SINGLE SELECTIVE INVERSION DYNAMIC NMR

APPLIED TO

COMPLEX ORGANOMETALLIC EXCHANGE

By

JANICE A. CRAMER,

B.Sc.

A Thesis

Submitted to the School of Graduate Studies

in Partial Fulfilment of the Requirements

for the Degree

Doctor of Philosophy

McMaster University

January, 1994

SINGLE SELECTIVE INVERSION DYNAMIC NMR

To Mom and Dad

DOCTOR OF PHILOSOPHY (1994) McMASTER UNIVERSITY

(Chemistry) Hamilton, Ontario

TITLE: Single Selective Inversion Dynamic NMR Applied to Complex Organometallic Exchange

AUTHOR: Janice A. Cramer, B.Sc. (University of Waterloo)

Supervisor: Professor A.D. Bain

Number of Pages: xiii, 193

ABSTRACT

Organometallic species often participate in complex multi-exchange processes. The existing dynamic Nuclear Magnetic Resonance (NMR) spectroscopic methods are of limited use in complex systems. The classical line-shape method generally cannot provide mechanistic detail, and the actual data analysis may well be intractable if multi-exchange processes are occurring. Spin relaxation methods are more appealing for complex systems as they can also provide mechanistic information. The one-dimensional selective inversion relaxation experiment is inherently more precise than the corresponding two-dimensional method, but was thought to be impractical for multi-site systems as a separate experiment is required for each site.

A one-dimensional selective inversion experiment in which all of the exchange processes are probed in a single experiment regardless of the number of sites was designed and tested for complex organometallic systems of the type $M_2(CO)_6(\mu\text{-}PPh_2)$ (μ_2-η^1:η^2-CCR) where M= Fe or Ru and R= -HC=CH_2 or -C≡CPr^i. Three potential exchange processes occur with these systems: trigonal carbonyl rotation on each metal atom and σ to π interconversion of the μ_2-η^1:η^2-CCR ligand between the two metal atoms. The single selective inversion method successfully determined the temperature dependence of the chemical exchange rates for these processes in the chemical systems under study. In all

cases, the line-shape data were in agreement with the single selective inversion values.

The strengths and weaknesses of each of the dynamic NMR methods are complementary in complex exchanging systems and it appears that in many cases the optimal experiment is a combination of the available methods. A recommended combination strategy incorporating the single selective inversion methodology with both 2D-EXSY and line-shape analysis is outlined.

Preliminary exchange studies on $Os_3(CO)_9(\mu\text{-}PPh_2)(\mu_3\text{-}\eta^1\text{:}\eta^2\text{:}\eta^2\text{-}C{\equiv}C\text{-}t\text{-}Bu)$ with qualitative 2D-ESXY experiments permitted the detection of 1) a minor isomer in exchange with the major isomer at low temperature (233 K) and 2) both delocalized and localized carbonyl exchange processes at higher temperature (253 K).

The chemical exchange process of the $\mu_2\text{-}\eta^1\text{:}\eta^2\text{-}HC{=}CH_2$ ligand in $Fe_2(CO)_6(\mu\text{-}PPh_2)(\mu_2\text{-}\eta^1\text{:}\eta^2\text{-}HC{=}CH_2)$ exhibited an interconversion barrier of 71 ± 6 kJ mol^{-1}. This was higher than expected, as most other vinyl and all acetylide complexes exhibit a barrier in the range of 42 to 55 kJ mol^{-1}.

The use of two structural features to predict the barrier is proposed: 1) strength of the π interaction as determined by the difference in $M\text{-}C_\alpha$ and $M\text{-}C_\beta$ bond distances and 2) asymmetry in the electronic donation to each metal as determined through the metal to ligand distances. Application of these two criteria have so far allowed prediction of the barrier in all cases found in the literature to date.

ACKNOWLEDGEMENTS

I would like to sincerely thank my supervisor Prof. Alex Bain for his patience and continued support while introducing me to his world of NMR. It was an enjoyable four years.

I am grateful to Prof. Arthur Carty, not only for supplying the interesting dynamic organometallic systems but also for his input and discussion on the inorganic aspects of the project. Special thanks to his co-workers Dr. Simon Doherty and Mr. John Corrigan who made the samples on my behalf.

I thank my committee Prof. Gary Schrobligen and Prof. Colin Lock, and my external examiner Prof. R. Morris for their helpful comments.

A special thank-you goes to Dr. Jim Britten and Mr. Dave Pole for their invaluable assistance in obtaining the crystal structure data and the sketches of the molecular structures, respectively.

I would like to thank my co-workers: Ian Burton, Lydia Lao, Bruce Fulton, Stephen Hughes, Greg Duns, Suzie Rigby, Frank Rathgeb, and *defacto* group member Tex (Chris Marvin) who were quick to offer encouragement when experiments didn't work and shared my joy when they did.

I also thank my other friends that I met at Mac (Elizabeth Jefferson, Kris Malisza, Dave Pole, Mike Malott, Mike Brown, Ian Bytheway, Akis Boyatzis, Al Postigo and Theresa Fauconnier) who lightened the days and nights in Hamilton.

Immense thanks to my parents and family for their constant love and support and for instilling in me the confidence and the tenacity to see this project through.

Financial assisance in the form of Scholarships from the Government of Ontario (OGS), and the Government of Canada (NSERC post-graduate), and Teaching Assistantships from the Department of Chemistry is gratefully acknowledged.

TABLE OF CONTENTS

LIST OF FIGURES

LIST OF TABLES

CHAPTER 1

INTRODUCTION

Part A: Introduction to Dynamic NMR

Molecules are often not rigid in solution. Individual atoms within the molecule can break and reform bonds creating different configurations, while bond rotation can occur to form different conformers of that molecule. These different configurations or conformers typically exist in a dynamic equilibrium in which the ratios of all of the species are fixed. The atoms within the molecule that are responsible for the rearrangement are said to undergo chemical exchange.

Chemically exchanging systems have long been of interest to chemists who seek to answer two fundamental questions: What is the nature or mechanism of the exchange between two or more chemical sites and what is the rate of that process? If there are only two sites undergoing exchange, the exchange can only occur *via* one mechanistic pathway. If the number of sites increases, the pathway by which the exchange occurs is no longer clear cut. In fact there may be more than one exchange process occurring, as is often the case with organometallic chemical species. As the number of processes increases it becomes more difficult to determine the rate of each process uniquely.

There are many instrumental techniques available to study chemical exchange. One of the most widely used is Nuclear Magnetic Resonance (NMR) spectroscopy. NMR spectroscopy has some notable advantages over other kinetic methods for studying chemical exchange.[1-4]

Separate signals are observed for each nucleus in a different chemical environment. The NMR spectrum, therefore, can give direct information about the actual parts of the molecule that are involved in the exchange. This allows even degenerate isomerization, in which the molecule rearranges to form a chemically identical molecule, to be studied.[4-6] NMR spectroscopy also allows the systems to be studied at equilibrium. A process at equilibrium occurs with no net reaction; it is reversible but occurs at a detectable rate. A technique that enables one to probe the exchange without disturbing the actual exchange equilibrium will give a better understanding of that exchange.

Dynamic NMR techniques have developed greatly since the late 1960's. This is primarily as a result of the advent of Fourier transform techniques, computer controlled spectrometers, and progressively more powerful numerical analysis methods. A variety of techniques are available depending on the rate of the process involved, and the type of information desired.[7] The optimal choice of techniques is dependent on many factors. One of the main factors is the time-scale of the reaction and how coincident that is with the corresponding time-scale of the NMR technique. There are separate NMR techniques that span the slow to fast regime of chemical exchange. Three techniques are suitable for studying exchange in the slow regime: line-shape analysis, one dimensional selective

inversion, and two dimensional exchange spectroscopy (2D-EXSY). Line-shape analysis also overlaps into the intermediate regime. The fast exchange regime can be studied by use of molecular correlation times from relaxation or cross-relaxation studies. This thesis has focussed on systems that undergo exchange that is slow on the NMR time-scale. Often the information that one can obtain from the three slow exchange NMR techniques is complementary. First the basics of NMR spectroscopy itself, then the three individual experimental techniques for slow exchange will be presented.

1.1 Basic Theory of Pulse FT-NMR[4]

When a sample is placed in a magnet, with an applied magnetic field B_o, the magnetic moments of all the nuclei sum to generate a bulk magnetization vector (M). At equilibrium, this vector aligns along the direction of the magnetic field (usually defined as the z axis). The force of B_o on M causes M to precess around B_o at a characteristic frequency (ν) which is defined as the Larmor frequency:

$$\nu = \frac{\gamma B_0}{2\pi} (in\ Hz) \qquad 1.1$$

where γ is the magnetogyric ratio and is a constant that is characteristic for each nucleus

Perturbation of the magnetization away from the equilibrium state is induced by applying a radio frequency (rf) pulse of irradiation perpendicular (normally along the x direction) to B_0. This field (B_1) interacts with M to produce a torque that rotates the magnetization vector towards the xy plane. The amount of rotation or pulse width is

determined by the duration of the pulse of rf irradiation. A 90° pulse width rotates M so that it is aligned with the y axis, where the detector is normally placed. When the B_1 field is removed, the magnetization vector M precesses about B_o at the Larmor frequency. Nuclei in different sites or chemical environments will all have slightly different Larmor frequencies or chemical shifts, so the total magnetization vector is a superposition of all their individual oscillating frequencies. This total magnetization induces an oscillating current that is detected in the receiver coils placed on the y and/or x axis. This induced signal was generated from a perturbed state and over time the magnetization will relax back to its equilibrium state. Once free from the induced field, the signal decays as a function of time and is called the free induction decay (FID). The FID is time domain (amplitude versus time) information and normally the frequency domain (amplitude versus frequency) information is of interest. The frequencies of all the individual chemical environments are extracted from the FID signal through mathematical procedures that transform the information from the time domain into frequency domain. The most common of these mathematical procedures is Fourier transformation (FT).

1.2 The NMR Time-Scale[1,6,7]

To choose the optimum NMR technique one must have an idea of the time-scale of the available NMR techniques. The sensitivity of any spectroscopic technique depends on the response time of that technique to the molecular motion. The time-scale is roughly related to the reciprocal of the frequency of the electromagnetic radiation used by that

technique. NMR spectroscopy is slow compared to IR spectroscopy that measures molecular vibrational changes (10^{12} to 10^{14} s^{-1}) and UV/visible spectroscopy that measures electronic changes (approx. 10^{18} s^{-1}). These motions have little direct effect on NMR spectra. However, slower motions that occur with rates between 10^{10} and 10^{-2} s^{-1} have been studied with NMR techniques.[7] There is no single defined time-scale for NMR as it depends on the type of NMR experiment done, which in turn is very much dependent on the observable NMR parameters of the chemical system under study. The observable parameters are normally signal intensities, chemical shifts, scalar couplings, and nuclear relaxation times.[7] These not only vary from one observed nucleus to another, but also from one molecular structure to another.

The type of experiment, and hence the ranges of rates that can be studied, are conveniently subdivided into three time regimes; the slow, intermediate and fast. The two extremes are the easiest to define. The slow regime occurs when the exchange lifetime is greatly in excess of the NMR time-scale. A spectrum of an ideal two site system in slow exchange should show two peaks, with no noticeable broadening, that are well separated in chemical shift. The intensity ratio of each peak gives the relative populations of each site and hence the equilibrium constant. In the fast regime, the lifetime is substantially less than the NMR time-scale and the spectrum is seen as a sharp singlet representing an averaged single site of all the individual species weighted by their respective populations. The intermediate regime naturally falls between the two extremes, and is seen as a gradual broadening until a broad singlet with a flat top is observed

followed by a sharpening in the signal until the fast regime is reached (Figure 1.1).[1,2]

There are several methods for studying chemical exchange that is slow on the NMR time-scale. The classical method is that of line-shape analysis, the time-scale of which is dependant on the modulation of the chemical shift parameters.[7] However, if rate processes are slow on the chemical shift time-scale, but fast on the relaxation time-scale, then NMR spin relaxation methods, such as selective inversion and 2D-EXSY, can be used to study the transfer of nuclear population from one site to another.

1.3 Line-Shape Analysis

Line-shape analysis is the classical method of rate determination by NMR techniques.[2,3] For the most part, it is suitable for rate processes that fall from the slow to intermediate regimes. The time-scale of line-shape analysis is typically in the region of $1\text{-}10^6$ s^{-1}, but this is very much dependent upon the nuclei being detected.[1,3,7] The difference between nuclei is related to the magnitude of the difference in frequency between exchanging sites and the operating frequency of the spectrometer. It is generally accepted that line-shape analysis can give extremely accurate rate data, especially in the intermediate regime.[1,3,8] However, it is often difficult to extract mechanistic information.

1.3.1 Theoretical Principles

As the rate of exchange increases from the slow regime to the fast regime, one begins to see an effect on the spectrum as the lines begin to broaden. Eventually, the

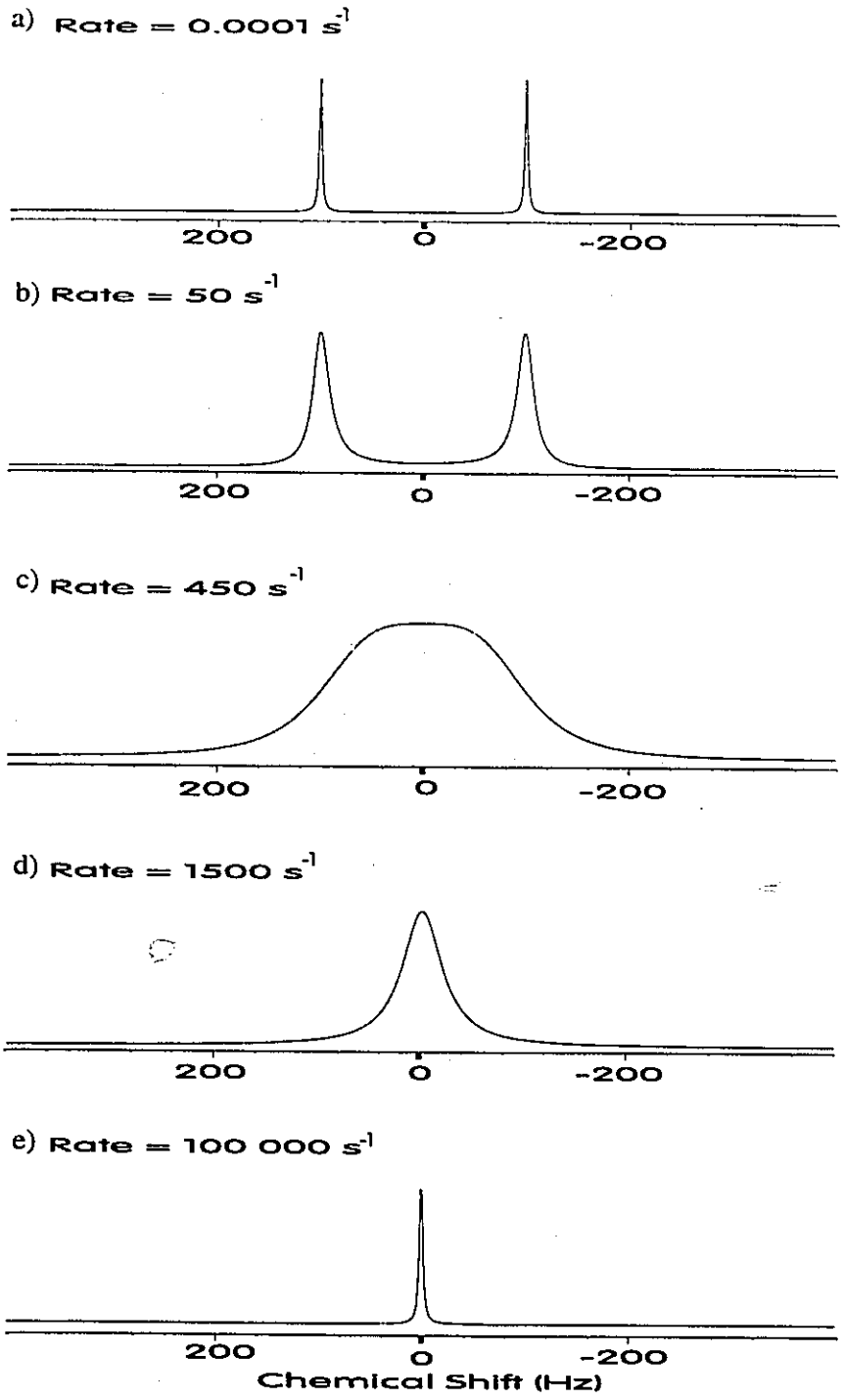

Figure 1.1 Calculated line-shapes for an equally populated two-site exchange: a) no exchange b) pre-coalescence c) coalescence d) post-coalesence e) fast exchange.

peaks will become so broadened that they merge and are said to coalesce. After this point no further exchange broadening is seen. If the rate is increased further, the broadened coalesced peak gradually narrows to form a sharp singlet caused by exchange that is fast in comparison to the NMR time-scale (Figure 1.1).

The exchange broadening can be explained as follows.[6] If an ensemble of spins is precessing at frequency ν_1, and then some spins briefly exchange into another environment with a different frequency, ν_2, before returning to their original site, then they will be out of phase with the spins that did not exchange. The accumulation of these phase errors with time leads to destructive interference in the FID and a loss of signal. As a result, the FID decays rapidly and the resulting Fourier transform produces a broad line. Below the coalescence point, the more frequently that spins visit another site with a different precession frequency, the faster the loss of phase coherence and the greater the line broadening. In the case of the fast regime, the spins change environments so quickly that there is not enough time to build any phase incoherence and the corresponding FID gives a sharp signal.

Clearly, the rate of exchange can then be monitored by measuring the extent of broadening. The total line-shape of the system is a function of the rate (or life-time) of the exchange, and the difference in frequencies between the two sites. One cannot precisely define the time-scale range of bandshape analysis for this reason. It is the chemical shift that is being modulated in this experiment, and modulation of the chemical shift is very much a function of the operating frequency of the spectrometer used and the

specific nuclei being observed. This is illustrated by comparing typical frequency differences between exchanging sites of ^{195}Pt and ^{1}H. Representative frequency differences for these nuclei are 1000 and 100 Hz, respectively[7]. The broadening due to exchange between sites can be observed at lower rates when the frequency difference is smaller and therefore the time-scale range for ^{1}H is lower than for ^{195}Pt. In the ^{13}C carbonyl exchange studies done in this thesis (with a 300 MHz NMR instrument), the frequency difference averaged between 300-500 Hz.

1.3.2 Total Bandshape Analysis[1-3,7]

The basic procedure involves obtaining the spectrum or line-shape in steps from the slow regime to the fast regime and matching each line-shape with a calculated lifetime or rate of exchange. Variation of the rate of exchange on the system is most commonly achieved by varying the temperature, but other means such as varying the pH, pressure, or catalyst concentration of the NMR sample have also been performed.

Several programs exist that will model the line-shape for a given rate. The basic procedure is the same; the estimated rate is varied until the program calculates a line-shape which simulates the experimental line-shape. At this point, one obtains the spectra as a function of both the temperature and the rate.

The simulated line-shape is matched with the experimental one through visual inspection and this procedure can be quite tedious. If there are many sites and/or reaction pathways, a line-shape that matches the spectra adequately may not be found. The most

rigorous of programs for simulating the line-shape DNMR5 has a built-in iteration procedure that will attempt to vary the rate itself until a correct match is found.[8] However, it has had limited success and this program can only handle up to 5 sites. Much of this work involved systems with more than the maximum allowed number of sites and this necessitated use of an alternate program (EXCHANGE) by McClung. However, this program is not applicable for systems with scalar coupling. This program requires the following input: the number of sites, frequency and relative population of each site, estimates of both the spectrometer line-width (in Hz) in the absence of exchange, the estimated rate of exchange, and also the exchange matrix.

The exchange matrix or map defines which sites exchange with each other. If more than one exchange process occurs simultaneously, these can be entered separately. One of the drawbacks of this procedure is that one must first make an educated guess as to which sites are exchanging and how many processes this involves. If the system is not too complicated and there is a marked difference in line-shape with differing exchange maps, then it may be possible to extract mechanistic information by varying both the rate and the mechanism. However, for complicated multi-site systems undergoing simultaneous exchange processes, as experienced in this work, it is imperative that the exchange map be defined accurately. In these cases, spin relaxation methods, particularly two dimensional techniques, are unsurpassed for outlining the mechanistic pathway between sites.

1.3.3 One Point Coalescence Approximation Method[1,2]

One can obtain an approximate value of rate of the exchange from the coalescence spectrum for systems which have equally populated sites and exhibit no scalar coupling. At coalescence, the rate of exchange (k_c) is given by:

$$k_c = \frac{\pi \Delta \nu}{\sqrt{2}} \qquad 1.2$$

In order to calculate the rate of exchange at coalescence, one must know the difference in frequency between the sites ($\Delta\nu$, in Hz) in the absence of exchange. However, since this rate value is virtually meaningless on its own, the free energy of activation ($\Delta G^{\ddagger}_c$) at coalescence is normally determined. In order to determine this value, the temperature at which coalescence (T_c, in Kelvin) has occurred must also be known. Rearrangement of the Eyring equation (1.3) gives the free energy of activation ($\Delta G^{\ddagger}_c$).

$$k_c = \kappa\left(\frac{k_B T_c}{h}\right) e^{\left(\frac{-\Delta G^{\ddagger}_c}{R T_c}\right)} \qquad 1.3$$

The constant κ is a transmission coefficient which depends on the nature of the process but is often taken to be unity,[1] k_B is the Boltzmann constant, h is the Planck constant and R is the gas constant.

This is at best an approximate method because it involves a single point calculation and is thus prone to large errors. Also, it is often difficult to determine the coalescence temperature exactly. Although the line-shape is most sensitive to small

deviations in the rate at coalescence, it is relatively easy to miss this temperature by ± 5 K. In addition, temperature variation of the chemical shift can give an error in the frequency difference ($\Delta\nu$).[1,2]

1.4 Spin Relaxation Methods and The Nuclear Overhauser Effect or (Enhancement)[5,9]

Nuclear Overhauser experiments have become an extremely powerful tool in the last decade for chemists and biochemists. Nuclear Overhauser enhancements are generated when excess spin population is transferred between energy levels within a molecule by electromagnetic radiation of the appropriate frequency.[9] In order for this to occur two conditions must exist: 1) There must be a connection or pathway between the two spin levels. This connection may be formed by dipole-dipole coupling or exchange coupling between the spin levels and 2) the spin population in the levels must be removed from equilibrium. The tendency to return to equilibrium drives the spin population to move or relax *via* the available pathways. In the recent literature, the term nOe has been used almost exclusively to refer to experiments probing the dipole-dipole coupling. In order to avoid confusion, spin population that is transferred in a transient experiment *via* an exchange coupling will be referred to as a chemical exchange transient (CET) and likewise the spin population that has been transferred *via* a dipole-dipole coupling will be referred to as an nOe transient (NOET).

In a transient experiment, the system is initially perturbed from equilibrium by

exciting one of the coupled sites and then the excitation energy is removed. The rates at which the CET or NOET grows and then decays is measured through the variation in the observed magnetization intensity of the coupled sites. During an exchange process, spins will exchange from one site to another perturbing the spin population in the energy levels. The return to equilibrium is characterized by the exchange rate (k) and the spin-lattice relaxation rate (T_1^{-1}).

The spin-lattice relaxation is a radiationless process that requires fluctuating fields of the appropriate frequency.[5] These fields originate from many sources, but the most common for nuclei of spin ½ is the dipole-dipole interaction. This mechanism of field generation arises from the interactions of neighbouring spin ½ magnetic moments as they undergo Brownian motion in the sample. The efficiency (or rate) of this relaxation is dependent on the distance between the nuclei and the molecular correlation time.[5]

Measurements of this relaxation rate in the absence of exchange can lead to determination of the bond distances since the relaxation rate depends on the internuclear distance. This has been utilized quite extensively and successfully to determine the structure of large biological molecules (plant alkaloids, penicillins, and antibiotics) that are sometimes difficult to determine with crystallographic techniques.[5,10] However, since exchange and relaxation are linked theoretically, their measurement and interpretation must be treated simultaneously.[11] If one can separate the effects of the two then one can obtain information about exchange. This necessitates that the exchange lifetime and the relaxation lifetime are of the same order.[5]

The two main types of CET experiments are one dimensional magnetization transfer and multi-dimensional exchange spectroscopy (EXSY). A brief outline of these experiments is given below.

1.4.1 Chemical Exchange Transient Experiments

One Dimensional (1D) Magnetization Transfer

The basic experiment involves perturbation of the spin system to generate the transient through selective excitation, and then allowing a variable delay to monitor the magnetization intensity of the exchange coupled sites as a function of time. There are two different 1D magnetization transfer methods; selective saturation and selective inversion.[5,6] The difference between the two methods lies in the manner in which the excitation occurs. In the case of a two-site exchange system, the saturation technique involves constant irradiation at one site.[12,13] The magnetization intensity of that site remains at zero throughout the experiment. This results in a CET being transferred to the unperturbed site and is observed in the change of magnetization intensity of this site as a function of time. In the selective inversion technique, a 180° pulse applied at one site selectively inverts the magnetization at this site. Initially the magnetization at this site will be negative and it will gradually approach the positive equilibrium magnetization intensity as the exchange-relaxation processes begin. The CET is most obviously observed in magnetization intensity of this site. The magnetization intensity at this site initially decreases as population is transferred from this site to the inverted site *via* the chemical

exchange process. Eventually an increase in intensity will be observed as relaxation begins to dominate the system (Figure 1.2).

The main advantage of the selective inversion experiment is that both signals can be monitored. In addition, the act of inversion perturbs the system 180° from equilibrium allowing a greater length of time to observe the exchange-relaxation process. These two advantages combine to increase the amount of information that one can observe from each spectrum. For these reasons, it is most often the method of choice.[6] Saturation transfer is advantageous if the relaxation of the irradiated site is fast in comparison to the exchange since saturation of that site will aid in removing this adverse effect.[5]

The disadvantage of both these methods is that in complex multi-site multi-exchange systems, a separate experiment, selectively exciting each site would have to be performed. This is not only time-consuming, but it is also difficult to perform a perfect selective excitation on a site that is close in frequency to others and this leads to errors.[5,14] An optimal technique that would allow one to probe all of the exchange rates in a single experiment would be a significant advance. A technique for a single optimal selective inversion experiment was designed and will be presented in this thesis.

There are various approaches to solving the time-dependence of magnetization intensity. Forsén and Hoffman[12,13] were the first to apply simplifying assumptions to the McConnell[15,16] or Gutowsky and Holm[17] equations that made extraction of the rate possible. However, there are many situations where these assumptions are not valid. Led

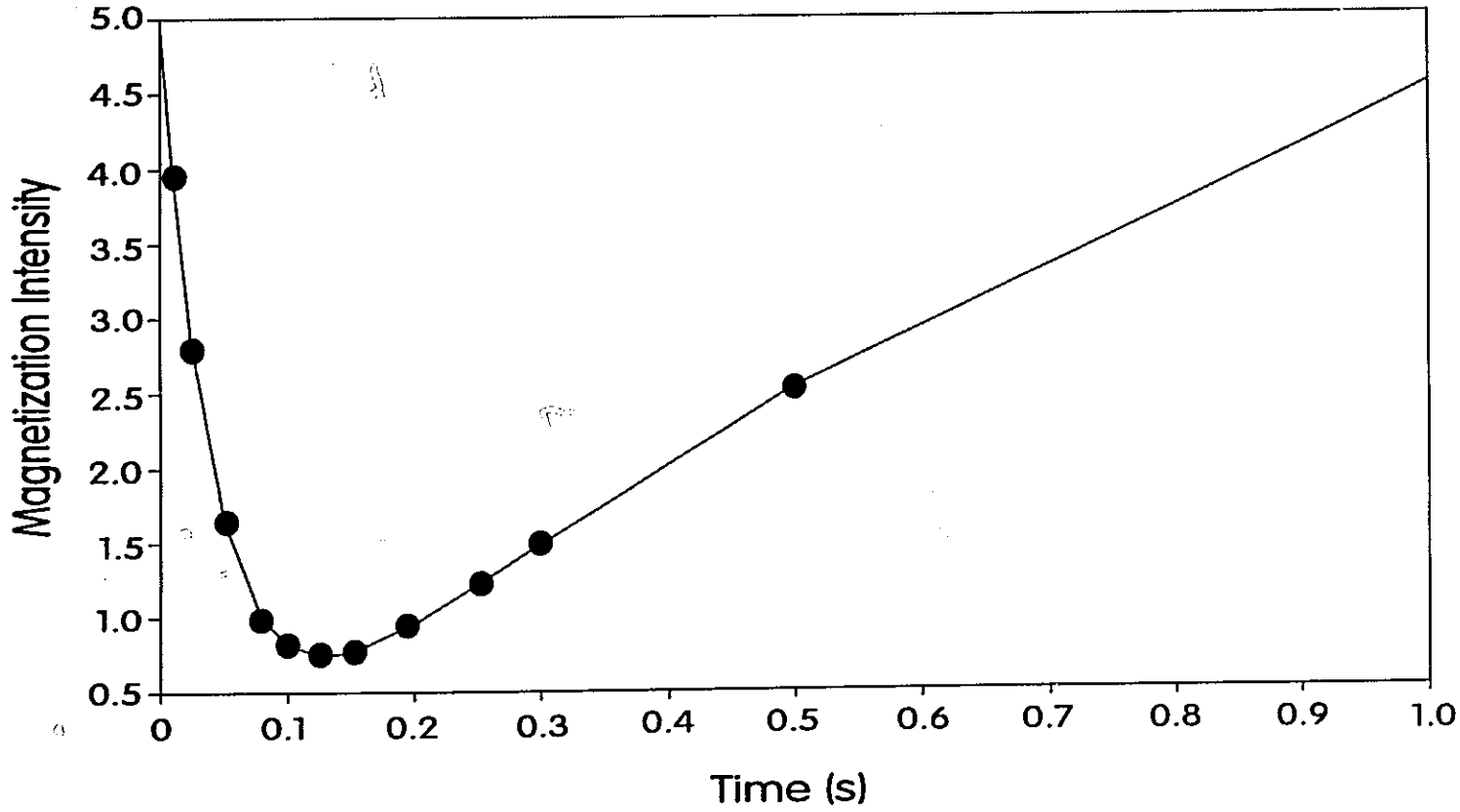

Figure 1.2 Plot of a typical chemical exchange transient (CET). The CET is formed by selectively exciting one site with respect to the other. This plot shows the magnetization of the positive site and the CET is observed as the dip in intensity as the magnetization is transferred from the positive site to the inverted site.

and Gesmar[18] proposed a more rigorous approach. This method is still not suitable for multi-site excitation as one can not account for imperfect excitation. The method of McClung[19] allows one to fit the data for multi-sites and multi-exchange processes in the presence of incomplete selective excitation. This is the only approach that permits the feasibility of a single selective inversion experiment. The program SIFIT[19] is a non-linear least squares fitting program developed by McClung that will iterate until the calculated magnetization intensities for each site sufficiently agree with the experimental data. It requires estimates of all of the rates of exchange, the spin-lattice relaxation rate for each site, and as with line-shape analysis, the exchange matrices that define the mechanisms of exchange. As a result of the iteration procedure, it is possible to vary the exchange mechanism along with the other variables to establish both the mechanism and the rates of exchange.[19]

Two-Dimensional Exchange Spectroscopy (2D-EXSY)[4,7,20,21]

If the main objective of the experiment is to distinquish one exchange mechanism over the other, the 2D-EXSY experiment is often superior. Cross-peaks arising from the transients occur between signals involved in chemical exchange, so often a simple visual inspection of the spectrum will pinpoint one mechanism over the other.[4,14] The basic pulse sequence is: $90°- t_1 - 90° - t_m -90° - t_2$

The first 90° pulse rotates the magnetization into the x-y plane and the signals are allowed to precess at their characteristic resonance frequency for an evolution period, t_1,

at which point they become frequency labelled. The second 90° pulse rotates the magnetization into the xz plane, effectively performing the 180° excitation (analogous to the 1D selective inversion experiment) required for magnetization transfer. The magnetization is then allowed to evolve for a fixed time, t_m, at which time the chemical exchange and relaxation processes occur. The final 90° pulse allows the net magnetization in z to be detected during time t_2. The experiment is repeated for n t_1 which results in the magnetization being obtained as a function of t_1 and t_2, $M(t_1,t_2)$. This is then double Fourier transformed to obtain $S(\omega_1,\omega_2)$.[4]

The means by which chemical exchange is observed in a spectrum demonstrates the clear advantage that the 2D method has in determining exchange matrices. The two sites A and X precess at ω_A and ω_X, respectively. If one examines one site, (A), during the labelling period, that site will contribute a component $\exp(i\omega_A t)$ in t_1 to $M(t_1,t_2)$. During the mixing time, t_m, some of site A spins will transfer to site B. These spins will precess at ω_B and will have a component $\exp(i\omega_B t)$ in t_2 contributing to $M(t_1,t_2)$. The result is that those spins labelled A in t_1, and B in t_2 will be observed as cross-peaks, while those spins that did not exchange with B are labelled A in t_1, and A in t_2 will be observed as diagonal peaks in the double Fourier transformed spectrum (Figure 1.3). Thus visual inspection of the spectrum gives the exchange matrix.[4]

The intensity of the cross-peaks is related to the mixing time and to the rate of exchange. Several approaches have been developed to extract the rate of exchange from the volume of the cross-peak.[4] One approach was to repeat the experiment over several

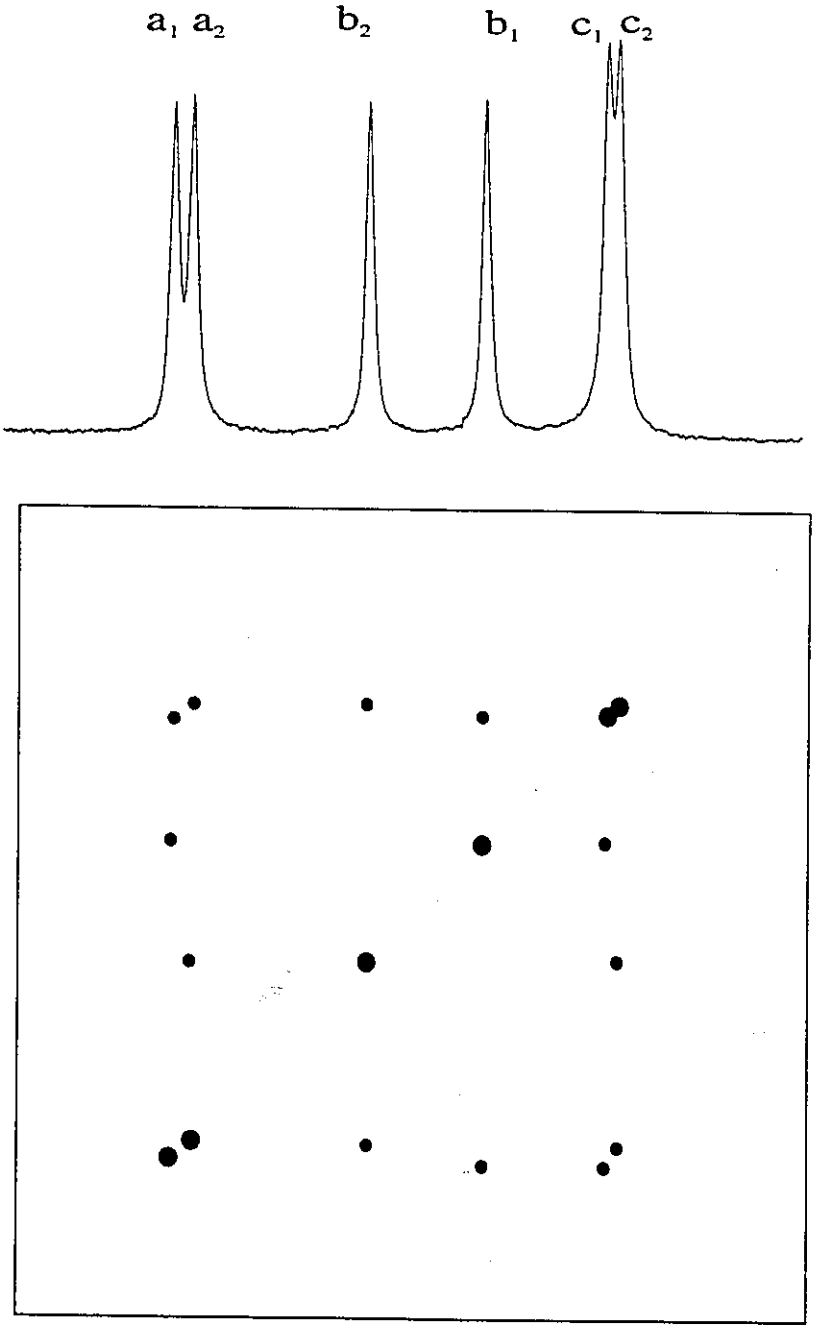

Figure 1.3 Representation of a 2D-EXSY spectrum showing carbonyl rotation in $Ru_2(CO)_6(\mu\text{-}PPh_2)(\mu\text{-}\eta^1\text{:}\eta^2\text{-}CC\text{-}i\text{-}Pr)$. The diagonal peaks represent the 1D ^{13}C spectrum of the carbonyl region and the cross-peaks represent the chemical exchange transient (CET) between exchanging sites.

short mixing times and plot the intensity of the cross-peak ($I_{ij}(t_m)$) as a function of the intensity of the diagonal peak ($M_j(t_m)$). The slope of the plot gives the rate k_{ij}. This is extremely time intensive and the use of low mixing times results in low intensity volume integrals that are difficult to measure accurately.[4] Another proposed method was to try to iterate to the correct rate. Given an initial guess for the rate, the cross-peak intensities are calculated. These are compared with the experimental values and the value of the rate is iterated until the experimental and calculated intensities converge. This was found to be too tedious.[4] In 1984, Perrin developed a method for explicitly solving the generalized equation for multi-site systems in order to extract the rates from a single mixing time value.[22]

Interpretation and quantitative analysis of 2D spectra are often complicated by the fact that cross-peaks can also arise from cross-relaxation and scalar coupling. Fortunately, techniques have been developed that either reduce or allow the identification of those peaks which arise from cross-relaxation.[4,20]

In multi-site systems, the mixing time is extremely crucial as second and third order cross-peaks can appear if the mixing time is sufficiently lengthy. This problem is illustrated in the work by Ramachadran *et al.*[23] in which the kinetics of halide redistribution occurring within a 1:1 M mixture of $SnCl_4$ and $SnBr_4$ were studied. They obtained 2D spectra at four different mixing times. The five different species ($SnCl_4$, $SnCl_3Br$, $SnCl_2Br_2$, $SnClBr_3$, $SnBr_4$) were observed in all of the spectra (Figure 1.4).

Magnetization transfer between the sites caused by halide scrambling reactions

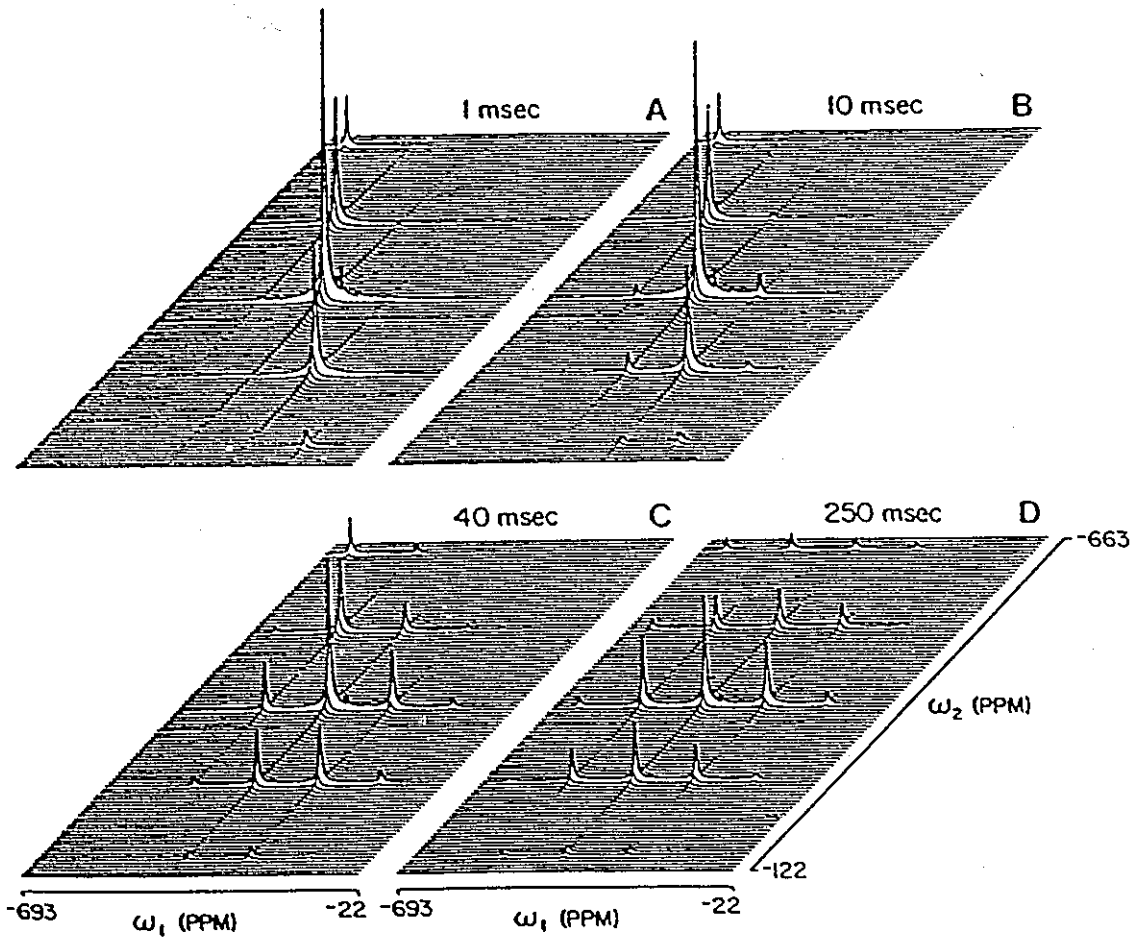

Figure 1.4 ^{119}Sn 2D-EXSY NMR spectra of a 1:1 mixture of $SnCl_4$ and $SnBr_4$ as a function of mixing time. As the mixing time increases, the number of cross-peaks increase. A) Only diagonal peaks B) First-order cross-peaks C) Second-order cross-peaks D) Third-order cross-peaks. *Figure 4.1 is reproduced from reference 23.*

was observed to increase in order as the mixing time lengthened. The fact that the higher order cross-peaks were observed as a function of mixing time allows one to conclude that the higher order peaks arose from single relayed halide exchanges and not from one step multiple halide exchange.[23]

Recently, Farrugia and Rae[24] published a study on a organometallic system with more than one exchange process occurring. They found that there was no optimal mixing time that would suit accurate evaluation of all the rate constants in the system and thus they turned to 1D magnetization transfer studies.

These studies illustrate quite clearly why 2D quantitative analysis is fraught with large experimental errors. If complex multi-site exchange can occur, a low mixing time is required to suppress higher order peaks. The low mixing time results in low peak volumes that translates into high experimental errors.[4]

1.5 Applications of NMR Techniques in the Slow Regime

One dimensional selective inversion techniques have some clear advantages, but many researchers are still using classical exchange methods (line-shape analysis or even worse, the one point coalescence approximation method). However, a review of the literature will show that the use of selective inversion and 2D techniques have steadily increased with the availability of accessible computer programs for the required numerical analysis.[19,21,25] Quite a few good reviews can be found that outline examples in the areas of organic, organometallic and biochemistry.[4,7,14,26]

In the organometallic area, the recent literature shows that the 1D selective inversion technique is becoming increasingly useful.[19,24,27-33] However, the 2D-EXSY technique is still the most popular (as demonstrated in many of the aforementioned reviews), despite the propensity for large errors in quantitative work, mainly because organometallic species typically involve multi-sites and many pathways. Most of the reported applications of 1D selective inversion involve few sites, since prior to the use of the technique presented in this thesis, a separate experiment was required for each site undergoing exchange, and as the number of sites increase, the experimental and computational time increases.

One area that has relied heavily on 1D magnetization transfer studies is that of enzyme kinetics.[34-38] Previous non-NMR kinetic methods had grave shortcomings. Stopped flow and temperature jump methods were utilized, but these require that the reaction be removed from equilibrium and its return to equilibrium is monitored to obtain the rate.[34,36] This differs from magnetization transfer, as in the NMR techniques the reaction equilibrium is always maintained; it is merely the initial spin populations in the energy levels that are perturbed from their equilibrium state. The only other method that permitted measurement at equilibrium was radioactive tracer analysis but this requires expensive and sometimes difficult radioactive labelling before the subsequent assay procedure.[34]

A comparison of one and two dimensional NMR magnetization transfer methods for measuring *in vivo* enzyme catalyzed exchange was made by Boyd *et al.* in which he

concluded that there was no significant advantage in going from 1D to 2D.[35] However, the 1D technique had some clear advantages. Normally, it is less difficult and more time efficient to obtain good quantitative data with 1D techniques.

The advantages and disadvantages of each dynamic NMR method have been alluded to in this introduction. Chapter 3 is devoted to presenting these advantages and disadvantages in full to illustrate when a particular method is most suitable.

1.6 Calculation of the Activation Parameters[2,3]

Often what is important to chemists is the activation barrier of a particular exchange process. This can be determined by obtaining the rate of exchange as a function of temperature through use of the Eyring equation (1.4).

$$k = \kappa\left(\frac{k_B T}{h}\right) e^{\left(\frac{-\Delta H^{\ddagger}}{RT}\right)} e^{\left(\frac{\Delta S^{\ddagger}}{R}\right)} \qquad 1.4$$

$\Delta H^{\ddagger}$ and $\Delta S^{\ddagger}$ are the enthalpy and entropy of activation respectively, and κ, k_B, h, and R are defined as in equation 1.3. This equation can then be rearranged to give:

$$\ln(k/T) = \frac{-\Delta H^{\ddagger}}{R}\left(\frac{1}{T}\right) + \frac{\Delta S^{\ddagger}}{R} + \ln\left(\frac{k_B}{h}\right) \qquad 1.5$$

A plot of ln(k/T) versus 1/T is linear, with a slope of $-\Delta H^{\ddagger}/R$, and an intercept of $\Delta S^{\ddagger}/R + \ln(k_B/h)$. The values for the enthalpy and entropy of activation are then obtained from a linear least-squares analysis of the plot.

Part B: Introduction to the Chemical System[39,40]

Interest in transition metal cluster chemistry has grown from the belief that one can gain insight into many catalytic processes involving metal surfaces by using bi- or polynuclear metal carbonyl compounds as models for these surfaces.[41] The actual chemistry at the metal atom in the transition metal complex is more readily probed *via* a number of spectroscopic techniques like NMR than those available for a metal surface. The application of the analogy between these complexes and the interaction of the organic molecules on the metal surface in the catalytic process has been the subject of a number of books and reviews.[41-50] In particular, it is believed that a key to the catalytic activity is linked to the ability of the organic moieties to form multi-site bonds to the metal surfaces.[40,41] Unsaturated organic ligands (CO, CN, RC≡C-, R_2C=CR-) are found to bind in a multi-site fashion and in many different bonding modes (i.e. η_1, sym-μ_2, μ_2-η^2, sym μ_3, μ_2-η^1:η^2 and μ_3-η^1:$\eta^2\mu_4$) to metal clusters (Figure 1.5).[40]

Another possible explanation for the high level of reactivity in clusters with unsaturated ligands is their ready ability to undergo intramolecular rearrangement. The dynamic molecular rearrangement is usually quite complicated in that as the number of metal atoms increase, so does the number of sites and it is not uncommon for these sites to exchange *via* more than one independent dynamic processes. As a result of this

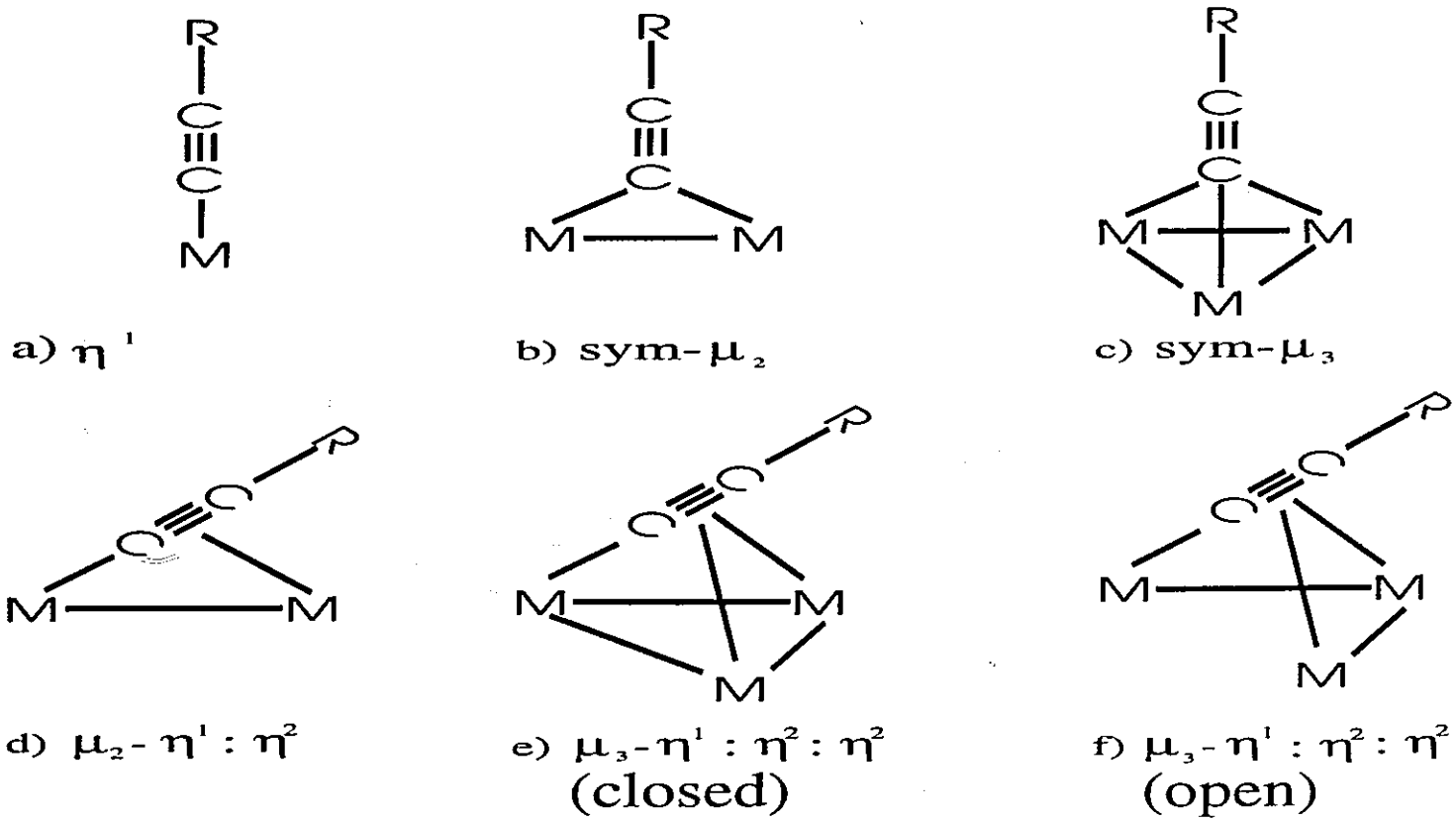

Figure 1.5 Bonding modes of an alkyne ligand on mono-, bi- and trinuclear metal frameworks.[39]

complexity, many of the older NMR studies have used the least accurate quantitative technique - that of one point coalescence data. Some of the more recent studies focus on the use of 2D techniques that are inherently less quantitatively accurate, but can accomodate multi-sites and multi exchange systems. These systems thus provide an excellent model to test a new dynamic NMR technique designed for accurate quantitation for complex systems. The molecules under study in this work are as follows:

1) $Ru_2(CO)_6(\mu_2\text{-}PPh_2)(\mu_2\text{-}\eta^1\text{:}\eta^2\text{-}C{\equiv}C\text{-}i\text{-}Pr)$

2) $Fe_2(CO)_6(\mu_2\text{-}PPh_2)(\mu_2\text{-}\eta^1\text{:}\eta^2\text{-}CH{=}CH_2)$

3) $Os_3(CO)_9(\mu\text{-}\eta^1\text{:}\eta^1\text{-}Ph_2P{=}O)(\mu_3\text{-}\eta^1\text{:}\eta^2\text{-}C{\equiv}C\text{-}t\text{-}Bu)$

An introduction to these systems will be given by first discussing the structural systematics of this class of compounds that contribute to its chemical reactivity, and then discussing the dynamic processes that are observed through NMR techniques.

1.7 Structural Systematics[40,51]

There are three main components of these systems that contribute to their unusual reactivity: the metal framework, the multi-site bound unsaturated organic ligand and the bridging phosphido or phosphidoxo ligand.

The Metal Framework:

The binuclear species have strong metal-metal bonds with resulting short metal-metal distances i.e. 2.7523(3) Å for **1** and 2.597(1) Å for **2**. In trinuclear systems, one can

either have a closed 48 electron structure with three metal-metal bonds or an open 50 electron framework with only two metal-metal bonds. The osmium trinuclear species **3**, has an open trinuclear structure with two strong metal-metal bonds, the other metal edge being essentially non-bonding. Each metal atom for all systems has a tripod of terminal CO ligands to form $M(CO)_3$ units. Localized scrambling of these ligands within the $M(CO)_3$ units is normally observed.[11,52-56]

The Phosphido,-oxo Bridge[40,51,57]

One of the major stumbling blocks to the use of organometallic complexes for catalytic processes is that the systems are susceptible to Lewis base degradation and the resulting fragmentation produces loss of catalytic material. It is thought that the use of a strong bridging ligand would maintain the polynuclear metal framework yet still allow for the necessary cleavage and reformation of the bonds in the catalytic process.

The phosphido ligand is believed to perform such a function. It forms strong rigid bonds that are chemically inert, yet flexible enough to allow for reactivity in other portions of the molecule. Maintenance of the polynuclear framework is of prime importance and this has been demonstrated. In some cases, even reversible M-M bond breaking and re-making has been shown to occur. Evidence has shown that the bridging phosphido group, under some conditions, acts as a non-innocent ligand that promotes certain nucleophilic and electrophilic reactions.[40,51]

The phosphido bridge is not the only suitable ligand. Interest has also been shown

in arsenido and phosphinidene bridging clusters. The phosphidoxo is a relatively new bridging ligand. The phosphorus atom bonds to one metal atom, while the oxygen atom bonds to the other along a metal-metal edge, forming an asymmetric bridge. This ligand is believed to have many novel properties that could induce increased reactivity under suitable conditions. It can bridge both non-bound metal centres, as in the case of the osmium species, **3**, and strongly bound centres, as in $Ru_2(CO)_6(\mu_2\text{-}O{=}PPh_2)(\mu_2\text{-}\eta^1{:}\eta^2\text{-}C{\equiv}C\text{-}t\text{-}Bu)$. The oxo portion is a hard base, while the phosphorus atom is a soft donor, this induces a large asymmetry in two homometallic centres.[57]

The unsaturated organic ligand:

One of the amazing features of these unsaturated ligands (alkenyl, alkynl, cyano) is the ability to form multi-site bonds and in a variety of fashions as illustrated in Figure 1.5.[40] In binuclear cases, the bridging ligand can bond in a sym-μ_2-η^1, asym-μ_2-η^1, or μ_2-η^2:η^1 mode. In addition, the ligand can either be coplanar with the metal-metal bond axis or not. In higher polynuclear species, the situation is more complex as a single alkyne ligand may donate (formally) between 2 - 6 electrons to a cluster depending on the mode of coordination. In addition to the bonding modes observed in the binuclear species, face-bridging μ_3 and μ_4 modes are also found in higher polynuclear species.[40] In general, as the number of metal atoms is increased in the bonding mode, the unsaturated bond lengthens. In the case of complex **3**, the alkyne is formally a 5 electron donor (one σ, and two π bonds). Orientation of the C-C bond is approximately perpendicular to one side of the

capped triangle. Despite the high formal donation the C-C bond is usually quite strong and the bond distance is short (1.27-1.32 Å).[40]

The μ_2-η^2:η^1 (π:σ) mode is of primary interest in this study as a result of its ability to exhibit both a high and low barrier to the fluxional motion. The bonding of high barrier alkene systems has been found to be significantly different from that of the low barrier alkyne systems. In the high barrier alkene cases, the ligand orients itself relatively perpendicular to the metal-metal bond axis, whereas the alkyne ligand is close to coplanar with the metal-metal bond axis. Along with this difference in geometry is a difference in the strength of the π bonds. In the low barrier alkene and alkyne systems, the α (to M) carbon atom is bound strongly to both metal atoms while the β (to M) atom is only weakly attached to the other metal atom. In high barrier alkene systems, the β carbon atom has been found to bond as strongly as the α carbon atom to the metal atom with π interaction.

If there is a difference in bonding strengths between the two interactions (σ and π), a substantial polarization occurs between the two metal atoms and the orientation of the ligand may well be responsible for the observed chemical reactivity and fluxionality.[40]

1.8 Chemical Exchange

Fluxionality in these chemical systems occurs with processes involving two separate ligand groups. The first is the carbonyl ligands that scramble in a delocalized[58-66] and/or localized[29,55,56,67-71] manner. In localized scrambling, the carbonyl ligands remain

on one metal atom and the motion involves a change in position of ligands on that metal, whereas in delocalized scrambling the ligands transfer from one metal atom to the other. The second fluxional ligand is the bridging acetylide or vinyl group and involves the σ to π interconversion of bonding modes between the bridged metal atoms (Figure 1.6).[72]

The localized scrambling of an inequivalent set of CO groups about a quasi-three fold axis can be explained in terms of a simple rotary motion, much like the mechanism described in Figure 1.7a. However, there exists another viable mechanism: that of successive pairwise motion (Figure 1.7b). It was realized that there was no substantive proof for either case, but throughout the literature, the simple concerted rotation motion is favoured intuitively on the basis of least motion effects.[53,55] Qualitatively, there is no difference between the two mechanisms as all of the carbonyl ligands scramble in either scheme. To determine which mechanism is in effect requires very accurate quantitative methods.

Alkyne systems, in general, show less variance in the barrier to the σ to π interconversion than with vinyl systems. The alkyne interconversion barriers range from 41-55 kJ mol^{-1} consistently.[40,73-78] Work on the original vinyl systems in the 1970's estimated these barriers to be within a similar range as the alkyne barriers.[79-81] Recently some vinyl systems have been shown to have much higher barriers; the iron vinyl complex, **2**, is one example.[78,82-84] The reasons for this behaviour will be discussed, with an explanation proposed in Chapter 5.

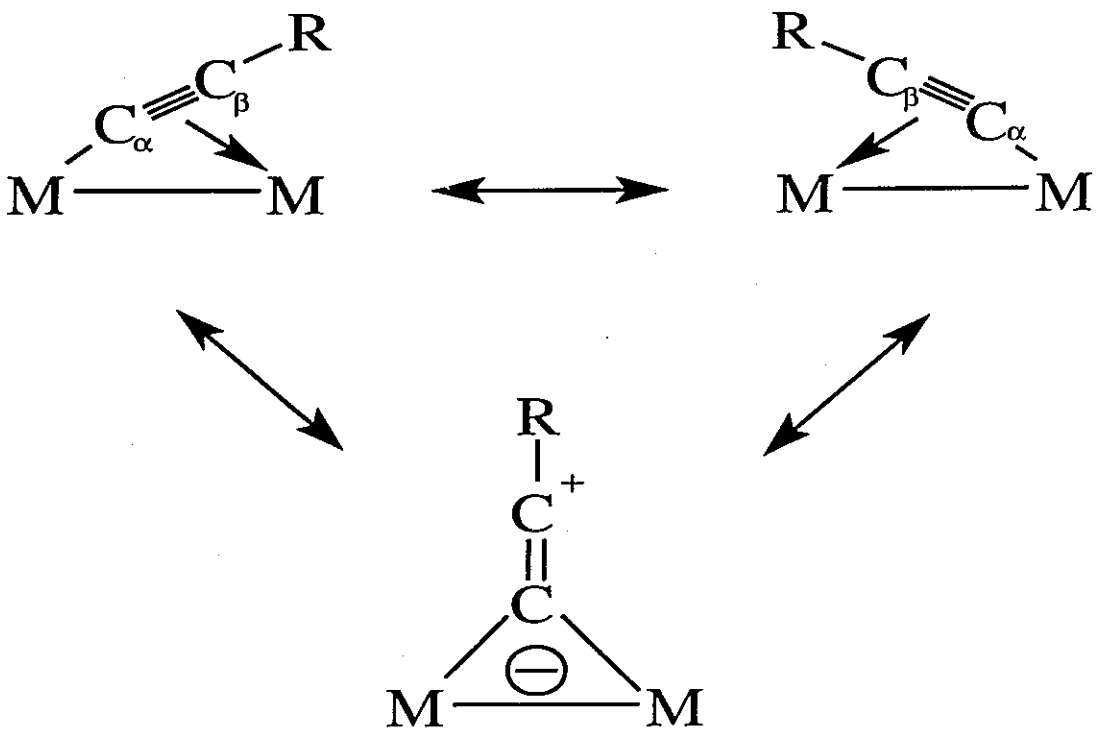

Figure 1.6 Windshield wiper fluxional process. The σ to π interconversion of the alkyne ligand between the two metal atoms is shown with the most probable transition state.

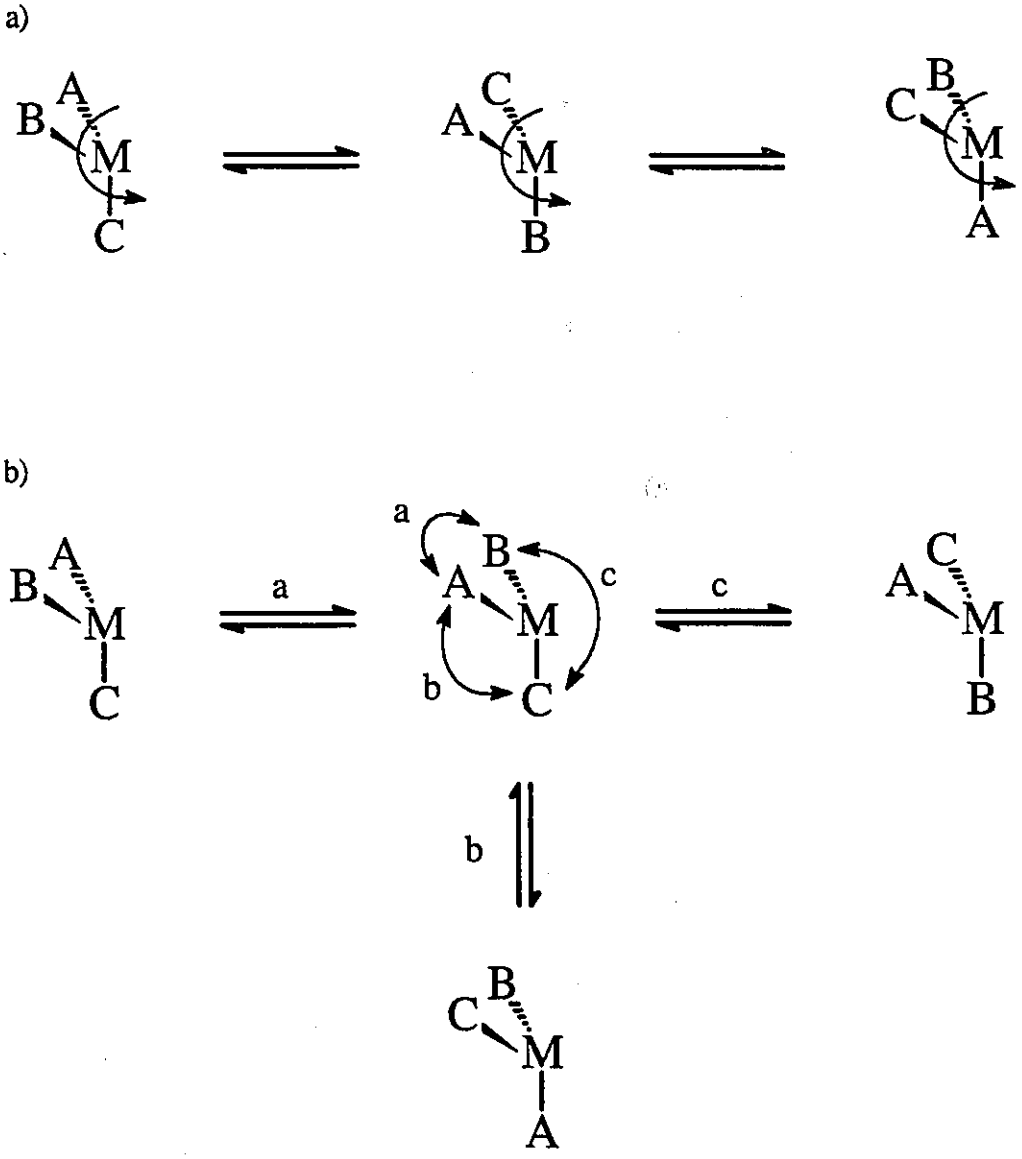

Figure 1.7 Possible mechanisms for tripodal carbonyl rotation a) concerted trigonal rotation b) successive pairwise exchange.

1.9 Objectives of the Thesis

Organometallic complexes often undergo complex exchange involving multi-sites and multi-exchange pathways. The classical dynamic NMR method of line-shape analysis often breaks down with these systems, and usually cannot provide mechanistic information. Spin relaxation exchange methods can be applied to complex exchange systems and provide mechanistic information. One-dimensional selective inversion studies were thought to be impractical because it was believed that a separate experiment had to be performed for each site present in the system.

The first objective was to design a selective inversion methodology that would allow all of the chemical exchange rate information to be obtained in a single experiment regardless of the number of sites and exchange processes. This methodology was tested by investigating the dynamics of the organometallic species of the type $M_2(CO)_6(\mu_2\text{-}PPh_2)(\mu_2\text{-}\eta^1\text{:}\eta^2\text{-}R)$ where R=-HC=CH_2, or -C≡C-*i*-Pr and M= Fe or Ru. These are challenging systems as there are six to twelve sites and at least three potential chemical exchange processes. The $\mu\text{-}\eta^2\text{:}\eta^1$ bound ligands undergo a process in which the σ and π bonds are interchanged between the two metal atoms. The carbonyl groups on each of the metal atoms undergo localized trigonal rotation. If the σ to π process is slow in comparison to the carbonyl rotation then the two carbonyl rotation processes can be measured independently. The carbonyl rotation itself may occur *via* two different mechanisms. This rotation by either mechanism results in a degenerate isomerism i.e. simple permutation of the carbonyl ligands about the metal that results in an

indistinguishable species from that of the original molecule, therefore extremely accurate quantitative work is required to distinguish between the two mechanisms and this is an exacting test system for the single selective inversion procedure.

The fluxional process involving the μ-η^2:η^1 bound ligands is more interesting from an inorganic structural point of view. In some alkene systems, the barrier to this exchange is higher than in other alkene systems and in all alkyne systems investigated to date. Currently there is no rationale that can predict or explain this behaviour. The second objective involved systematically probing the structural features of high and low barrier systems reported in the literature to gain a better understanding of this behaviour.

CHAPTER 2

SELECTIVE INVERSION MAGNETIZATION TRANSFER

2.1 Historical Background

The original magnetization transfer methodology was presented in 1963 by Forsén and Hoffmann[13] for a two-site equally populated system. At that time, all NMR experiments were done with continuous wave (cw) spectrometers, and not surprisingly this technique did not become popular until Fourier transform (FT) spectrometers became readily available. In 1964, Forsén and Hoffmann[12] generalized the theory for n sites and presented experimental results on a three-site system. Dahlquist *et al.*[85](1975) were one of the first to popularize the selective inversion experiment. This experiment perturbs the system 180° from equilibrium as opposed to 90°. This allows for a greater length of time to observe the transient, and permits both signals to be monitored which provides more information, and therefore, greater precision.[5,6] Prestegard[86], in 1977, was the first to apply the methodology to a two-site system with unequal populations. Although examples of magnetization transfer experiments on three sites can be found in the literature, the technique was both time-consuming and awkward for systems with more than two sites.

Improvements in the design of magnetization transfer experiments for chemical

exchange have been developed as more powerful numerical analysis methods and faster computers have become more accessible. The original approach of Forsén and Hoffmann applied simplifying approximations to the fundamental chemical exchange equations that permitted one to obtain the rate information from a straight line, given by a semi-log plot.[13,87] Led and Gesmar[18] proposed a more rigorous approach that corrected for the simplifying assumptions and used a non-linear least-squares program to fit the data. In 1986, they generalized this approach for *n* sites.[88]

The study of the dynamics in organometallic complexes has to a large extent prompted improvements to the methodology. Many organometallic systems have numerous sites, thus an efficient experiment is required. In addition, many of these systems have more than one possible exchange process and information about the mechanism is also desirable. The methods of both Grassi *et al.*[25] and McClung *et al.*[19] allow one to fit the data to different mechanistic pathways. This has the effect of incorporating a probe for mechanistic information. The work presented in this thesis proposes a more efficient experiment for multi-site and multi-exchange systems in that all of the exchange rate information is obtained in a single experiment.

The McClung approach was adapted for this experiment for two reasons. The manner in which it probes for the mechanism is more sophisticated and, more importantly, it fits the initial magnetization intensity. This was originally incorporated to correct for imperfect selective excitation but it also allows one to create any initial magnetization for each site, as opposed to only $(+)M_\infty$ or $(-)M_\infty$, as in the previous

approaches.

The single experiment allows one to create a set of initial magnetizations that would create sufficient excitation from at least one site to probe each exchange process. If this is done properly, one would only need a single experiment to obtain the rate information. With modern pulse methods virtually any initial non-equilibrium state can be produced. One needs an optimal set that will give sufficient information about each of the exchange processes of interest. The determination of an optimal set goes beyond the field of NMR investigations of chemical exchange as the need to find optimal conditions occurs any time there is freedom to choose the experimental parameters.[11] This set can be found by use of the criterion developed here.

The dynamics of the localized carbonyl scrambling in $Ru_2(CO)_6(\mu\text{-}PPh_2)(\mu_2\text{-}\eta^1\text{:}\eta^2\text{-}C{\equiv}C\text{-}i\text{-}Pr)$ was examined as a test case. This is an ideal system as there are six sites and three exchange rates, and particularly accurate rate data is required for mechanism elucidation. The scrambling of the carbonyl ligands on either metal atom can be explained with a simple rotary motion or three successive pairwise motions (Figure 1.5): both of which involve three separate rate mechanisms. These two mechanisms are qualitatively indistinguishable. One would expect, however, that all three rates would be equal in the rotary motion, and not in the successive pairwise mechanism. To distinguish between these two mechanisms, exceptionally accurate rate data is required. The theory and experimental approach for the generalization of a single magnetization transfer experiment for multi-site and multi-exchange systems is given along with the experimental results for

the tripodal carbonyl rotation in $Ru_2(CO)_6(\mu\text{-}PPh_2)(\mu_2\text{-}\eta^1\text{:}\eta^2\text{-}C{\equiv}C\text{-}i\text{-}Pr)$.

2.2 Theory of Magnetization Transfer

Conceptually, one can understand the theory of magnetization transfer by examining an energy diagram for the chemical exchange process (Figure 2.1).[5] In this process site A is slowly interconverting to site X with a rate constant of k_a, while the reverse of that reaction is occurring with rate k_x. At equilibrium, each species has a Boltzmann distribution in its spin state and there will be separate equilibria for both the upper and lower spin levels. Since the process is undergoing slow exchange on the NMR time-scale, two resonance signals, one for A and one for X, are observed each with an intensity that is proportional to the difference in spin population between the upper and lower levels.

In the selective inversion experiment, a 180° pulse is applied to site A. This inverts the population of the upper and the lower spin levels of site A. At t=0, a negative peak of near equilibrium intensity results at site A, and a positive peak results at site X of equilibrium intensity. The upper level of site A will experience an increase in population, while the lower will experience a decrease. The system will attempt to regain equilibrium by transferring population *via* the chemical exchange and relaxation processes. The chemical exchange process moves the population laterally across both the upper and lower levels with a rate of k_x and k_a respectively, while the spin-lattice relaxation of A

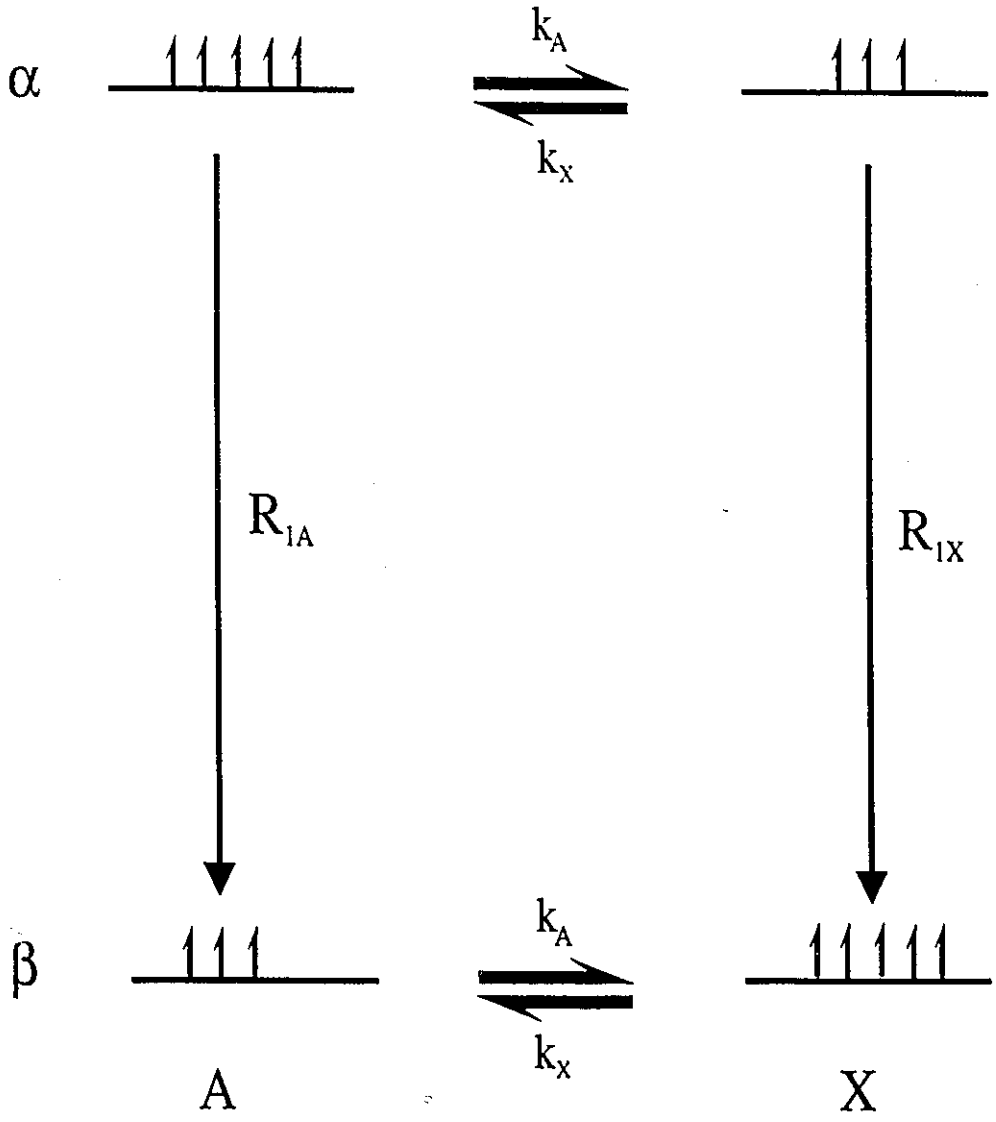

Figure 2.1 Energy diagram for a two-site chemical exchange process. The effect of selective inversion at site A is shown. The excess population in the upper level of A will recover back to equilibrium *via* both the spin-lattice relaxation and exchange rate.

and X, with a rate of R_{1a} and R_{1x}, returns the upper population to its respective lower level.[5]

This leads to a competition between the chemical exchange and the relaxation processes. If the relaxation is significantly more rapid than the exchange, the population differences between the upper and lower states of the selectively inverted peak rapidly regain equilibrium before the chemical exchange transient can be observed. If the exchange is much faster than the relaxation, exchange broadening is normally observed in the signals and that leads to increased error in the rate determination. The ideal situation occurs when the two rates are comparable with the exchange rate being slightly larger than the relaxation rates.[5] This translates into exchange rates that fall into the range of 10^{-2} to 10^{2} s^{-1} for protons. Other nuclei with significantly shorter, or longer T_1 values will have different ranges.

The ^{13}C NMR signals of the carbonyl ligands were used to probe all of the exchange processes presented in this thesis. The T_1 values of metal carbonyls have a large component that is caused by chemical shielding anisotropy (CSA) relaxation.[89-91] This relaxation mechanism is field dependent with the relaxation increasing as the square of the field.[1,92] While optimal resolution of the signals is desirable, the requirement of a slightly lower relaxation rate than the chemical exchange rate often forces the use of intermediate field strengths with metal carbonyl complexes. A 300 MHz NMR instrument was used for the bulk of this work and the measured exchange rates ranged from 33 to 0.085 s^{-1}.

2.3 Numerical Analysis

The McConnell,[15,16] or Gutowsky and Holm[17] equations were the first to describe the time dependence of the magnetization under the condition of chemical exchange and are based on the Bloch equations.[1] The manner in which these equations are formulated, and are solved differentiate between the dynamic NMR methods and between the various approaches for 1D magnetization transfer. One can conveniently group the 1D magnetization transfer approaches by formulation. The groups of Forsén and Hoffmann, and of Led and Gesmar formulate the equations similarly, with no attempt to incorporate mechanistic constraints. The Grassi *et al.* and McClung *et al.* methods use an exponential matrix formulation and both incorporate a strategy for mechanistic determination. The approaches of Forsén and Hoffmann combined with that of Led and Gesmar will be discussed briefly, and then those of Grassi *et al.* and of McClung *et al.*, will be presented with the emphasis being placed on the latter as this was the method chosen for this work.

2.3.1 The Approach of Forsén and Hoffmann[12,13,93] and Led and Gesmar[18,88]

In the Forsén and Hoffmann approach, they made simplifying assumptions that, in a two site case, both relaxation rates were equal and that there was perfect saturation at one site. A plot of log $(M_{zA}(t)-M_{zA}(\infty))$ versus time is linear (where A is the unsaturated site) and this allowed determination of the relaxation exchange rates from the resulting slope and intercept.

Led and Gesmar noted that the assumption that the relaxation rates are equal will

not hold for all cases, and the second assumption that perfect selective saturation or inversion is generated will never occur. They resolved the problem by formulating the equations with additional variables and then obtaining extra data to solve these variables independently. The extra data are obtained through complementary experiments in which each signal is successively inverted, and the magnetization intensities of both sites are measured for each inversion. In a two-site system, one can then obtain four independent equations for the four unknowns (k_a, k_x, R_{1a}, R_{1x}).

A non-linear least-squares fitting program was used to extract the rate parameters. However, the fundamental equations are expressed with variables that are complicated with respect to the relaxation and exchange rates and no mechanistic information can be obtained with this approach. The technique can be adapted for *n* sites but complementary data must be collected for each site to solve for all the variables. This becomes excessively time-consuming as *n* increases.

2.3.2 The Approaches of Grassi *et al.*[25] and McClung *et al.*[19]

In these two approaches the time dependence of the z magnetizations undergoing chemical exchange is described by the following differential equation:

$$\frac{d[M - M(\infty)]}{dt} = A[M - M(\infty)] \qquad 2.1$$

The manner in which the matrix **A** is defined distinguishes the two approaches. The matrix is defined in the following manner by Grassi *et al.*:

$$A_{ij} = \begin{cases} k_{ji} & i \neq j, \\ -\sum_{l=i}^{n} k_{il} - \frac{1}{T_{1i}} & i = j, \end{cases} \qquad 2.2$$

The rate constants, k_{ji}, represent all of the rates for which magnetization is transferred from site j to site i, and in complex multi-site exchange that may occur through more than one mechanism. In the method of Grassi *et al.*, one can place constraints on the individual rate elements (k_{ji}) and on the relaxation rates (T_{1i}^{-1}). These constraints allow one to fix some elements as constants. However, some exchange mechanisms impose certain relationships between rate elements and these relationships cannot be indicated.

In the method developed by McClung, the actual exchange pathways for each of the potential exchange mechanisms (α_i) are incorporated in the matrix formulation of **A**.

$$A_{ij} = \begin{cases} \sum_{\alpha} K^{\alpha} \prod_{ji}^{\alpha} & i \neq j, \\ -\frac{1}{T_{1i}} - \sum_{\alpha} \sum_{l=i}^{n} K^{\alpha} \prod_{il}^{\alpha} & i = j, \end{cases} \qquad 2.3$$

K^{α} is the rate constant for a particular rate mechanism as opposed to that from one site to another and Π^{α} is the matrix of exchange coefficients that describes the α exchange mechanism. Thus, the product of the rate constant and the exchange coefficients connects the site to site magnetization transfer caused by exchange. The Π matrices describing the tripodal carbonyl rotation are given in Figure 2.2.

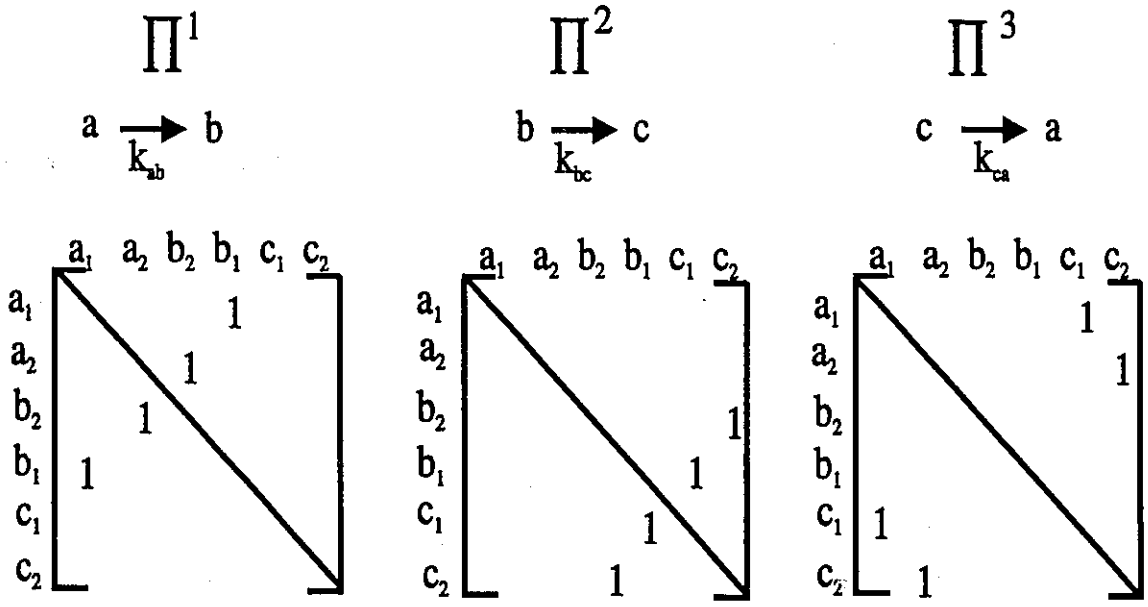

Figure 2.2 Π exchange matrices for carbonyl tripodal rotation. The first matrix takes carbonyl ligand a into b, the second takes b into c and the third takes c into a. All three matrices were entered to determine each rate individually, or one matrix encompassing all three rotations may be entered to determine a single rate.

It should be noted that the cross-relaxation terms caused by nuclear Overhauser effects from dipolar relaxation have not been included. In most exchange work they are ignored as the cross-relaxation term is usually negligible in comparison to the rate constant in the regime that one can normally study and this is especially so with spin-dilute nuclei (i.e. natural abundance to 30% enriched ^{13}C compounds).[11,14,29]

The non-linear least-squares program (SIFIT), developed by McClung[19] uses a adapted Marquardt algorithim and allows the following parameters to vary: k^{α}, $1/T_{1i}$, as well as the equilibrium and the initial magnetizations. The magnetization intensities at these points were not varied in the Mann approach. It is important to fit both the equilibrium and initial magnetization as there is as much error in these points as there is at any other variable delay time.[19] In fact, it is impossible to measure at exactly t=0 and as a result there will always be more error in M(0).

2.4 The Generalized Single Selective Inversion Experiment

The ability to fit the initial magnetization is an important feature for developing a single experiment for selective inversion in multi-site systems. The fact that McClung's program fits M(0) permits one to generate any initial magnetization state, instead of creating an initial state in which one site is perturbed from equilibrium (inverted peak) and the others are not (positive peaks). In a generalized single site experiment all of the sites will need to be perturbed from equilibrium to some extent and the exact value of each requires fitting.

2.4.1 Experimental Design

The pulse sequence used for the single selective inversion experiment is simple with just two pulses separated by a delay:

90° - τ - 90° - VD - 90° - FID(acquire)

A selective 180° pulse can be generated by more than one method. The most common is the DANTE (Delays Alternating with Nutations for Tailored Excitation)[95] pulse sequence. This consists of a series of short pulses separated with a delay of about a millisecond. If the pulses are on resonance the effect will be additive; that is *n* pulses each with a tip angle of ϕ add together to give a total pulse of angle *n*ϕ, for site A and no other site. Unfortunately, *n* must be at least 30. This can be quite time-consuming and small errors in ϕ will sum to give larger errors. Consequently, other pulse sequences are sometimes used.[1,6,96] The advantage of the DANTE sequence is that it generally allows for more selective excitation. In this work, rigorous selective excitation is not required since it is desirable to have all of the sites excited to some extent as with the 2D-EXSY experiment. This pulse sequence is more robust because there are only two pulses, and most importantly it allows the flexibility required to allow the design of the single generalized selective inversion experiment for multi-site and multi-exchange systems.[11] There are two experimental variables, the transmitter offset (O1) that defines ν_o, and the delay time, τ, both of which can be varied independently to define a whole family of

initial magnetizations, $M(0)_i$, given by equation 2.4. Figure 2.3 is an example of a typical excitation showing the difference in initial magnetization between sites.

$$M(0)_i = -M(\infty)_i \cos(2\pi\omega_i\tau) \qquad 2.4$$

where $\omega_i = (\nu_i - \nu_o)$

A variable time delay (VD) is incorporated after the last 90° pulse to follow the effects of the relaxation and the chemical exchange processes as they evolve with time. The magnetization is acquired and then a relaxation delay of five times T_1 is allowed to ensure that the magnetization intensity reaches its equilibrium value before the next scan.

Peak Intensity Measurement

It is crucial that one can obtain the peak intensity measurements as accurately as possible within a reasonable length of time. Thus both the acquisition parameters and the method of data processing are important in minimizing the error. There are four potential sources of error: 1) instrumental noise, 2) digitization error, 3) truncation error, and 4) phase error.[97-99]

Of the four errors only instrumental noise does not affect the accuracy, only the precision as the noise is assumed to be random and unbiased. With these assumptions, one cannot predict the noise at any one point given the value of the noise at any other point and the noise will average to zero over long time.

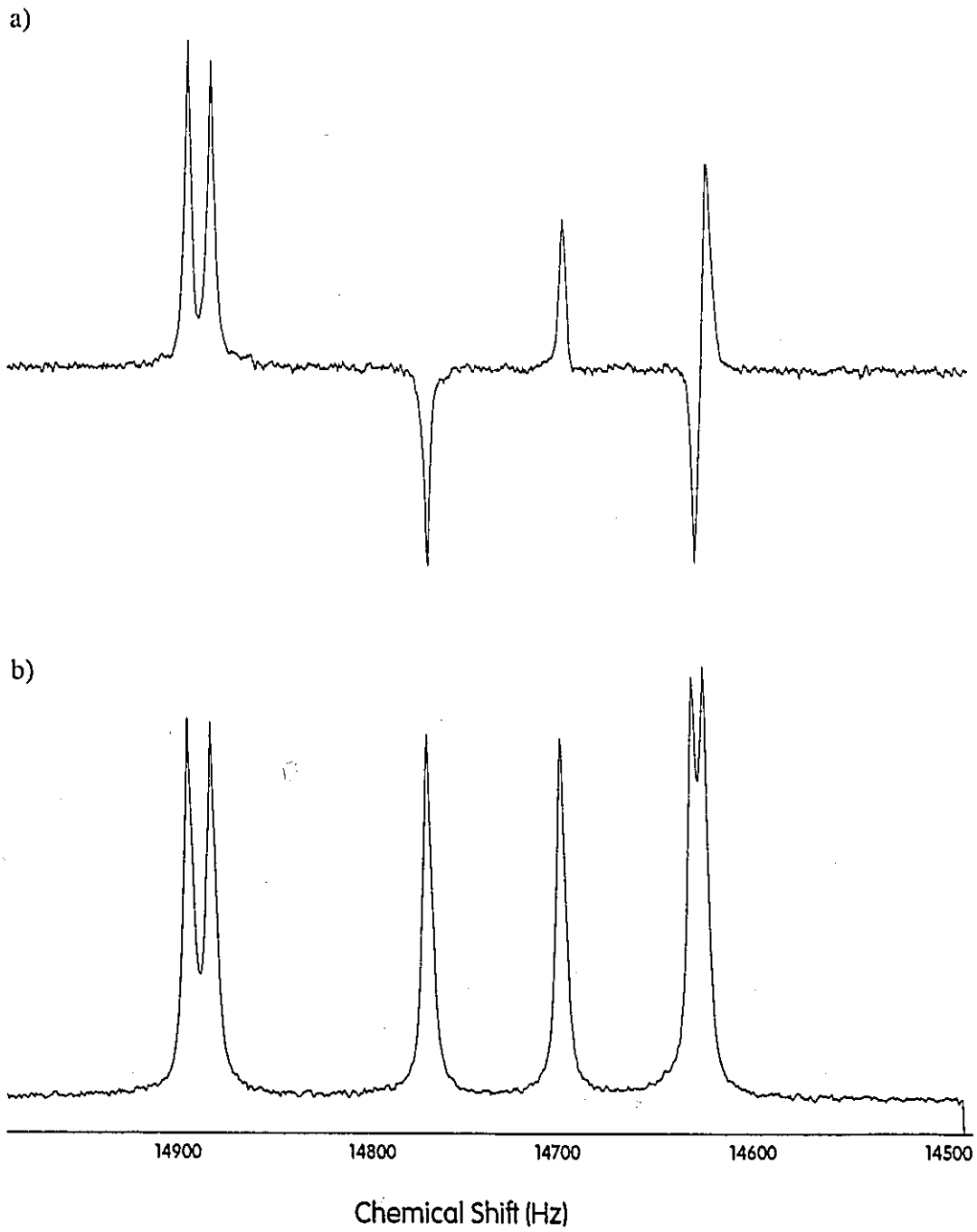

Figure 2.3 Typical single selective inversion excitation. a) ^{13}C spectrum of the initial magnetization b) ^{13}C spectrum of the equilibrium magnetization

With Fourier transform techniques, digitization error occurs directly as a result of measuring the peak intensity at discrete uniformly spaced frequencies as opposed to continuously over the whole frequency range of the peak. This also results in truncation error since the whole frequency range ($+\infty$ to $-\infty$) is not sampled and the ends are clipped. Phase errors, as their name implies, occur if the peaks are phased incorrectly and can cause distortion in the baseline.[97-99]

There are several techniques with which one can overcome these errors. Peak heights are considered more reliable than peak integrals when the peaks involved are not excessively line broadened. Normally with measurements on systems in the slow regime as in T_1 experiments, peak height measurements are preferred.[4,100,101] Truncation error is not as important with peak height measurements as only the maximum point is measured and not the whole peak as with integrals. Baseline distortion is more severe with an integral measurement, since a non-zero baseline will cause slope and curvature of the integral which means that the value of the integral depends strongly on the choice of the endpoints. With peak heights the baseline simply adds or subtracts a constant from the intensity.[100,101]

Digitization error is a considerable factor with either measurement and can cause large biases.[97-99] This can be minimized by acquiring the spectra with a large number of points. The instrumental noise error is potentially more of a factor with peak heights since one is measuring one point (the maximum) as opposed a range of points in which the error has a greater opportunity to cancel. However, this is negated to a large extent as the

point that is being measured is the maximum point so the relative error caused by instrument noise should be at its lowest and as one increases the number of scans, the noise becomes more unbiased. Zero filling also helps to reduce instrumental noise error.[96]

In any case, the errors of any one individual magnetization measurement are minimized as the data analysis is normally accomplished with a nonlinear least-squares fitting routine that calculates the best fit based on all of the data points. As long as enough data points are measured in the exchange regime, one poor data point will not severely affect the result.

2.4.2 Optimization of the Initial Conditions[11]

Equation 2.3 demonstrates that all the sites are coupled by the exchange-relaxation matrix with the off-diagonal terms containing the rate constants and the diagonal terms containing the sum of the relaxation and rate constants. The exchange-relaxation processes are dependent on the initial state, M(0), as evident from equation 2.1, or more specifically the difference between the equilibrium and initial state. However, it is possible to control the initial magnetization through experimental design and thus the exchange and relaxation at any given site will depend on the initial states of *all* the other sites in the system. In principle, any experiment that probes any one of the parameters should give information on all the others. In practice, the amount by which one can accurately measure small differences in magnetization intensity limits the extent to which poorly designed experiments allow determination of the rates. This necessitates that initial

conditions are chosen that will produce an exchange-matrix with strong off-diagonal contributions. This occurs when the difference in initial magnetization states between exchanging sites is maximized.

Pictorially, this can be understood by examining the two-site energy diagram in Figure 2-1.[5] A T_1 experiment inverts the populations of the upper and lower states in both sites. The population difference between site A and site X in both the upper and lower states is zero and thus the probability of the exchange pathway providing a means of returning to equilibrium is nil, unless the difference between R_{1A} and R_{1X} is excessively large, in which case eventually there will be some difference between the two sites. Equilibrium will instead be regained *via* the spin-lattice relaxation pathway. In the selective inversion experiment, only one site inverts the population between the upper and lower states and this maximizes the difference in populations between site A and site X in both the upper and lower levels, which maximizes the probability of the equilibrium being regained through the exchange pathway ahead of the relaxation pathway.

2.4.3 The Partial Derivative Criterion[102]

Mathematically, the dependence of the initial conditions on the rate process can be determined from the partial derivatives of the magnetizations with the respect to the particular rate coefficient (dM_i/dk^{α}).[11,100,102] When these partial derivatives are large for the sites involved in a particular exchange mechanism, it indicates that the set of initial conditions from which that partial derivative arose is sensitive to that rate process. This

contribution can be quantified and demonstrated mathematically.[102]

The general calculation of the partial derivatives of the magnetizations in equation 2.1 with respect to all the parameters is complicated, since both the eigenvalues and eigenvectors are functions of the parameters.[19] For simple two-site and three-site problems, the relaxation-exchange matrix can be diagonalized algebraically, so the functional forms can be determined. These provide useful prototypes for more complex systems.[102]

The simplest case is a two-site exchange in which both sites are equally populated case and have the same relaxation rate. If r is the relaxation rate and k is the exchange rate between the two sites then the specific form of the equation is

$$\frac{\partial}{\partial t}\begin{bmatrix} M_1(\infty) - M_1(t) \\ M_2(\infty) - M_2(t) \end{bmatrix} = -\begin{bmatrix} r+k & -k \\ -k & r+k \end{bmatrix}\begin{bmatrix} M_1(\infty) - M_1(t) \\ M_2(\infty) - M_2(t) \end{bmatrix} \qquad 2.5$$

The time dependence of magnetization intensity of site one is given in equation 2.6 from 2.5,

$$\begin{aligned} M_1(\infty) - M_1(t) = {} & \frac{1}{2}\left[e^{-(r+2k)t} + e^{-rt}\right]\left[M_1(\infty) - M_1(0)\right] \\ & + \frac{1}{2}\left[-e^{-(r+2k)t} + e^{-rt}\right]\left[M_2(\infty) - M_2(0)\right] \end{aligned} \qquad 2.6$$

This shows the familiar behaviour of a two-site system. If both sites are perturbed equally, the system relaxes with the spin-lattice relaxation rate, r. If M_1 is selectively inverted, it relaxes using both spin relaxation and exchange.

From the point of view of experimental design, the object is to measure the exchange rate with the greatest precision. This occurs when the parameters maximize the partial derivative of M_1 with respect to k. The solution for the partial derivatives with respect to k is given by equation 2.7 from 2.6.

$$\frac{\partial}{\partial k}[M_1(\infty) - M_1(t)] = -t\,e^{-(r+2k)t}\,[M_1(\infty) - M_1(0)] + t\,e^{-(r+2k)t}\,[M_2(\infty) - M_2(0)] \qquad 2.7$$

Examination of equation 2.7 reveals some important points. As expected the partial derivative is at a maximum if the magnetization of one site is completely inverted and the other site is not perturbed. Secondly, it does not matter which site is inverted. Thirdly, a non-selective inversion will give data that do not depend on the exchange rate, k. The partial derivative with respect to the rate vanishes under the assumption of equal relaxation rates. Large differences in the relaxation rates must be present in order for the partial derivative to be appreciable. Finally, when the partial derivative is varied as a function of time, a maximum occurs at t=1/(r+2k). This is characteristic of exponential decay, and was observed previously in the inversion-recovery T_1 experiment. The three sites equally populated case also demonstrated that a selective inversion of one of the sites allowed an excellent measurement for the exchange rate. This approach was also extended for unequal populations in the two-site case. The situation is more complex because now there are two rates to consider: the forward rate coefficient, k_f, that takes site 1 into site 2, and the corresponding reverse rate coefficient, k_r. The results showed for a

case where the ratio of the populations was arbitrarily set to four, and the slower exchange rate is three times the relaxation rate. Of course, the principle of detailed balance requires that the equilibrium magnetizations be in the same ratio as the forward and reverse rate constants i.e. $M_1/M_2=k_r/k_f$.

Analytically solving for the partial derivative allows the following conclusions.[102] As with the non-selective T_1 experiment, the sensitivity of the experiment with respect to the rate is at a maximum in time at the reciprocal of the rate (a combination of k_f, k_r and r), and this maximum is very broad. Thus, the choice of sampling times is not crucial. The data are more sensitive to the forward rate, as it is four times larger than the reverse. Figure 2.4 shows the difference upon inverting the major and minor sites. Both figures show a broad maximum in the curve, but the curve (Figure 2.4a) in which the minor peak is inverted shows a low sensitivity to the reverse rate. Inversion of the minor site will only perturb the major site minimally. The act of inverting the major site, on the other hand, shows relatively large sensitivities to both rate coefficients. The magnitude of the partial derivatives demonstrates that the optimal experiment would be inversion of the major site, and to follow the CET in the minor site.

The analytical solutions derived for two and three site cases clearly demonstrate that the optimal result can be obtained if one searches for a maximum in the partial derivative of the magnetization with respect to the rate of interest. In general, the maximum in the partial derivative curve with time is broad so the choice of variable delay times is not crucial.

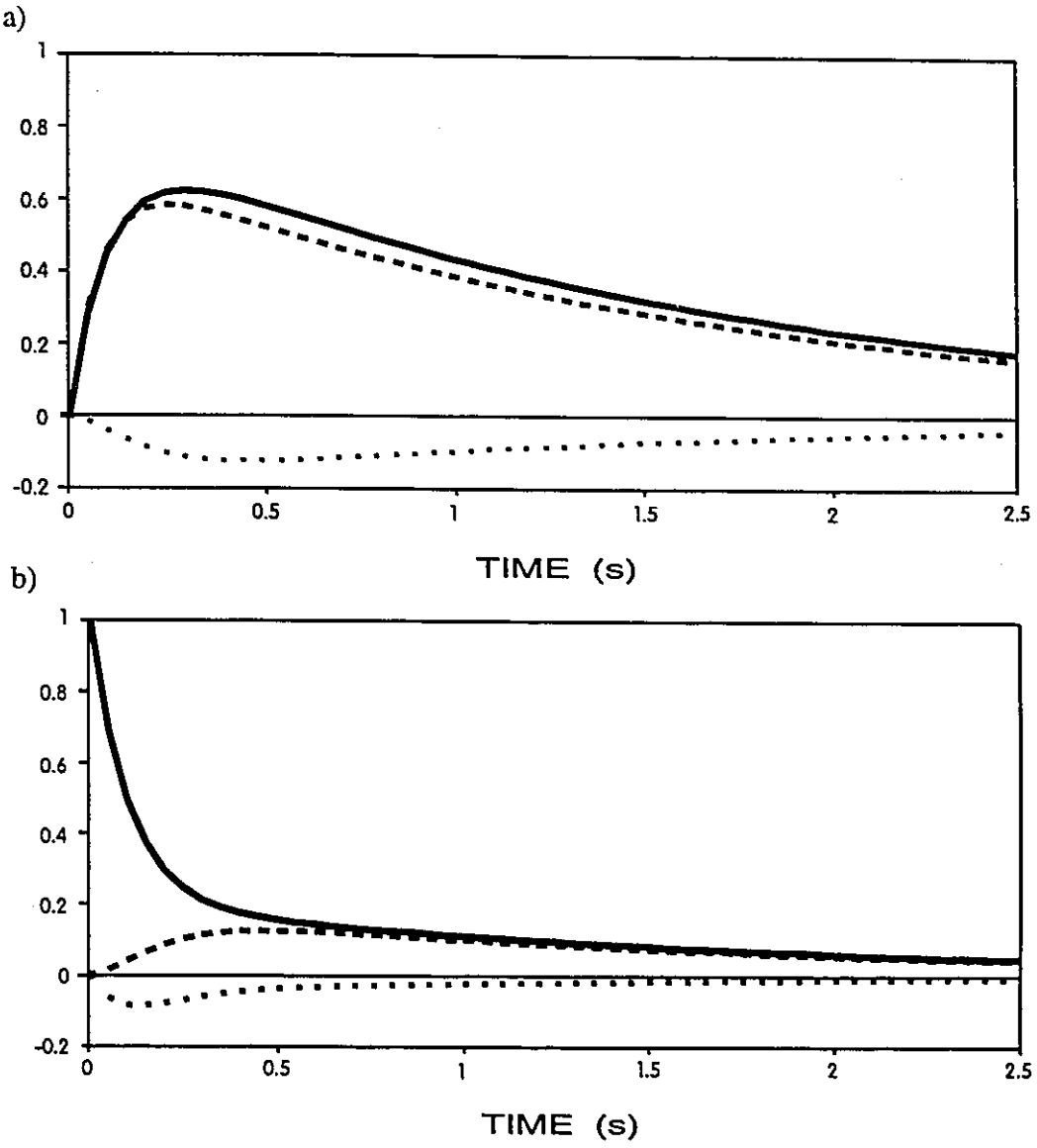

Figure 2.4 Plot of magnetization intensity and partial derivatives as a function of time in a two-site unequal population case. a) Inversion of the minor site (1), $M_1(eq.) - M_1(0) = 1$ and $M_2(eq.) - M_2(0) = 0$ b) Inversion of the major site (2), $M_1(eq.) - M_1(0) = 0$ and $M_2(eq.) - M_2(0) = 4$. In both plots the relaxation rate, $r = 0.3$, $k_f = 3.6$ and $k_r = 0.9$. The plot of the magnetization of the minor site (1) is given by the solid line and the other two lines are represent the partial derivatives with respect to k_r (positive dashed line) and to k_f (negative dotted line).

The partial derivatives as a function of time with respect to all the parameters are difficult to solve analytically for multi-site exchanges since both the eigenvalues and eigenvectors are functions of the parameters. A numerical solution for the partial derivatives with respect to all the parameters has been published and is incorporated into the SIFIT program. An additional program was written to extract these values from the program. The partial derivatives that are of interest are those with respect to the rates (dM_i/dk^α). The partial derivatives themselves are functions of the experimental variables (τ, and O1) that determine the initial state. In the test system, $Ru_2(CO)_6(\mu\text{-}PPh_2)(\mu_2\text{-}\eta^1\text{:}\eta^2\text{-}C{\equiv}C\text{-}i\text{-}Pr)$, there are six sites and three possible rates, therefore there are eighteen partial derivatives of interest. A contour map of each partial derivative as a function of these two variables can be constructed. Figure 2.5 is an example of a typical plot.[11] A peak on the contour plot implies that the partial derivative is large and therefore, the corresponding transmitter offset and delay time is sensitive to that particular rate process (for that particular site). The transmitter offset and delay must be chosen such that there is at least one site that is sensitive each rate process in a single experiment. Examination of the contour plot shows that there are many sets of initial conditions that give comparable values for the partial derivatives but there are distinct time delay values that are poor. Furthermore, there are additional contributions to the errors in the experiment, other than uncorrelated random errors. As a result, the partial derivative map does not provide a complete picture. In the simple T_1 experiment, the partial derivatives did not give a perfect correlation with the observed errors. However, the partial derivative criterion is

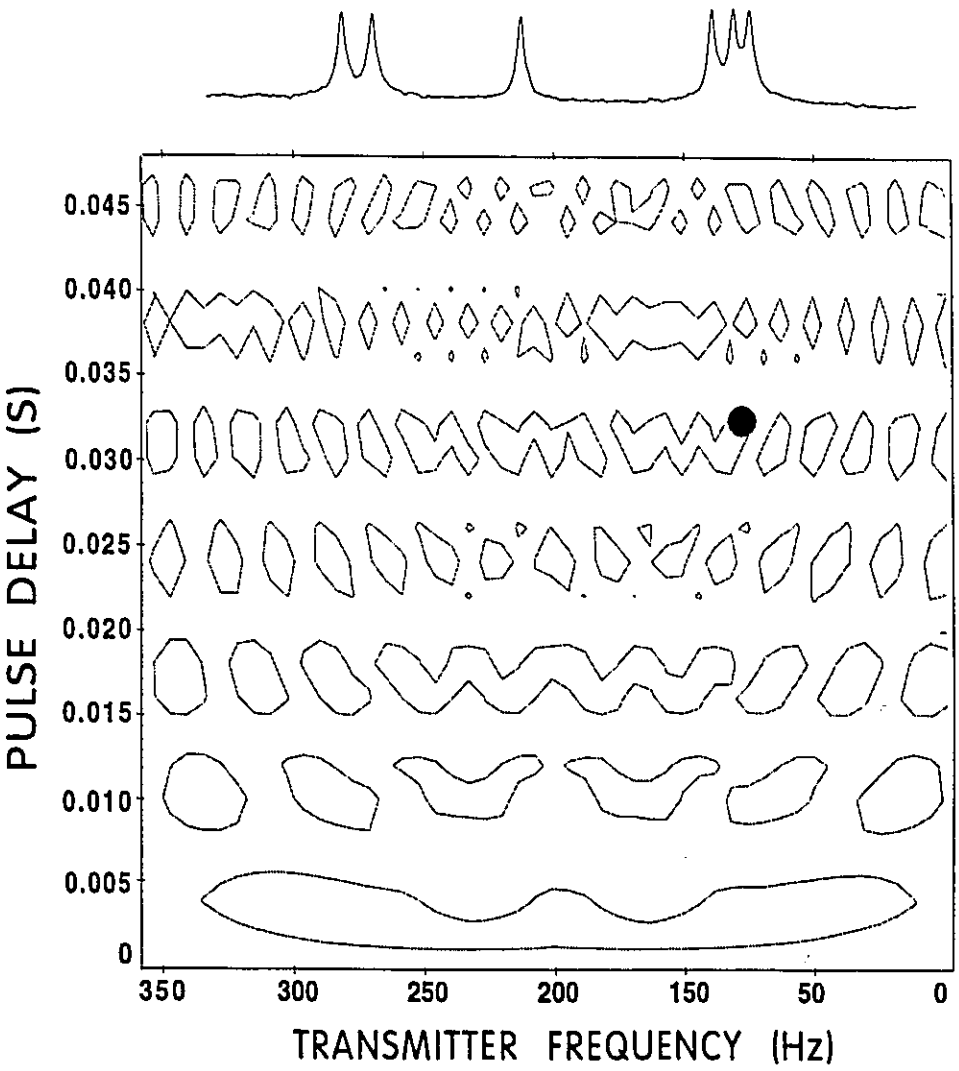

Figure 2.5 Typical contour plot of the partial derivative of the magnetization intensity (c2) with respect to the rate (b to c) for $Ru_2(CO)_6(\mu\text{–}PPh_2)(\mu_2\text{-}\eta^1\text{:}\eta^2\text{-}CC\text{-}t\text{-}Bu)$. The frequency scale in the contour plot matches that of the spectrum on top. The black dot indicates the values used in actual measurements.

a useful qualitative guide to designing a sensitive experiment. The partial derivatives with respect to the rate are, of course, dependent on the rate so one must have reasonable estimates of the rate coefficients to obtain reliable partial derivatives. However, this is true for any dynamic NMR experiment. Often, as in this work, the rate coefficients were estimated from preliminary results. However, in some regions the contours are broad and so the design of the experiment is tolerant to some error in the partial derivatives. The optimal choice of parameters lies in the region with a broad high contour of the partial derivative.[11]

Calculation of the initial magnetizations as a function of the transmitter offset and time delay is possible *via* equation 2.4, and this can be used as an alternative method to determine the initial conditions (transmitter offset and delay time). One conclusion from the explicit calculations of the partial derivatives for two and three sites, is that if at least one site is inverted with respect to another site, defined by each particular exchange process, then acceptable measurements for all of the rates are possible. In this method, the initial parameters (the offset and time delay) are varied until acceptable initial magnetizations are found. One clear advantage of calculating the theoretical values of the initial magnetization is that it provides verification that the experimental spectrometer conditions have been set correctly. The pulse sequence is quite robust, but it is possible to set the pulse width and relaxation delay incorrectly.

2.5 Experimental Section

2.5.1 Preparation of the NMR Samples

Approximately 0.2 g of $Ru_2(CO)_6(\mu\text{-}PPh_2)(\mu_2\text{-}\eta^1\text{:}\eta^2\text{-}C{\equiv}Pr^i)$, **1**, (approximately 30% ^{13}CO labelled) was dissolved in 1 mL of deuterated chloroform-*d* (MSD Isotopes, 99.8% D) and placed in a 5 mm thin wall NMR tube. A stream of nitrogen gas was passed through the sample for a few minutes to deoxygenate it.

2.5.2 Temperature Control

All of experiments were performed on the Bruker AC-300 spectrometer that is equipped with a Bruker B-VT 2000 variable temperature unit. The temperature readings were measured with an external copper-constantan thermocouple (placed in an empty 5 mm NMR tube) positioned in the probe and allowed to equilibrate for 30-45 minutes. The sample was then placed into the probe and allowed to equilibrate for 15-30 minutes before data accumulation.

2.5.3 The Selective Inversion Experiments

The selective inversion experiments were recorded on a Bruker AC-300 MHz spectrometer, equipped with a quadrinuclear (^{31}P, ^{13}C, ^{1}H,and ^{19}F) 5 mm probe tuned to ^{13}C (operating frequency of 75.47 MHz).

The pulse program INVREC2P.AUR was used for both the selective inversion experiment and the separate T_1 experiment. The pulse sequence for this program is as

follows: D1 - 90° - D2 - 90° - VD -90° (acquire). The values for the pulse sequence parameters that varied with experiment are found in Table 2.1. The parameter D1 is the relaxation delay to ensure that the magnetization intensity is back to its equilibrium value before the next scan is acquired and should be set to $5xT_1$. The D2 delay is τ, one of the initial conditions that can be varied to achieve selective excitation.

For all of the experiments D1 was set to 15 seconds. The Fourier transform size (SI) and acquisition size (TD) were set to 2K. The spectral width was set to 976 Hz. This gave a acquisition time of 1.05 seconds with a digital resolution of 0.95 Hz/pt. The number of scans was 64 for the first experiment and 32 for the other two experiments. All experiments were performed at a temperature of 300K.

A ^{13}C spin-lattice relaxation experiment was also done. The τ (or D2) value for the T_1 was set to 0.00001 s. The magnetization intensities as a function of the variable delays for each site were entered into non-linear least-squares program for T_1 determination (T1CALS). The calculated values for each of the sites are as follows 1.05, 1.06, 1.07, 1.07, 1.26, and 1.25. The ^{31}P spin-lattice relaxation rate was measured at T=300 K and was found to be 0.32 s^{-1}.

The selective inversion data were analyzed by use of FLOPSI (a modified C version of SIFIT [19]). The ^{13}C spin-lattice relaxation time was fixed to the measured values while all other parameters were allowed to vary.

Table 2.1 Parameters for the Carbonyl Rotation Selective Inversion Experiments

Offset Frequency (O1) Hz	Time Delay (τ) seconds	Variable Delays (VD) seconds
14651.3	0.033	0.001, 15.0, 0.5, 0.1, 1.0, 0.25, 0.75, 0.15, 2.0, 0.4, 0.05, 0.35, 0.6, 3.0, 0.4, 0.8, 0.075, 0.175, 0.45, 0.9, 0.3, 1.5, 1.1, 0.2
14907.7	0.033	0.001, 15.0, 0.5, 0.1, 1.0, 0.25, 0.75, 0.15, 2.0, 0.4, 0.05, 0.35, 0.6, 3.0, 0.4, 0.8, 0.075, 0.175, 0.45, 0.9, 0.3, 1.5, 1.1, 0.2
14651.3	0.020	0.001, 15.0, 0.5, 0.1, 1.0, 0.25, 0.75, 0.15, 2.0, 0.4, 0.05, 0.35, 0.6, 3.0, 0.4, 0.8, 0.075, 0.175, 0.45, 0.9, 0.3, 1.5, 1.1, 0.2

2.6 Results and Discussion

At low temperature, there are twelve sites for the carbonyl ligands in $Ru_2(CO)_6(\mu$-$PPh_2)(\mu_2$-η^1:η^2-C≡C-*i*-Pr). All six carbonyl groups are distinct as the acetylide ligand is fixed in one orientation and each CO ligand shows a coupling to ^{31}P in the bridging phosphido ligand. At higher temperatures, the acetylide ligand undergoes motion similar to a "windshield wiper" (Figure 1.6) that creates a plane of symmetry between the two metal atoms resulting in only three distinct CO ligands and therefore six sites with the ^{31}P coupling. The carbonyl rotation begins around -10 °C at which temperature the acetylide ligand is in fast exchange and can be neglected. A spectrum demonstrating these features is found in Figure 2.6.

Three separate exchange matrices (Figure 2.2) were entered into SIFIT and this enabled the measurement of the individual rates for each of the individual carbonyl exchanges (a→b, b→c, c→a). Since there is more than one possible set of initial conditions that give acceptable data, a selective inversion experiment was performed for three different sets of initial conditions at the same temperature (room temperature) to determine if the initial excitation produced a bias. The calculated rates for the individual rate processes for the carbonyl rotation are shown in Table 2.2.

Each exchange process has 4 NMR signals that are involved in the exchange mechanism. In the first two sets of initial conditions, there is at least one site that is excited with respect to each exchange process, whereas in the latter set, the a → b process was not probed. The data for that set of initial conditions would not converge until the

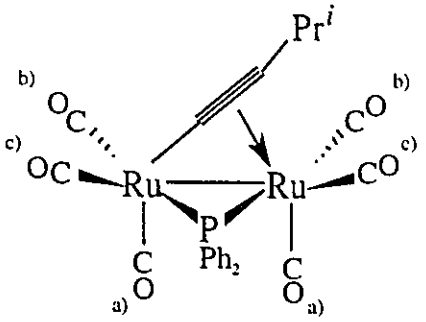

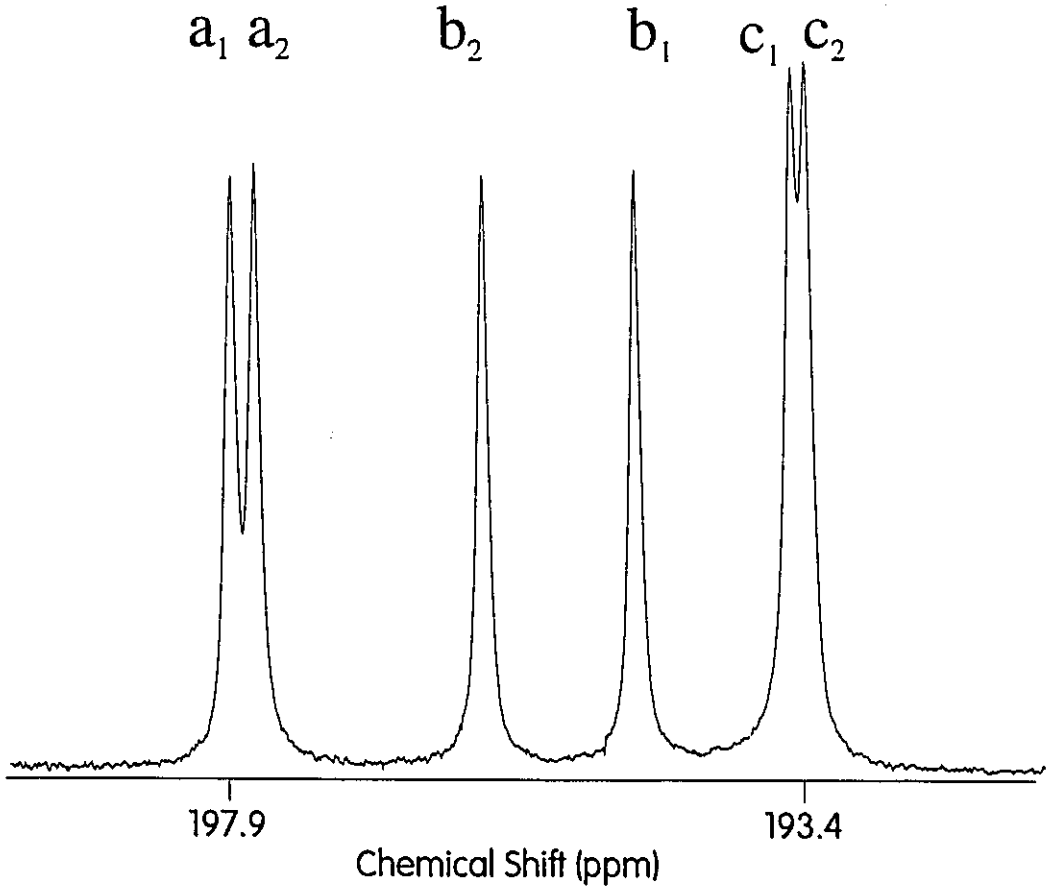

Figure 2.6 Carbonyl region ^{13}C spectrum of $Ru_2(CO)_6(\mu\text{-}PPh_2)(\mu_2\text{-}\eta^1\text{:}\ \eta^2\text{-}CC\text{-}i\text{-}Pr)$ at 300 K. The labelling scheme is shown above.

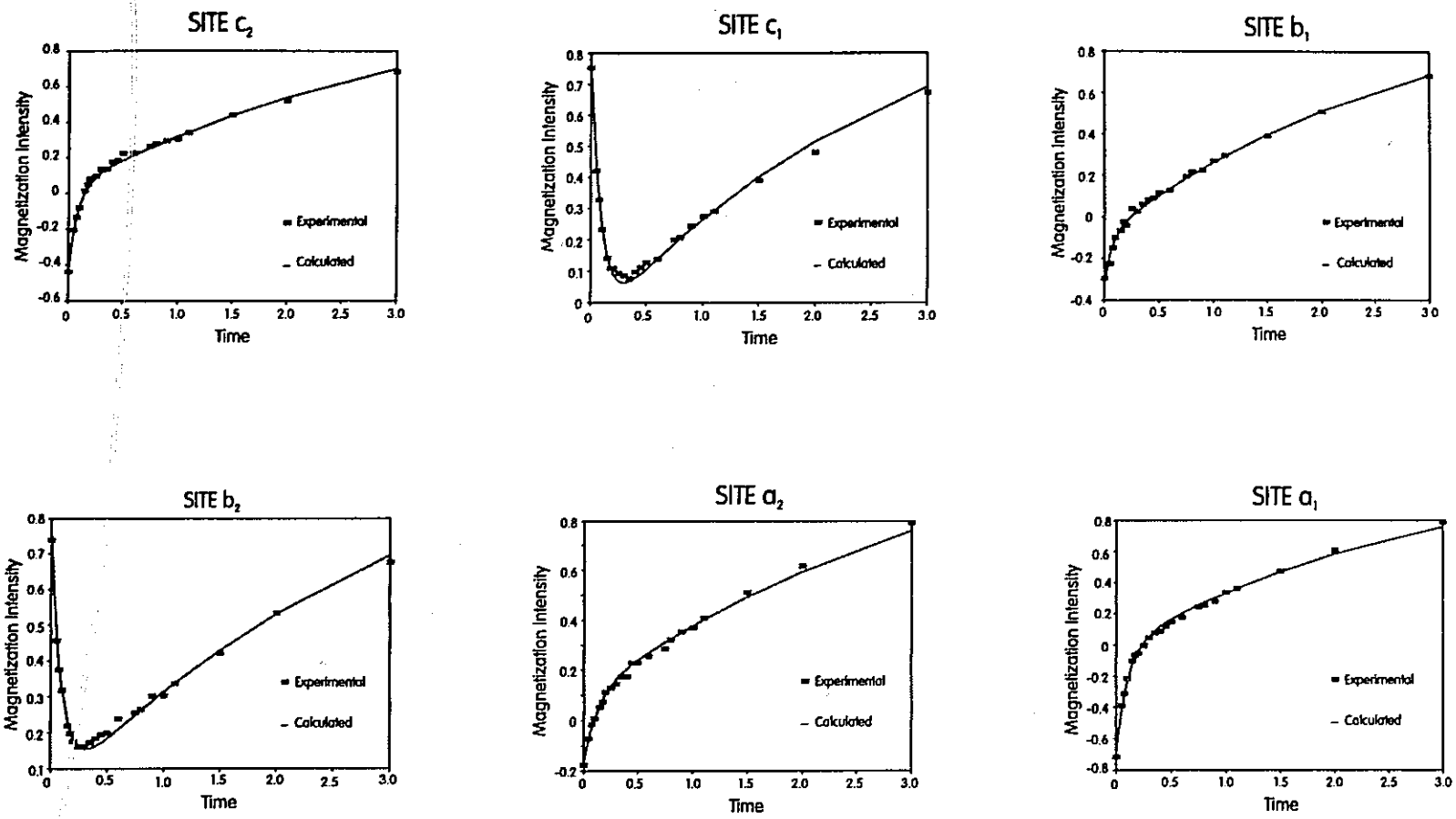

Figure 2.7 Typical plots of the calculated versus experimental selective inversion data. The data from experiment 1 at 300 K is shown.

Table 2.2 Initial Conditions and Carbonyl Ligand Exchange Rates for each Selective Inversion Experiment

Initial Conditions			Process		
Transmitter Offset (O1)	Time Delay (τ)		a $\rightarrow$ b	a $\rightarrow$ c	b $\rightarrow$ c
Site 1 (c2)	0.033	Rate k (s^{-1})	3.6	3.1	2.7
		Error ($\pm 2\sigma$)	0.4	0.4	0.5
Site 5 (a2)	0.033	Rate k (s^{-1})	3.0	4.4	5.0
		Error ($\pm 2\sigma$)	0.8	0.8	0.8
Site 1 (c2)	0.020	Rate k (s^{-1})	fixed (3.0)	3.1	3.1
		Error ($\pm 2\sigma$)	N.A.	0.9	0.9

rate for that process was fixed at 3 s^{-1}, an approximate average value from all the processes from the other two sets. When this was done, the other two values converged to 3.1 s^{-1}. These data demonstrate that there is no dependence on the selective excitation as long as all of the exchange processes are probed. The first set of data in Table 2.2 has lower errors because the spectra were obtained with twice the number of scans. Figure 2.7 shows typical agreement between the measured data and the final fit.

These data also show that the three pairwise exchange rates are equal within experimental error. While this does not entirely rule out a pairwise mechanism, it strongly suggests a concerted process. If the three pairwise processes were separate, then the three barriers must be very close in energy to produce three equivalent rates. If all the barriers are the same, then the distinction between pairwise exchange and a concerted mechanism becomes unclear.[11]

2.7 Conclusions

The single selective inversion methodology is feasible in multi-site and multi-exchanging systems through use of the partial derivative criterion. This criterion gives essential guidance in determining an acceptable set of initial conditions for the single selective inversion experiment.

The partial derivative criterion states that when the parameters maximize the partial derivative of the magnetization intensity with respect to a particular rate process, the experiment will be sensitive for that rate determination. This was proven

mathematically for two and three site systems. In a two-site, equally populated system, the maximum occurs when one site is completely inverted and the other site is not perturbed. It does not matter which site is inverted and a non-selective inversion does not give data that are dependent upon the rate of exchange. The maximum of the curve is a function of the both the relaxation rate and exchange rate, but it is quite broad and thus the choice of sampling times is not crucial. In an unequally populated two-site system, the optimal experiment is one in which the major site is inverted since this results in maximal perturbation.

Although comparable calculations are difficult mathematically for multi-sites, the conclusions that were determined from two and three site systems are applicable to multi-site systems. In general, acceptable data will be obtained if there is at least one site that is inverted with respect to another site with which it is exchanging for each rate process that is being probed. In addition the partial derivative curve is broad so the choice of sampling times is not crucial.

There can be more than one acceptable set of initial conditions. In a comparison of three acceptable initial conditions, it does not appear that a bias in the rate determination is observed as all of the rates were observed to be equal within experimental error.

The three pairwise exchange rates corresponding to the carbonyl ligand rotation in $Ru_2(CO)_6(\mu\text{-}PPh_2)(\mu_2\text{-}\eta^1\text{:}\eta^2\text{-}C{\equiv}C\text{-}i\text{-}Pr)$ at 300 K are equal within experimental error and this strongly suggest a concerted mechanism.

CHAPTER 3

COMPARISON OF DYNAMIC NMR METHODS AND ERROR ANALYSIS

Each of the dynamic NMR methods for chemical exchange rates in the slow regime has its own set of strengths and weaknesses. These factors must be considered when choosing the appropriate method for a particular experiment. Often the strengths and weaknesses in one method complement those of another and a combination of experiments is, in fact, the best experimental method.

There are certain problematic areas that are common to all dynamic NMR methods. The most severe of these is error in the temperature measurement. It is possible to calibrate the probe temperature and modern variable temperature units are extremely stable. However, there will always be some temperature gradient in the NMR tube itself, so at best the error in the temperature is approximately ± 2 K. The error in the temperature is most readily apparent in the activation parameters, as these are determined from the temperature dependence of the rate of reaction.

Another problem common to all methods is that one must have knowledge of the rate, and of the mechanism of the exchange before the data can be fully analyzed. The extent to which this is a problem is very much dependent on the NMR method.

The dynamic NMR methods in the slow exchange regime are compared with the following criterion in mind: convenience of the method both in the spectral acquisition and in the data analysis, time constraints, and errors in the obtaining the rate information. The errors in determining the activation parameters will be discussed, and then as a conclusion, a combination strategy incorporating the single 1D selective inversion methodology with both line-shape analysis and 2D-EXSY is outlined.

3.1 Line-Shape Analysis

3.1.1 Convenience

Spectral Acquisition

Acquisition of the spectrum is easiest with the line-shape method. There is virtually no set up other than that for a normal 1D spectrum. Care must be taken in obtaining the appropriate frequency range with good digitization. As with all methods, the signal to noise must be sufficiently high, but this is only potentially difficult at coalescence. At coalescence, the signal is at its broadest, and if the difference in frequencies is large, then the signal will resemble a broad smear just barely over the baseline. More scans are then required to obtain an acceptable signal to noise ratio.

Knowledge of the spin-lattice relaxation time is not usually required to acquire the spectrum. Saturation effects are less of a problem since one is not measuring the magnetization intensity directly, but rather the line-shape. If the spin relaxation time is significantly different between sites, saturation effects could arise but only if the exchange

rates are of the same order as the relaxation time, but this would only occur at the lowest temperatures.

Normally, one does not require knowledge of the rate of reaction before obtaining acceptable spectra since the experimental spectrometer conditions do not depend on the rate. However, to determine the rate constants accurately, one must be able to obtain the spectrum at a temperature in which no exchange broadening is present. In addition, ideally one would like to obtain more spectra around the coalescence temperature. If these temperatures are within NMR capabilities, then they are found by trial and error. Trial and error spectra can be obtained quickly and thus these are found relatively easily. One must, however, ensure that a sufficient length of time is allowed between spectral acquisition for temperature stabilization.

Data Analysis

The convenience that was gained in obtaining the spectrum is lost in the data analysis. One major problem in line-shape analysis is that the exchange map linking the appropriate site with each rate constant must be known. If the spectra and exchange processes are sufficiently simple they may allow for an educated guess. There are many instances when this is not possible, as is the case with the preliminary line-shape studies that were done on complex **3**, $[Os_3(CO)_9(\mu\text{-}Ph_2P{=}O)(\mu_3\text{-}\eta^2\text{-}C{\equiv}C\text{-}t\text{-}Bu)]$. Initially, examination of the spectra showed carbonyl rotation on one metal atom. At slightly higher temperatures, the spectra were too complicated to interpret. Instead, 2D exchange spectra

were obtained and an unexpected exchange pathway corresponding to delocalized carbonyl scrambling was observed.

The other significant problem is that the key analysis is not done by computer. The recommended computer programs can only generate calculated spectra given the frequencies of the sites, estimated line-widths in the absence of broadening, the exchange pathways, and the estimated rates.[2,3] The actual rate extraction is done by hand through tedious trial and error matching of the experimental and calculated spectra for each temperature. Some line-shape programs have attempted to incorporate an iterative line-shape fitting routine.[8] Unfortunately these have met with little success. It is possible to import both the calculated and experimental spectra into computer graphics packages (i.e. Word-Perfect 6.0 or Coreldraw 3.0) to facilitate the matching process. The spectra can then be overlapped and the comparison is made easier.

A severe disadvantage in multi-site and multi-exchange line-shape analysis is that there is only one parameter (the line-shape). If there are n exchange mechanisms occurring simultaneously, then there are n dependant parameters that must be varied simultaneously and since there is only one parameter with which to fit, there may be more than one solution that will give an acceptable fit and many more that will not. In such cases, determination of individual rates may well be intractable.

3.1.2 Time Constraints

Ideally, there will be more spectra acquired around the coalescence temperature

as these line-shapes are inherently more sensitive to the exchange. The acquisition of these spectra is more lengthy as the signal to noise will be at its worst for these points. In general, however, acquisition of the spectra for line-shape is the most expedient of the methods as there are fewer experimental values to pre-determine before acquiring the spectra.

Computational time should never be a constraint with any method, as powerful computers are readily available today. Unfortunately, the main data analysis is off-line and as such can be exceedingly time-consuming. If one is most concerned with obtaining instrumental time then line-shape analysis would be the method of choice, provided the data can be analyzed. The time required for the line-shape analysis can be reduced considerably if one has a good approximate of the rate before the analysis.

3.1.3 Errors in Determining the Rate

There are several problems in accurate rate determination with line-shape analysis even if one neglects the problem of uniqueness of solution in multi-site and multi-exchange systems.

The first is that there are several parameters (other than the exchange rate) that affect the line-shape that are also temperature dependant. These include the chemical shifts, coupling constants, and the effective transverse relaxation time, T^*_2, for each site.[2] There will always be an error in the temperature measurement so a method that has additional temperature dependant parameters compounds the error.

One estimates the chemical shifts and coupling constants at the temperature below which exchange occurs, but the chemical shift is often strongly temperature dependant.[1,2] This is caused in part by the temperature variation in the solute-solvent or solute-solute interactions.[2] Although rarely done, this can be corrected for somewhat by measuring the chemical shift as a function of temperature in the slow regime and fitting the relationship to the lowest polynomial possible. There are errors involved with this procedure because of the covariant nature of the change in the chemical shift with the rate, but this is minimized by measuring the relationship in the slow regime only.[2]

The effective transverse relaxation time, T^*_2, controls the natural line-width that must be entered as a variable for the line-shape program. The dependence on the line-shape by T^*_2 is greatest in the slow and fast regimes. In fact, in the slow regime the line-shape is affected in the same manner by the rate of exchange and by T^*_2.[2] For two equally populated sites in exchange, it is not possible to differentiate the effect of T_2 broadening from that of rate broadening. In unequally populated cases, one sees a differential broadening effect between rate and T^*_2 effects. There have been various approaches to correcting for the T^*_2 temperature dependence. It appears that the optimal approach is to introduce a reference signal that one considers to have a similar T^*_2 temperature dependence, but does not undergo exchange. The transverse relaxation contribution would then be extracted from the reference signal.[2]

Another error that can lead to poor results in the fast and slow regimes are the presence of small couplings that cannot be resolved in the slow regime.[2,3] The signal is

distorted from a true Lorentzian line-shape and this leads to rates that are undervalued in the slow regime and overvalued in the fast regime. In addition, the line-shapes are inherently less sensitive to the rate when the signals are sharp. This occurs in both the slow and fast regimes. The coalescence spectrum is inherently more sensitive to the rate, but unless sufficient signal to noise is obtained, the fit of this spectrum is susceptible to high errors.[1]

Both of these problems can have devastating effects on the activation parameter evaluation. The line is fit more strongly from the data points at both ends, and this is where the error is the largest.[1,2]

3.2 2D-EXSY

One of the true advantages of the 2D experiment over 1D techniques is that unique solutions are possible.[4] In complex chemical exchange, a particular site may experience transients from more than one site. In 1D magnetization transfer all of these transients are summed together in the magnetization of that particular site. One must rely on the non-linear least squares program to extract the transient contribution of each site by fitting the magnetization intensities of each site in the exchange matrix. A two-dimensional spectrum separates the transient contributions as separate cross-peaks. Each cross-peak is a measure of the transfer of magnetization from a single site to that of another. This attribute coupled with the fact that all sites are excited at once (provided that an optimal mixing time is used) demonstrate the advantages of the 2D experiment for mechanistic

determination.[4,14]

3.2.1 Convenience

Obtaining the spectrum

Two-dimensional spectra are more difficult to acquire than one-dimensional spectra. One must first set the time domain in both dimensions. The primary consideration for accurate quantitation is sufficient spectral resolution. This determines the digitization, and as such largely determines the accuracy in measuring the peak area.[4,103] The spectral resolution is inversely related to the acquisition time, t_2, as in 1D spectra and therefore the requirement for spectral resolution must always be balanced with the length of time to complete the experiment. In order to ensure a square matrix, the time domain in t_1 is one half that of t_2.[103] Since one repeats the experiment for nt_1, the larger the frequency range the greater the time-length of the experiment. It is then important to minimize the spectral width to include only the peaks of interest. Normally only a gap of 5-10% is left on either end to avoid instrumental distortions.[103] There is, however, a greater probability of folded peaks from sites that are outside of the spectral window in 2D spectra than in 1D spectra. The filters that remove folded peaks can only be placed in F2, so a test 1D spectrum might not show the presence of a folded peak that will be detected in F1 in the actual 2D spectrum.[103]

Phase-cycling is incorporated in the experiment to improve the quality of the spectra through artifact suppression.[4,103,104] Usually, the greater the number the scans the

more efficient the suppression, but again, length of experimental time is a consideration.

The pulse sequence is not overly complicated in comparison to other 2D experiments, but the 90° pulse width requires accurate calibration to ensure that the quality of the spectra is maximized. Ideally, one would like to set the relaxation delay to five times the spin-lattice relaxation time, but this is not always feasible because of time constraints.

Another problem is that optimal values of key parameters must be pre-determined. The most important of these parameters is the mixing time, τ_m, which is dependent on the rate of exchange, k, and on the relaxation rate, T_1^{-1}. A number of studies have shown that the ability to obtain useful information is dependant on setting this value optimally.[4,14,21,24,105,106] If the value is set too short then the cross-peaks will be small or non-existent. If the mixing time is too long, then there is a potential for higher order peaks or loss of signal intensity because of T_1 relaxation. Basically, this requires that one has a good approximation of both the exchange and relaxation rates before beginning the experiment. The T_1 value can be determined relatively quickly with an independent T_1 experiment, and normally the rate can be estimated from line-width of the signals.

If more than one process is occurring and the rates are widely different, then there will not be a single optimal mixing time and more than one experiment must be performed. More than one experiment per temperature is extremely time-consuming especially when spin-dilute nuclei are being probed.

Data Analysis

Processing the data is also more difficult in two dimensions.[4,103,104] Normal one-dimensional techniques processing techniques are not always sufficient. Linear prediction is strongly recommended for multi-dimensional spectra as the spectra are frequently acquired with low resolution and as a result the peaks are often truncated.[103] Zero-filling will not normally improve the spectrum drastically and heavy apodization will suppress data points at the end of the FID. This has the effect of decreasing the signal to noise ratio and distorting the relative intensities of the cross-peaks.[103]

Baseline distortions are also more prevalent and difficult to correct than with 1D spectra. Artifacts such as t_1 noise, quadrature images, axial peaks, and J-coupling peaks are normally retained if insufficient scans were obtained, so extra cosmetic steps might be required to improve the quality of the spectrum.[20,103,104] All aspects considered, considerable experience and effort is required in order to obtain useful 2D-exchange spectra.

3.2.2 Time Constraints

Accurate quantitation of data can be extremely time-intensive. The main reason, as previously discussed, is the need for highly digitized spectra obtained over multiple mixing times.

As mentioned previously, substantial qualitative mechanistic information is

obtained from visual inspection of the 2D spectrum, provided that an acceptable mixing time is used. This mixing time is, of course, more difficult to ascertain if there is more than one process occurring. However, if one seeks only qualitative mechanistic information, one is not as concerned about digitization error and the suppression of artifacts and as a result the spectra can be obtained more quickly.

3.2.3 Errors in Rate Constant Determination

Errors arising from the integration of peak areas and peak volumes have three major sources of error in both one and two-dimensional spectra; spectrometer noise, digitization and truncation. All of these errors are more severe in two dimensional spectra. The 2D errors can approximated as a product of the 1D errors i.e. a 10% error in a 1D spectrum would translate into a 100% error in the 2D spectrum.[98,99,107] So even if one minimizes these errors, the errors in 2D spectra would always be considerably greater than those in 1D spectra. In addition, one is normally required to minimize the length of the 2D experiment, and this is done at the expense of the digitzation and truncation error.

Recent work by Weiss *et al.*[99] has investigated the later two errors in peak area and volumes in the *absence* of noise. They found that typical experimental parameters gave errors for 1D peak areas in the region of 10%, and up to 100% if unfavourable conditions (but not overly unreasonable) are used. With the two-dimensional peak volumes, 100% errors are not inordinate under typically good conditions. The errors could be reduced somewhat if spectra are obtained as a function of the mixing time. The data

could then be fit by use of a non-linear least-squares routine as with 1D experiments. This is normally precluded because of time constraints.[4]

The accordion 2D-EXSY experiment is a potential solution to this problem. In this relatively recent variation on the 2D-EXSY experiment, the mixing time is varied without increasing the total time of the experiment.[108,109] This is done by incrementing the mixing time synchronously with the evolution time, t_1. This leads to peak distortions, however, and the rate is calculated from the peak-widths rather than from the cross-peak intensities. Special line-shape analysis is required to extract the rate.[110] Severe problems are encountered with multi-site systems or when peaks overlap.[4]

Recently, Yarnykh *et al.*[110] have published the mathematical formalism (and program) for a computerized least-squares line-shape analysis for the 2D accordion experiment.[110] They presented the first three-site exchange analyzed by this technique and reported increased precision in the rate determination. They noted that one still requires high digital resolution and good signal to noise to avoid large errors. The advantages to this experiment are clear in that it is no longer a one point kinetic method and the computer analysis allows for iteration that may correct for instrumental error.[110]

So far the only error that has been discussed has been that caused by digitization and truncation. All magnetization transfer methods are optimally done in the slow regime without excessive exchange broadening. Abel *et al.*[21] reported an error analysis that included the effect of temperature on the precision of the rate determination. This is an important factor to consider as most reported error analyses pertain more to 2D-NOESY

studies that optimally involve no exchange.[98,99]

The errors in the Abel study were categorized into three areas i) the finite S/N ratios of the computed spectra, ii) instrumental drift during the course of the experiment and iii) errors in the 2D integral integrations. They assumed that the first error is a constant, proportional to the spectral noise level regardless of the signal intensity. The temperature dependence on the signal is accounted for by including the loss of signal caused by the spin-lattice relaxation (this is more important at long mixing times), the increase in S/N as the temperature is lowered because of the Boltzmann factor ($S/N \propto T^{-1}$), and the lowering of the rf receiver coil noise ($S/N \propto T^{-1/2}$). Most importantly they included changes in the signal width caused by exchange broadening.[21]

The errors of spectrometer drift and integration were treated as percentage errors of the signal intensities. The assumed errors were ± 2% for the instrumental drift and ± 1% for the error in integration. Clearly, this is severely understated, given the errors from digitization and truncation discussed previously. They also assumed that the errors of each exchange process are independent, i.e. that the covariances are equal to zero.

Under these assumptions, they found that there was a narrow temperature range (273-243 K) in which the errors were under 10%; below or above that range, they increased substantially. The low temperature regime has extremely weak cross-peaks, while at high temperatures there was appreciable exchange broadening.[21] This analysis demonstrates that the error can be quite substantial even when one virtually neglects the large error due to digitization and truncation.

Another source of error not present in line-shape analysis is the contribution of cross-relaxation. The cross-relaxation contribution is intrinsically indistinguishable from the exchange contribution. As a result, the quantity that one actually measures is the exchange rate minus the cross-relaxation rate. The cross-relaxation contribution is negligible when the dipole-dipole contribution to the spin-lattice relaxation is not efficient. This is the case if spin-dilute nuclei (such as natural abundance to 30% enriched ^{13}C samples) are used to probe the rate or when the exchange involves small molecular systems.[9,20,111]

A potentially greater source of error occurs if the optimal mixing time cannot be set. This was demonstrated in a study by Farrugia and Rae in which they re-examined the fluxional processes of $Ru_3(CO)_9(\mu\text{-}H)(\mu_3\text{-}\eta^2\text{-}C{\equiv}C\text{-}t\text{-}Bu)$.[24] This molecule undergoes several fluxional processes with widely differing rates. There exists no single optimal mixing time that will induce low errors for all the rate processes.

Initially, Farrugia and Rae[24] attempted 2D exchange studies. The 2D spectrum (Figure 3.1) demonstrated that all of the sites exchange with each other as expected and that the cross-peak intensity of I_{ed} was twice as that of I_{bd} and I_{be}. Determination of the mechanism required accurate quantitation of the rate constants, since this spectrum demonstrated that all sites exchanged. Large errors were produced in the rates of exchange from three different mixing times (0.2, 0.5, 0.6) at 275 K (Table 3.1).

Examination of Table 3.1 shows where the problem lies. The rate k_{ac}, is much larger than the rest, and the optimal mixing time for this rate will be significantly shorter

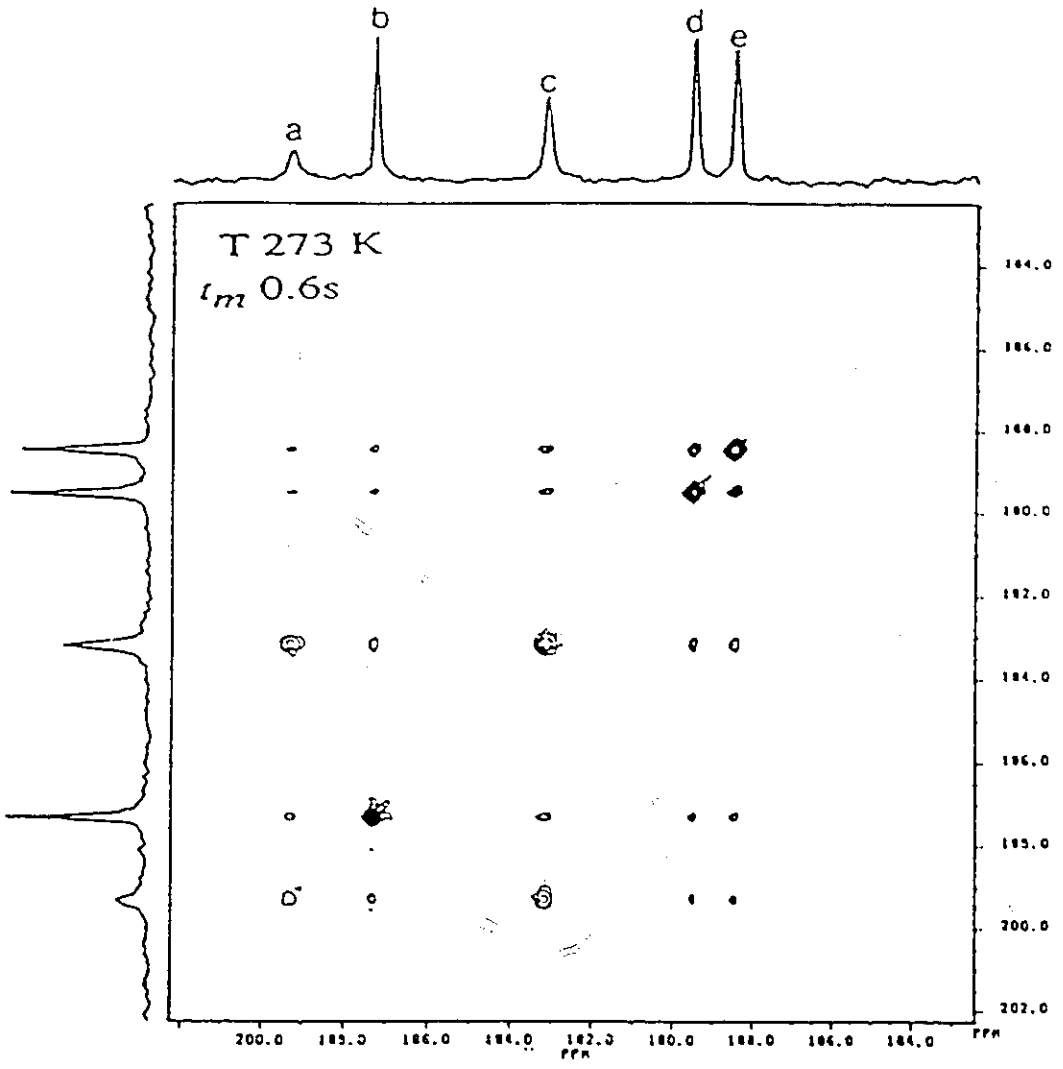

Figure 3.1 $^{13}C\{^1H\}$ 2D-EXSY carbonyl spectrum of $Ru_3(CO)_9(\mu\text{-}H)(\mu_3\text{-}\eta^2\text{-}C{\equiv}C\text{-}t\text{-}Bu)$ at 273 K. Note that all of the carbonyl ligands exchange with each other, and that the cross-peaks corresponding to exchange between carbonyl ligands a and c are much more intense than the others. *Figure 3.1 is reproduced from reference 24.*

Table 3.1 2D-EXSY Exchange Rates in the Study of $Ru_3(CO)_9(\mu\text{-}H)(\mu_3\text{-}\eta^2\text{-}C{\equiv}C\text{-}t\text{-}Bu)$[24]

	k_{ij}				
	a	b	c	d	e
a		0.94 ± 0.5	26.8 ± 7.0	0.17 ± 0.60	0.17 ± 0.60
b			0.35 ± 0.2	0.09 ± 0.08	0.09 ± 0.09
c				0.48 ± 0.25	0.48 ± 0.25
d					0.92 ± 0.18

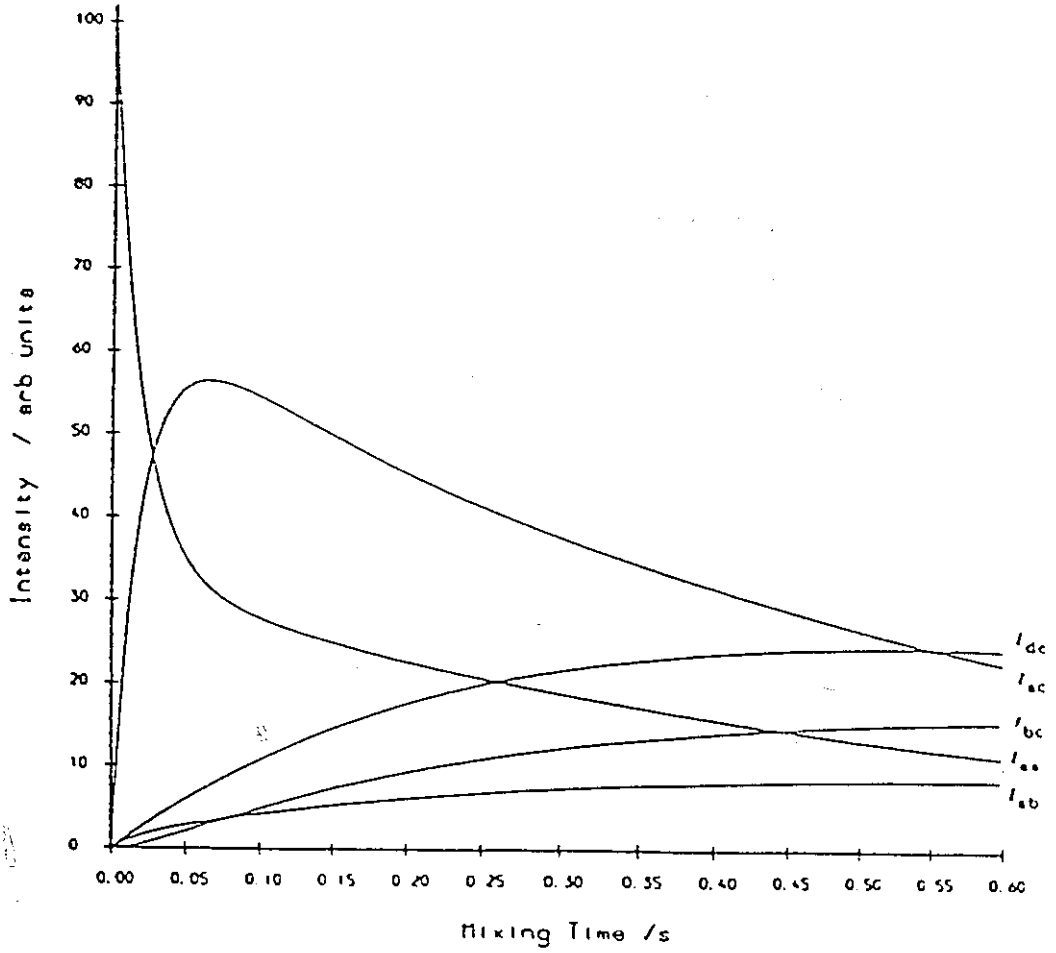

Figure 3.2 Calculated dependence of the peak intensity on the mixing time for $Ru_3(CO)_9(\mu\text{-}H)(\mu_3\text{-}\eta^2\text{-}C{\equiv}C\text{-}t\text{-}Bu)$. *Figure 3.2 is reproduced from reference 24.*

than for the others. This is demonstrated in Figure 3.2. The optimal mixing time to measure k_{ac} is 0.02 s, but at that mixing time the intensities of the other cross peaks will be very small. If one uses a compromise mixing time of 0.1 s, then the intensities of the diagonal peak, I_{aa}, and the cross peak, I_{ac}, will be insensitive to the mixing time. This also increases the error in k_{ab}, k_{ad}, k_{ae} since the intensity of the diagonal peak, I_{aa}, is low as well as the respective cross-peaks.[24] This demonstrates quite clearly that the assumption by Abel *et al.*[21] that the errors in the rates are independent is false because each cross-peak intensity is dependent on the intensities of the two diagonal peaks. Those two diagonal peaks may be involved in other exchange processes and so the rate coefficients are not determined independently.

This case also demonstrates that it is not always advantageous to probe all of the rates at once. For this reason, the 1D magnetization transfer technique in which all of the sites are selectively inverted in separate experiments was done. The data were then analyzed with use of the constraint method of Mann.[25] They concluded from this rate information that delocalized CO scrambling was not occurring as originally reported, but rather rotation of the alkynyl ligand occurs in concert with hydride migration.

3.3 The Single Selective Inversion Method

The only 1D magnetization transfer method that will be discussed here is the single selective inversion method. In many ways, the advantages and disadvantages are very similar to the 2D-EXSY method since both are magnetization transfer methods.

However, there are some differences and these along with the similarities will be discussed.

3.3.1 Convenience

Spectral Acquisition

As this is a 1D experiment, it is less difficult in many regards than the 2D experiment. For example, folding of peaks is less of a problem, and as a result the frequency limits are set more easily. The actual pulse sequence is similar to the 2D experiment, and again the 90° pulse calibration and the T_1 determination must be done accurately before beginning the experiment. The total experimental time per variable delay is significantly less so the magnetization transfer is determined as a function of the variable delay (or mixing time). The optimal number of scans can be determined easily as test spectra can be obtained relatively quickly.

The single selective inversion method is more difficult with respect to the number of optimal parameters that require determination prior to obtaining the spectra. As with the 2D experiment, ideally, the exchange and relaxation rates must be known in order to perform the experiment. In quantitative experiments, it is especially important to set the equilibrium relaxation delay to five times the spin-lattice relaxation time. One must determine the correct temperature regime and this involves knowledge of the approximate rate. The approximate rates of exchange and relaxation are also used to determine the range of variable delays. Since more than one variable delay is used, this is not as crucial

as in the 2D experiment. However, it is best if the majority of variable delays sample the chemical exchange transient and not the T_1 curve. It is possible to design the experiment such that the first few variable delays will determine if one is sampling in the correct range. If these spectra determine that the range was incorrect, the experiment may be stopped and reset without losing excessive instrumental time.

In a single experiment in which all of the rates are probed, one must know both the transmitter offset and that pulse delay that will optimally excite the system. The process of obtaining the partial derivatives and choosing an optimal set, as described in Chapter 2, can be tedious if there are many sites and exchange processes. The alternative method of calculating the initial magnetization by varying the pulse delay and transmitter offset from the known mathematical formula can be more expedient and allows verification of other parameters that require setting. This process could also be tedious unless one uses intuition and knowledge of the exchange pathways to guess an acceptable excitation. It is conceivable that a good guess could not be made and that the full partial derivative method would be required.

Data Analysis

The actual processing of the spectra is easier than even those from line-shape analysis. Line-shape spectra around coalescence can be difficult to phase correctly as the signal can be quite broad, while those of the selective inversion technique must have sharp signals, and as such, are easy to process.

As with line-shape analysis, one must also enter the exchange map. It is, however, relatively facile to iterate over both the rate and the exchange map to determine the mechanism.

3.3.2 Time Constraints

The greater the accuracy in the determination of the rate coefficients, the longer the experimental time. As one increases the number of variable delays, scans, and the amount of digitization the more one approaches the length of time required for a 2D experiment. The result, however, is a more accurate rate constant.

3.3.3 Errors in Rate Constant Determination

As with the 2D experiment, the largest source of error comes from poor signal to noise, digitization and the presence of truncation. It is not as severe as in 2D spectra as the error in a 2D experiment is the product of that for a 1D experiment.[98,99] The error in 1D is normally around ten percent, but with careful work this can be reduced in half.

Again the error of cross-relaxation contribution would be present as this is a magnetization transfer experiment. The errors also increase with temperature, as with the 2D experiment. Exchange broadening increases the errors as one increases the temperature. As one lowers the temperature, the relaxation rate dominates the matrix and the exchange rate is relatively insensitive to the experimental conditions.[21]

The one significant source in error over that of 2D magnetization transfer is that

the covariances will be significantly larger in a one-dimensional experiment. If a particular site experiences a transient from more than one site, then these transients will be observed in that signal together and not as separate cross-peaks. The fitting routine must separate each contribution. The more contributions observed in a signal the greater the likelihood of a false minima. This is alleviated somewhat as one obtains a series of magnetizations as a function of the variable delay and therefore there is more information to fit than in the 2D data set with a single mixing time.

As a result, the covariance should be reported as the error and not the simple variance. Unfortunately, with multi-site and multi-exchanging systems, one is required to calculate the covariances over a large dimension space and this is difficult. Currently, no selective inversion program calculates the covariance, and thus the reported errors of the rates may be severely underestimated. One possible solution for reducing the covariance is to avoid or minimize certain contributions by judicious choice of the selective excitation and it is possible to do this with the partial derivative criterion.

As was mentioned previously, the exchange map alone will not always determine the mechanism. Often accurate rate coefficients corresponding to each exchange map element are required. The McClung approach[19] that allows one to enter the actual set of exchange maps permits the fit of each as a separate of set of exchange coefficients. This allows maximum flexibility in fitting the data and aids considerably in the mechanistic determination.

The errors in the individual rates should be less than with 2D methods especially

if one can reduce the covariances through selective excitation of each exchange process. Smaller error allows greater confidence in applying the relative magnitude of the rates towards mechanistic determination.

3.4 Errors In Activation Parameters

Most often in organometallic studies, the exchange rate is not of prime importance, but rather the "barrier" to the exchange which is determined from the activation parameters ($\Delta G^{\ddagger}$, $\Delta H^{\ddagger}$ and $\Delta S^{\ddagger}$).[2] This information is obtained from the temperature dependence on the rate and is given by equation 3.1

$$k = \kappa \frac{k_B}{h} e^{\frac{-\Delta G^{\ddagger}}{RT}} \qquad 3.1$$

where $\Delta G^{\ddagger} = \Delta H^{\ddagger} - T\Delta S^{\ddagger}$

The error in $\Delta G^{\ddagger}$ is not overly sensitive to the errors in the temperature but this is not the case with $\Delta H^{\ddagger}$ and $\Delta S^{\ddagger}$.[2] These parameters are normally calculated by use of a non-weighted linear least squares analysis of ln (k/T) versus 1/T that results in a slope of $-\Delta H^{\ddagger}/R$ and an intercept of $\Delta S^{\ddagger}/R + \ln(k_B/h)$. With non-weighted data, the data points at the ends contribute more to the calculated line then do those in the middle. This is potentially disastrous for line-shape analysis, since the coalescence data points are generally considered more accurate than those in the fast or slow regime, but they have less effect in defining the line.[1]

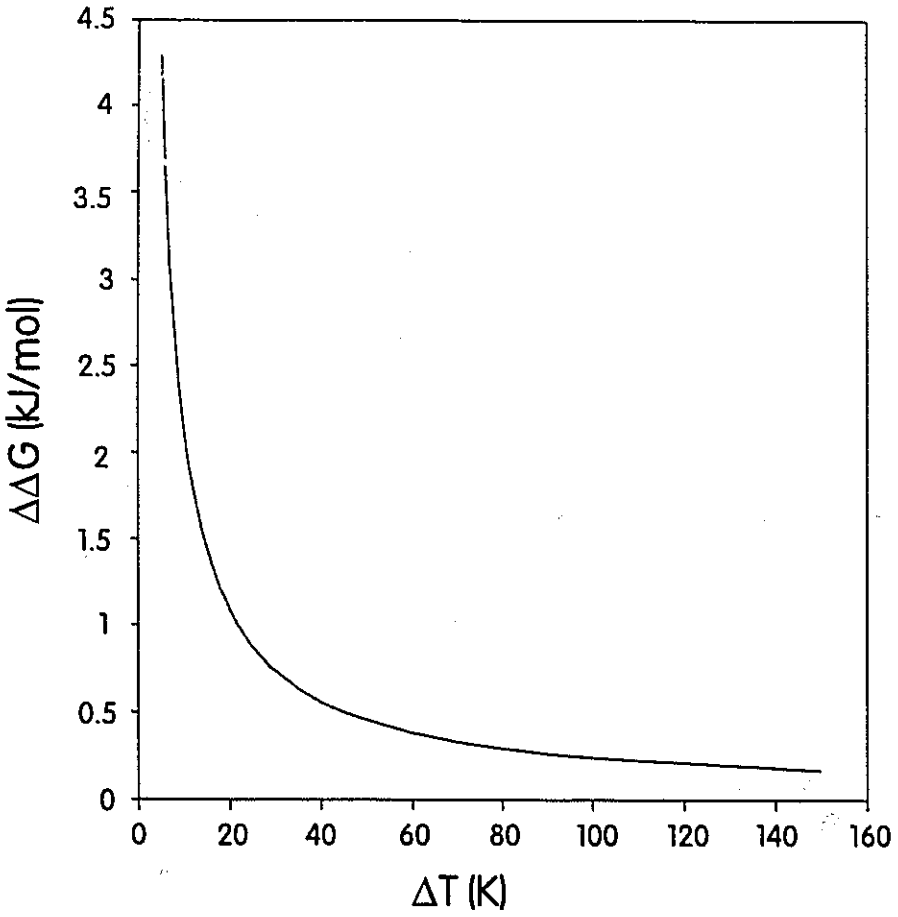

Figure 3.3 Variation in ΔG with range of temperature. Calculation was done as per reference 2.

Naturally, the more data points one obtains *via* any method, the more degrees of freedom and hence the greater the confidence in the error. The temperature range over which these points are obtained will also affect the error in these parameters. As demonstrated in Figure 3.3,[2] the temperature range should be extended as much as possible as possible. Magnetization transfer studies (both 1D and 2D) are more accurate in the slow regime, while line-shape analysis is more sensitive to the rates in the intermediate regime. It then makes sense to extend the range by combining these two methods to obtain activation parameters with lower error.[112-114]

Both line-shape and selective inversion data were combined for the complexes **1**, and **2**, and precision of the line was improved. This was especially important for complex **2**, as only three data points over a narrow temperature region could be obtained by the selective inversion method.

3.5 Conclusions

The strengths and weaknesses of each of the dynamic NMR methods seem to complement each other and it appears that in many cases the optimal experiment for complex systems with multi-site and multi-exchange processes would be a combination of one or more of these methods. This section serves to summarize the strengths and weaknesses of each method and outlines a combination strategy for optimal results in complex exchange.

Accurate exchange rates can be determined from line-shape in the coalescence

region, at intermediate temperatures, provided that the exchange map is known. If more than one process is occurring, line-shape analysis cannot normally provide information on the mechanism, and thus is not recommended for systems that undergo complex multi-exchange (unless one has prior knowledge of the mechanism and the approximate rates).

The 2D exchange experiment is unsurpassed for determining the exchange pathways, but unless highly digitized spectra are obtained, the errors involved in the quantitation can be excessive. Highly digitized spectra are possible to obtain within a reasonable experimental time if the frequency range containing all the peaks of interest is not excessive. Line-shape analysis and 2D methods are completely co-dependent with multi-site and multi-exchange systems. The 2D experiment requires an approximate rate to determine the optimal mixing time. This is best determined by obtaining the line-shape spectra approximating the rate from the exchange broadening. The full analysis of the line-shape spectra in many cases cannot be accomplished without the exchange map and this is most easily provided from the 2D experiment.

Quantitation of the data in the slow regime is best performed with 1D selective inversion magnetization transfer data as the errors will, in most cases, be lower than with the corresponding 2D data. In some cases, this ability to quantitate more accurately leads to mechanistic determination. The 1D method also requires an approximation of the rate from the line-shape spectra in the slow regime. Whenever possible the line-shape data from the intermediate region should be combined with the selective inversion data to increase the confidence in the activation parameters.

If, however, one seeks qualitative information, the 2D experiment is strongly recommended, but will not always provide the mechanism without proper quantitation. There are situations when the 2D experiment is expected to give better quantitation. This would occur when the spectra can be obtained with good digitization and when the ability of the 2D experiment to separate the contributions of the each transient from different sites into individual cross-peaks is crucial. In addition, if one is working with a 100% abundant nuclei (i.e. ^{31}P, or ^{1}H) it may be possible to perform the experiment with use of multiple mixing times since each experiment can be accomplished with significantly less scans than with natural abundance ^{13}C samples.

3.5.1 Recommended Combination Strategy for Complex Exchanging Systems

Faced with an unknown multi-site and multi-exchanging system, one should first obtain the line-shapes as a function of temperature to approximate the rates in the low temperature regime. Fast qualitative 2D spectra should be obtained at the appropriate temperatures and mixing times as determined from the line-shape analysis. This will provide the exchange pathways and one should have sufficient information to set an optimal 1D single selective inversion magnetization transfer experiment to obtain the slow regime data points.

The temperature dependence of these points can be extended to provide approximate rates for the intermediate region. Matching of the line-shapes then requires fine-tuning only. This will considerably reduce the length of time required to extract the

rate information from the line-shape spectra. The Eyring plot is then redrawn to include the line-shape data and this should increase the confidence level of the activation parameters.

CHAPTER 4.

CARBONYL SCRAMBLING

4.1 Introduction

One of the first complexes to be studied with dynamic NMR techniques was $[C_6H_8Fe(PF_3)_3]$ in 1970.[115] At that time, ^{13}C NMR was extremely difficult and axial-equatorial exchange was investigated for the PF_3 substituted complex. The advent of ^{13}C NMR opened up the study of organometallic rearrangement and in particular carbonyl scrambling.[116-122] One can find many examples of binuclear,[58,60,123-130] trinuclear[61-63,131-135] and tetranuclear[64,66,136-139] complexes in which carbonyl scrambling occurs *via* motion from one metal center to another. It was not until 1974, that Forster *et al.*[67] published the first evidence for localized axial-equatorial carbonyl exchange in trinuclear carbonyl compounds. They were studying both simple, mixed and related compounds of $M_3(CO)_{12}$ (M=Fe, Ru, and Os). The study was complicated because these compounds do not exchange *via* a single generalized mechanism. In the case of $Ru_3(CO)_{10}(NO)_2$, the most plausible mechanism had to be that of localized axial-equatorial exchange since the compound could not form bridged CO intermediates. The probability of bridged carbonyl intermediates decreases as one goes down a triad. The presence of bridging carbonyl

groups in compounds of second and third row metals have been observed when other ligands in the system are strong donors.[70]

In 1975, both Aime *et al.*[70,71] and Cotton *et al.*[55,56,68] presented further evidence of localized carbonyl group rotation on individual metal atoms. Aime was studying the substituted acetylenic complexes $[HM_3(CO)_9(\mu_3\text{-}C{\equiv}C\text{-}t\text{-}Bu)]$ (M=Ru, and Os). Both the osmium and ruthenium analog show localized axial-equatorial exchange on the metal atoms, but only the ruthenium analog shows exchange between the metal atoms *via* bridged intermediates.

By far the most prevalent examples of localized axial-equatorial exchange occur when one finds $M(CO)_3$ units in the complex, and when the structure does not allow for bridged intermediates.[29,67,69-71,140,141] This is the case with $HM_3(CO)_9(\mu_3\text{-}C{\equiv}C\text{-}t\text{-}Bu)$ (M=Ru and Os)[70] and $HRu_3(CO)_9L$ (L=olefin)[142] where the larger radii and different electronic requirements of ruthenium and osmium inhibit carbonyl ligand bridging. First row metal complexes can also undergo localized exchange if they contain large enough ligands to inhibit the carbonyl bridging. This is the case with the following iron examples (acenapthylene)$Fe_2(CO)_5$[55] and (cyclooctatriene)$Fe_2(CO)_6$[56] that contain large rigid polyolefins that sufficiently inhibit bridging. In the former case, there are two iron environments: one with three carbonyl ligands, the other with two. Only the $Fe(CO)_3$ unit scrambles amongst itself and it does not exchange with the carbonyl ligands in the $Fe(CO)_2$ unit.

Localized scrambling can occur *via* a simple rotary motion, or that of successive

pairwise motion. Qualitatively, there is no difference between the two mechanisms as the carbonyl ligands all scramble amongst themselves *via* either scheme. In the case of the simple rotation one would expect that the rates between all three exchanges would be the same, since it is a concerted motion. With the successive pairwise mechanism, one would expect the barrier of one of the carbonyl exchanges to be higher than the barrier for the other two. In order to determine the mechanism, one then requires very accurate rate data on the exchange between all three carbonyls.[11]

Localized carbonyl scrambling is exhibited in all three of the molecules studied. Selective inversion and line-shape experiments were completed for **1**, $Ru_2(CO)_6(\mu\text{-}PPh_2)(\mu\text{-}\eta^1\text{:}\eta^2\text{-}C{\equiv}C\text{-}i\text{-}Pr)$, and **2**, $Fe(CO)_6(\mu\text{-}PPh_2)(\mu\text{-}\eta^1\text{:}\eta^2\text{-}HC{=}CH_2)$ to determine accurately the activation parameters. Two-dimensional studies on **3**, $Os_3(CO)_{10}(\mu\text{-}Ph_2P{=}O)(\mu\text{-}\eta^1\text{:}\eta^2\text{-}C{\equiv}C\text{-}t\text{-}Bu)$ demonstrated the presence of delocalized carbonyl exchange, in addition to localized carbonyl rotation. The results from the studies on these compounds are presented.

4.2 Carbonyl Scrambling in $Ru_2(CO)_6(\mu\text{-}PPh_2)(\mu\text{-}\eta^1\text{:}\eta^2\text{-}C{\equiv}C\text{-}i\text{-}Pr)$

In compound **2**, $Ru_2(CO)_6(\mu\text{-}PPh_2)(\mu\text{-}\eta^1\text{:}\eta^2\text{-}C{\equiv}C\text{-}i\text{-}Pr)$, the carbonyl rotation exchange occurs well after the acetylide interconversion and these two processes do not interfere with each other in the carbonyl spectra. For this reason, it was the system of choice to test the single selective inversion technique. The spectral details were presented in Chapter 2, along with selective inversion results at room temperature. These details will be repeated here briefly to ensure readability.

At low temperature, all six carbonyl ligands are distinct as the acetylide ligand is fixed in one orientation and each carbonyl ligand shows a coupling to the phosphorus from the bridging phosphido ligand, resulting in twelve sites in total. At higher temperatures, the acetylide ligand undergoes σ to π interconversion. This creates a plane of symmetry between the two metal atoms resulting in only three distinct CO ligands, and therefore six sites with the ^{31}P coupling. The carbonyl rotation process begins around -10° C, at which temperature, the acetylide ligand is in fast exchange and can be neglected.

The initial goal of this experiment was to measure the individual rates for each of the individual carbonyl exchanges (a→b, b→c, c→a) separately with the expectation of differentiating between a concerted rotation and a successive pairwise mechanism. The results from the selective inversion studies at a single temperature demonstrated that the three exchanges are equal within experimental error.

Selective inversion and line-shape data were obtained as a function of temperature. Table 4.1 shows the experimental temperatures along with the measured rates and Figure 4.1 shows the temperature dependence. The selective inversion data compare very well with the line-shape data. It was found that the fit improved if all three rates were constrained to be equivalent. The barrier is given from the plot of the temperature dependence (Figure 4.1) with $\Delta H^{\ddagger} = 59 \pm 3$ (3σ) kJ mol^{-1} and $\Delta S^{\ddagger} = 0.035 \pm 0.003$ (3σ) kJ deg^{-1} mol^{-1}.

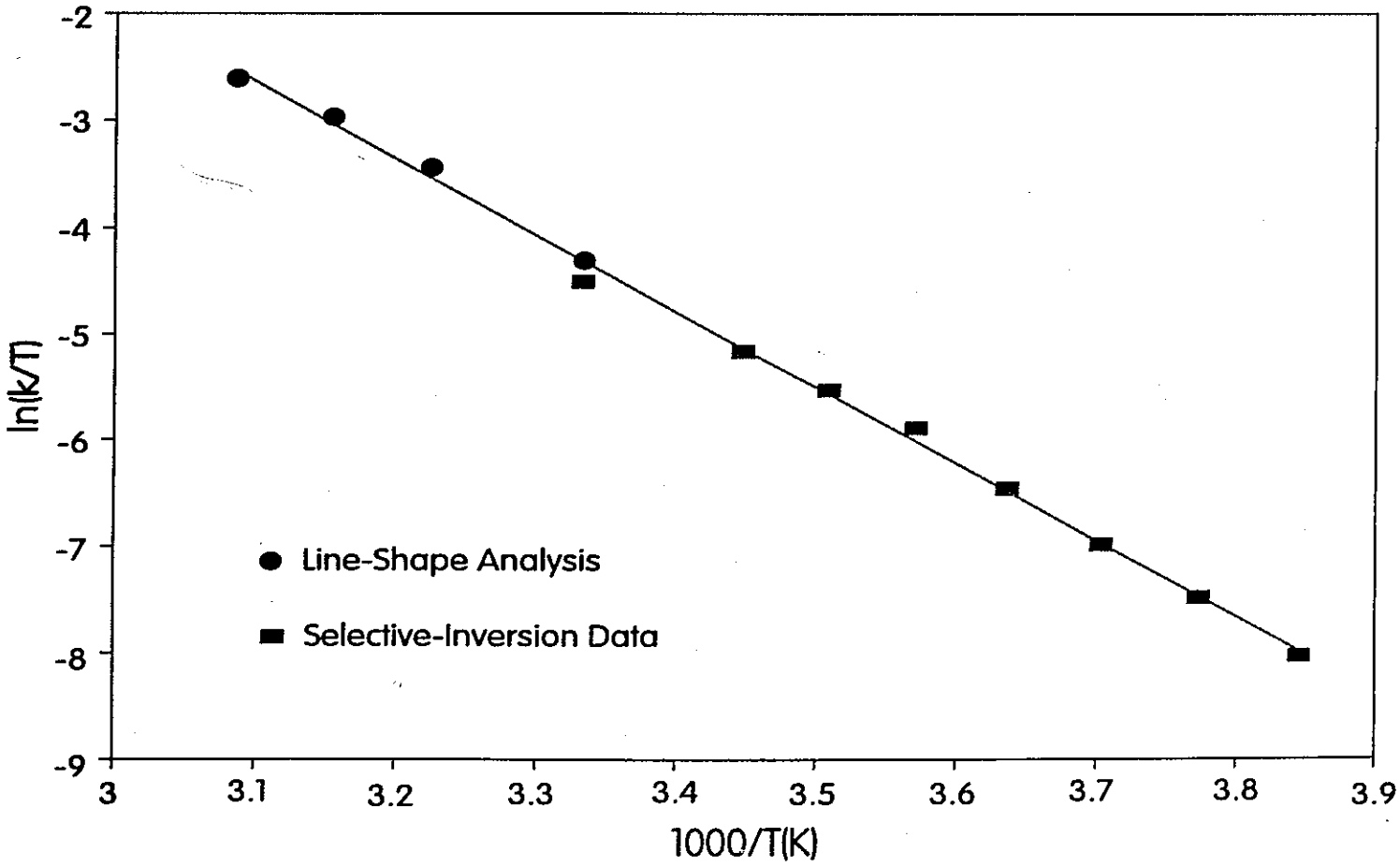

Figure 4.1 Temperature dependence of the carbonyl rotation process of $Ru_2(CO)_6(\mu\text{-}PPh_2)(\mu\text{-}\eta^1\text{:}\eta^2\text{-}CC\text{-}i\text{-}Pr)$. Both the single selective inversion and the line-shape data were combined.

Table 4.1 Temperature Dependence of the Carbonyl Rotation Process in $Ru_2(CO)_6(\mu\text{-}PPh_2)(\mu_2\text{-}\eta^1\text{:}\eta^2\text{-}C{\equiv}C\text{-}i\text{-}Pr)$

Temperature (K)	Rate (s^{-1})
260[a]	0.085
265[a]	0.15
270[a]	0.25
275[a]	0.43
280[a]	0.77
285[a]	1.12
290[a]	1.65
300[a]	3.3
300[b]	4
310[b]	10
317[b]	16
324[b]	22

a)Selective inversion data b) Line-shape data

One of the criticisms of magnetization transfer methods is that the temperature range for which one can measure data is thought to be quite narrow. However, the selective inversion data for this system shows quite a wide range.

This, and the data presented in Chapter 2 demonstrated that the three pairwise exchange rates are equal within experimental error. While this does not entirely rule out a pairwise mechanism, it strongly suggests a concerted process. Several studies of localized carbonyl exchange can be found whereby a concerted mechanism was concluded. Hawkes *et al.*[69,141] studied the carbonyl rotation in $[Os_3H_2(CO)_{10}]$ and $[Ru_3(\mu\text{-}H)(CO)_9(MeCCHCMe)]$. In the former case, two of the carbonyl ligands are equivalent, so there is only one rate. In the latter case, the processes are distinguishable and the rates were found to be equal within experimental error. Again this was considered strong evidence that the mechanism was concerted rather than pairwise exchange. Beringhelli *et al.*[29] have published work on the intramolecular rearrangement of $[Re_3(\mu\text{-}H)_4(CO)_9(NCMe)]^-$. Two of the metal atoms have three distinct carbonyl ligands. The scrambling rates were found to be equal at three different temperatures within experimental error. A more recent study by Farrugia *et al.*[24] of $Ru_3(\mu\text{-}H)(\mu_3\text{-}\eta^1\text{:}\eta^2\text{:}\eta^2\text{-}C{\equiv}C\text{-}t\text{-}Bu)(CO)_8(PMe_2Ph)$ also concluded a concerted mechanism for the $Ru(CO)_2(PMe_2Ph)$ group.

4.3 Localized Carbonyl Rotation in $Fe_2(CO)_6(\mu\text{-}PPh_2)(\mu_2\text{-}\eta^1\text{:}\eta^2\text{-}HC{=}CH_2)$

This system provides a challenging test model for any kinetic studies. Unlike the

ruthenium system, the dynamic processes are not well separated. Three independent processes (Figure 4.2) occur as follows: rotation of the carbonyl ligands on one iron atom, rotation of the carbonyl ligands on the other iron atom, and then the σ to π interconversion of the vinyl ligand.

Well separated processes are ones in which the preceding exchange process is in fast exchange before the next process begins. This is not the case with this system (Figure 4.3). The first discernable broadening for the initial process is observed around 195 K and significant broadening caused by the second set of carbonyl ligands begins before the onset of fast exchange for the first process. Around 275 K, the first carbonyl rotation is in fast exchange while the second set of carbonyl ligands is approaching the coalescence point. Shortly thereafter, the onset of the vinyl interconversion occurs and the compound decomposes before coalescence.

This non-separation of processes creates difficulty for both the line-shape and selective inversion experiments. In line-shape analysis, there is only one parameter to fit, that of the signal shape. If more than one rate parameter strongly influences the line-shape, it is difficult to separate each contribution, even by trial and error. In this case there are three rate parameters that affect the line-shape. In order to analyze the line-shape spectra effectively, one must be able to fix the two of the rates, while the third rate is being probed.

With the generalized single selective inversion technique, one can tailor the experiment to exclude the exchange processes that are not of interest. Selective inversion

a)

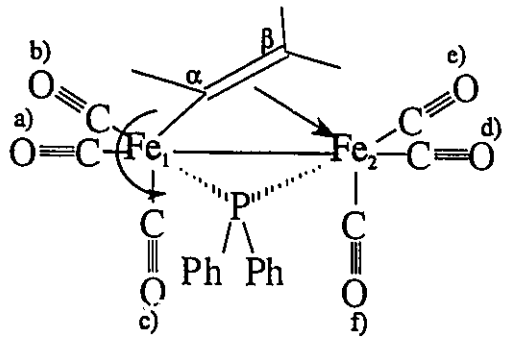

b)

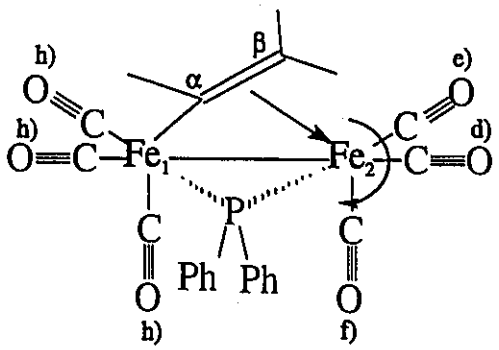

c)

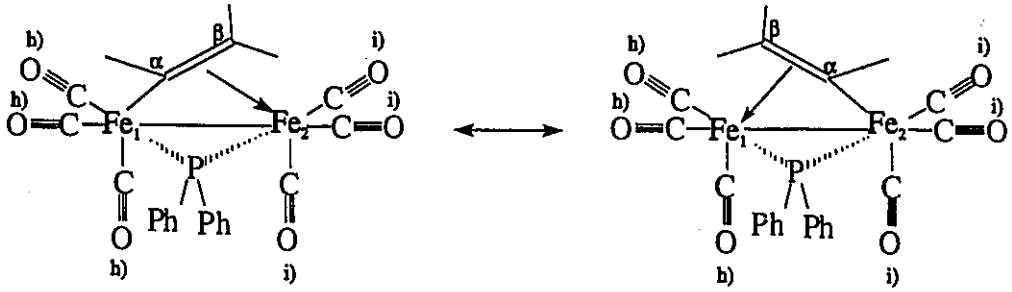

Figure 4.2 The three independent exchange processes of $Fe_2(CO)_6(\mu\text{-}PPh_2)(\mu_2\text{-}\eta^1\text{:}\eta^2\text{-}HC{=}CH_2)$. a) Carbonyl rotation on Fe_1 b) Carbonyl rotation on Fe_2 c) σ to π inter-conversion

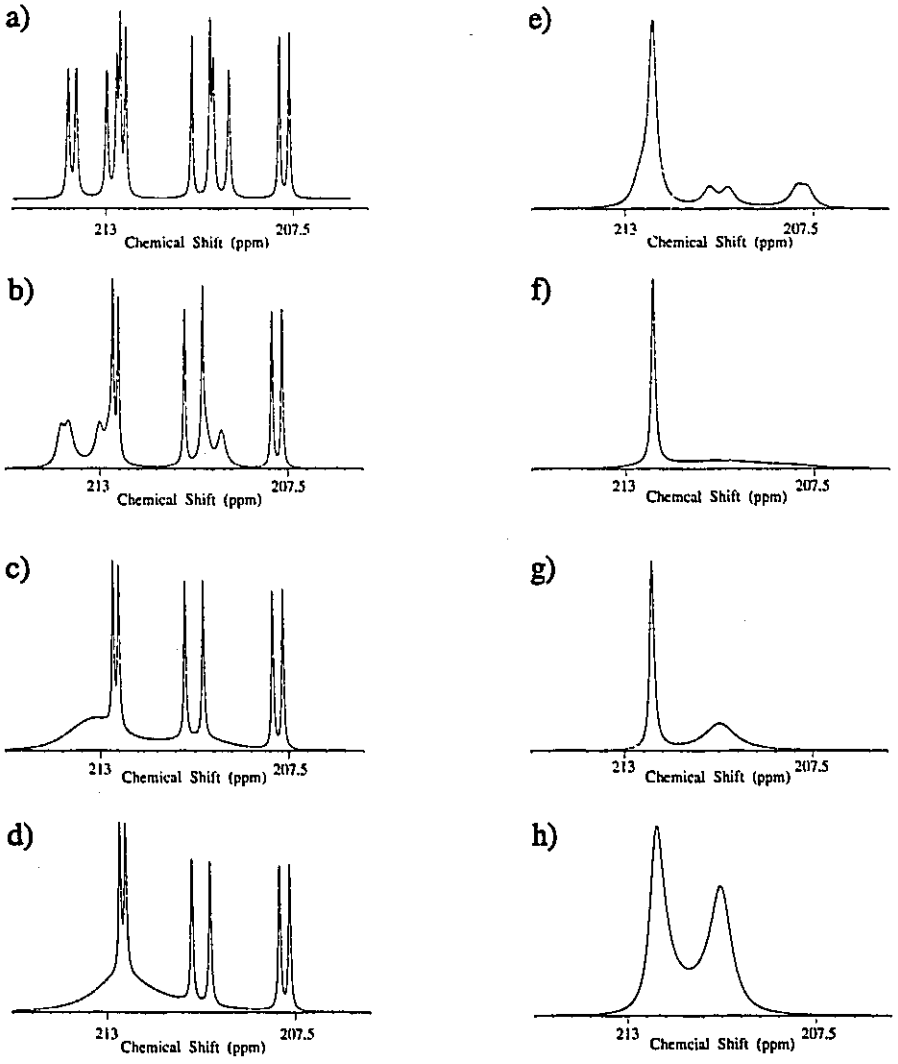

Figure 4.3 Calculated line-shapes for $Fe_2(CO)_6(\mu\text{-}PPh_2)(\mu\text{-}\eta^1\text{:}\eta^2\text{-}HC{=}CH_2)$. The rates were calculated using the slope and intercept from the temperature dependence plot for each process. a) T= 173K, rates (1.8, 0 , 0 s^{-1}) b) T= 193K rates (22, 0.02, 0 s^{-1}) c) T= 213K rates (183, 0.4, 0 s^{-1}) d) T= 223K rates (459, 1.5, 0 s^{-1}) e) T= 253K rates (4750, 39, 0.1 s^{-1}) f) T= 273K rates (17072, 237, 1.5 s^{-1}) g) T= 293K rates (51787, 1127, 14 s^{-1}) h) T= 313K rates (136919, 4406, 93 s^{-1})

experiments may still be difficult as one must work in a narrow rate regime where the rate is just slightly higher than the relaxation rate, and the appearance of broad signals due to other processes may decrease the temperature range further. However, three points will define a line, albeit imprecisely, and from this one can extrapolate the rates into the line-shape regime. In this manner, one can determine the approximate values for the rates to facilitate the line-shape analysis. The temperature dependence of all three processes was determined by combining the line-shape and the selective inversion data. This increases the range of rates that can be measured and hence decreases the error in the activation parameters.[2]

The σ to π interconversion process acts to equalize the metal centres and hence the rotation of the carbonyl ligands on each metal. One is able to differentiate between the two sets of carbonyl rotations in this case because the vinyl windshield wiper motion has a higher barrier than the carbonyl rotation and hence occurs later.

The selective inversion and line-shape data were combined in the analysis of both carbonyl rotation processes. The temperature dependence for the first process is presented in Table 4.2 and Figure 4.4, while that of second process is found in Table 4.3 and Figure 4.5.

Only two selective inversion data points could be obtained for the first process. At lower temperatures, the relaxation rate sufficiently competes with the chemical exchange rate, and at higher temperatures the peaks are exchange broadened. Since this process occurs over a range of approximately 40 °C without interference from the second

Table 4.2 Temperature Dependence of the First Carbonyl Rotation Process as Determined by a Combination of Line-Shape and Selective Inversion Data

Rate (s^{-1})	Temperature (K)
2.1[a]	175
4.7[a]	180
8[b]	185
28[b]	195
140[b]	211
310[b]	219
500[b]	223

a) Selective inversion data b) Line-shape data

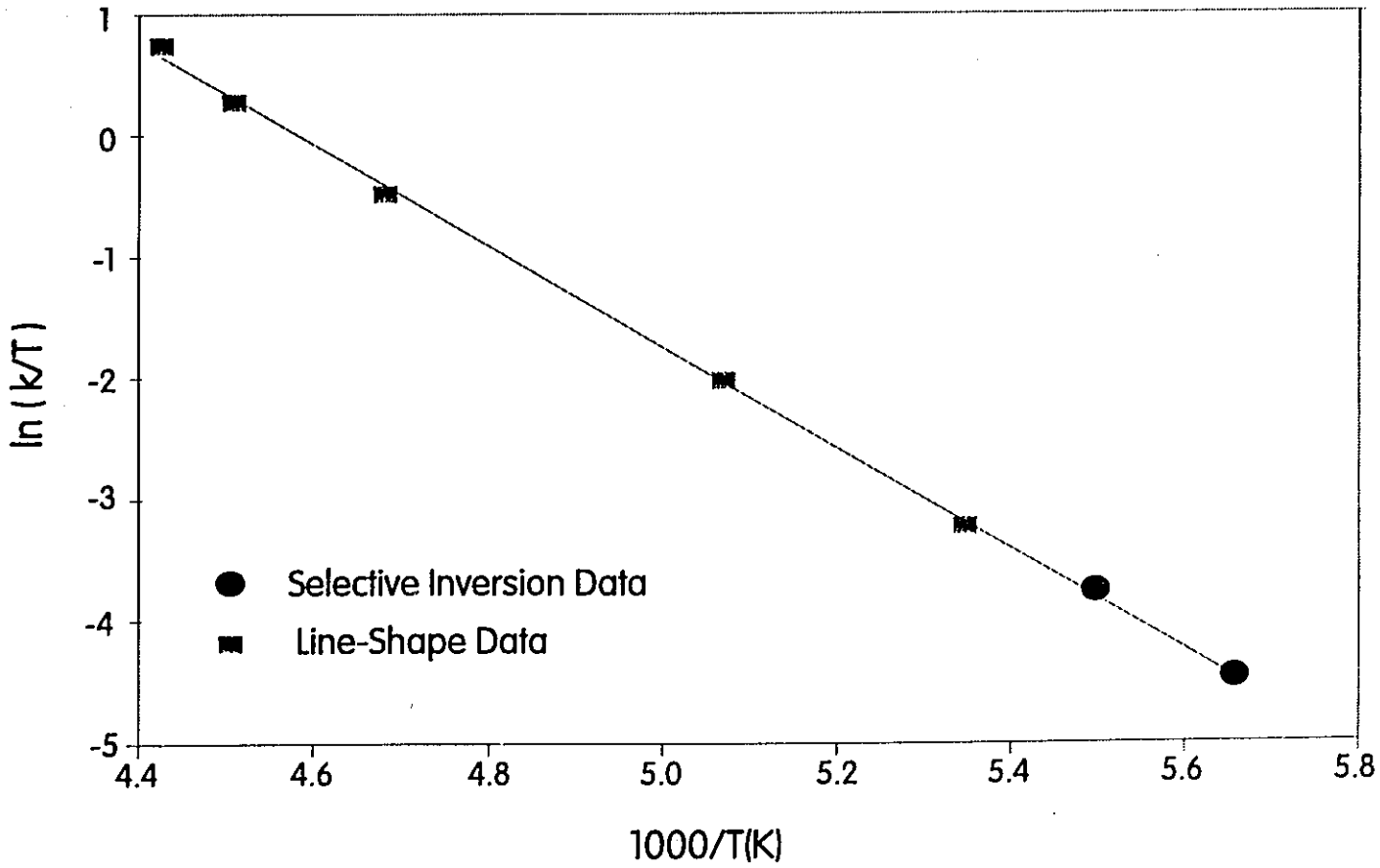

Figure 4.4 Temperature dependence of the first carbonyl rotation process for $Fe_2(CO)_6(\mu\text{-}PPh_2)(\mu\text{-}\eta^1{:}\eta^2\text{-}HC{=}CH_2)$.

Table 4.3 Temperature Dependence of the Second Carbonyl Rotation Process as Determined by a Combination of Line-Shape and Selective Inversion Data

Rate (s^{-1})	Temperature (K)
1.0[a]	220
3.4[a]	230
6.0[a]	235
1000[b]	290
1400[b]	295
1800[b]	300

a) Selective inversion data and, b) Line-shape data

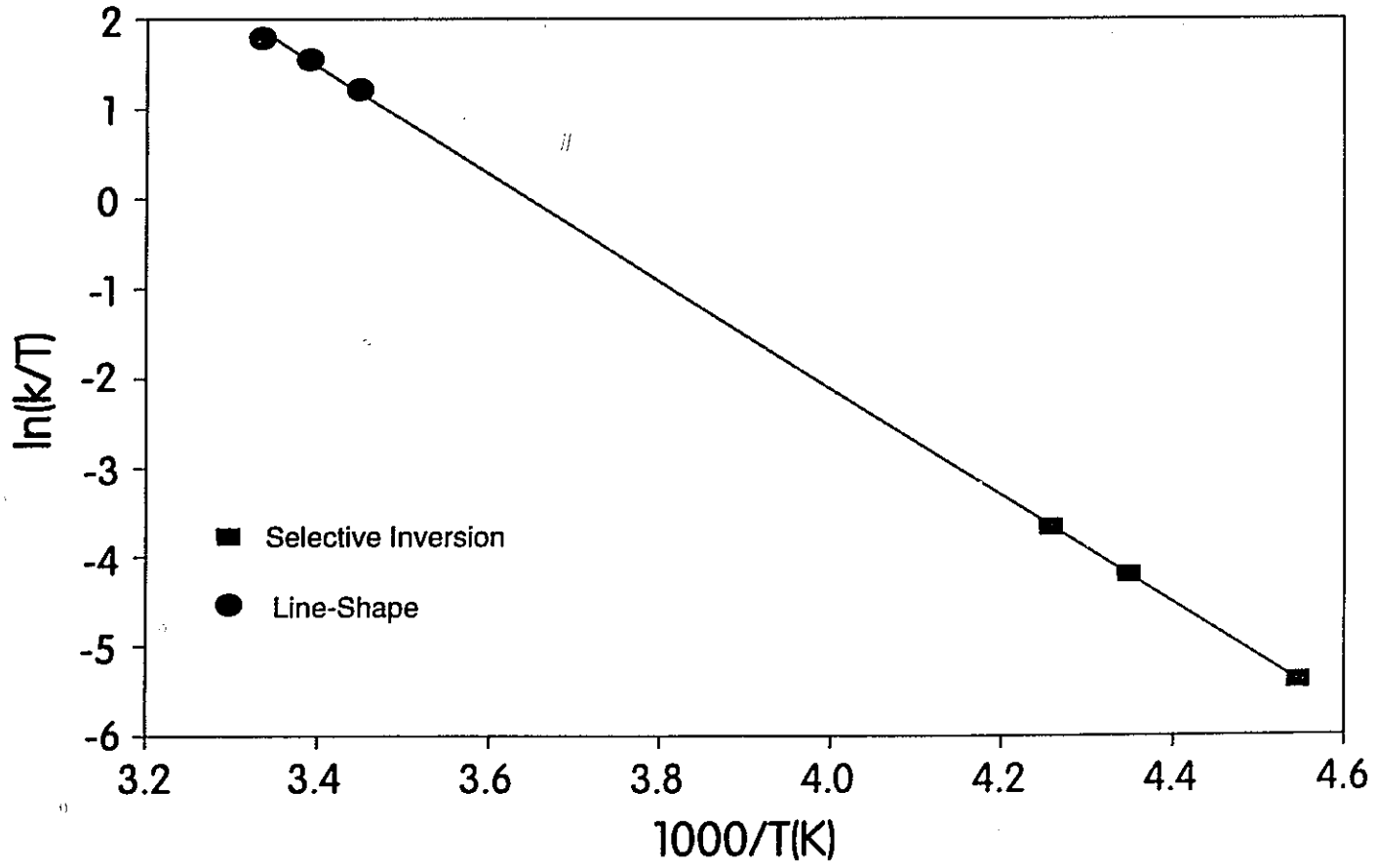

Figure 4.5 Temperature dependence of the second carbonyl rotation process for $Fe_2(CO)_6(\mu\text{-}PPh_2)(\mu\text{-}\eta^1\text{:}\eta^2\text{-}HC{=}CH2)$.

process, it is possible to use the line-shape data alone. However, the activation parameters are determined more accurately if one can determine the extreme points more accurately and extend the range of points.[2] The selective inversion data determine the very slow rates more accurately and will also define a line that can approximate the rates to facilitate the line-shape analysis.

The selective inversion studies for the second process could only be obtained over a narrow range. In this instance, it is a direct result of the presence of more than one exchange process overlapping. As one decreases the temperature, the signal from the first carbonyl set becomes more prominent and interferes with the signals corresponding to one carbonyl ligand and as one increases the temperature the carbonyl ligand with a small $^2J_{P\text{-}C}$ is too broadened to distinguish each peak of the doublet.

Line-shape analysis of the second process is hindered by the need to have accurate values for the first (carbonyl rotation on the other metal) and third (alkene motion) processes. The line-shape analysis of the first process, coupled with the selective inversion results of the second and third process gave the temperature dependence for all of the rate processes and extension of the subsequent Eyring plots allowed extrapolation of approximate rates for the coalescence region. This combination allowed the best possible rate measurements; selective inversion for the slow regime and line-shape for the coalescence region.

As expected the dramatic difference in the temperature at which each process begins translates into a large difference in the barriers. The temperature dependence of

the first process gave activation values of $\Delta H^{\ddagger} = 36 \pm 2$ (3σ) kJ mol^{-1} and $\Delta S^{\ddagger} = 0.037 \pm 0.002$ (3σ) kJ deg^{-1} mol^{-1}, while the temperature dependence for the second process gave the values of $\Delta H^{\ddagger} = 50 \pm 2$ (3σ) kJ mol^{-1} and $\Delta S^{\ddagger} = 0.016 \pm 0.002$ (3σ) kJ deg^{-1} mol^{-1}.

Aime *et al.*[70] have shown that the barrier to localized carbonyl scrambling is controlled more strongly by electronic factors rather than steric. The higher the ligand charge donor ability, the lower the barrier, as was also found with mononuclear carbonyl complexes.[72,143] In the work by Aime *et al.*, they studied the trinuclear systems $M_3(CO)_9(\mu\text{-}H)(\mu_3\text{-}\eta^1\text{:}\eta^2\text{:}\eta^2\text{-}C{\equiv}C\text{-}t\text{-}Bu)$ (M = Ru and Os) and found that the metal atom that was σ bound to the acetylenic carbon atom had the lowest barrier, while the two metal atoms that were π bound to the acetylene exhibited slower exchange. If this is accepted, then one would conclude that in $Fe_2(CO)_6(\mu\text{-}PPh_2)(\mu_2\text{-}\eta^1\text{:}\eta^2\text{-}HC{=}CH_2)$, the first carbonyl rotation occurs on the iron atom that is σ-bound to the vinyl ligand and the second carbonyl rotation occurs on the iron atom that is π-bound to the vinyl atom.

4.4 Carbonyl Scrambling in $Os_3(CO)_9(\mu\text{-}Ph_2P{=}O)(\mu_3\text{-}\eta^1\text{:}\eta^2\text{:}\eta^2C{\equiv}C\text{-}t\text{-}Bu)$

The $Os_3(CO)_9(\mu\text{-}Ph_2P{=}O)(\mu_3\text{-}\eta^1\text{:}\eta^2\text{:}\eta^2C{\equiv}C\text{-}t\text{-}Bu)$ compound exists in two isomers. The major isomer is shown in Figure 4.6a. At -40 °C, peaks of extremely low intensity corresponding to a minor isomer are observed. A 2D-EXSY experiment was undertaken and cross-peaks were observed between the minor and major peaks and this demonstrates that the two isomers are in exchange. The 2D exchange spectrum that demonstrated interconversion between the two isomers is given in Figure 4.7. The X-ray structure of

an iron analogue (Figure 4.6b) shows that the alkyne is σ and π bonded to different metal atoms and this is most likely the structure of the minor isomer.

As one increases the temperature, the two isomers are in fast exchange and the initial line-shape analysis shows exchange among three of the carbonyl signals. This is indicative of carbonyl rotation on one metal atom. Soon after this temperature, the onset of more than one exchange process occurs and the line-shapes become too complex to elucidate the exchange processes. This is complicated by the fact that assignment of the carbonyl ligands, at that point, was rather sketchy. The only carbonyl signals that could be identified were those caused by carbonyl ligands attached to the osmium atom bound to the phosphorus atom. These show $^{2}J_{P\text{-}C}$ coupling to the phosphorus atom, and these are not the three carbonyl ligands that are undergoing exchange. The exchanging carbonyl ligands must then be either those on the osmium with the σ alkyne bond, or those on the osmium atom bonded to the oxygen atom of the bridging phosphidoxo ligand.

A 2D exchange spectrum (Figure 4.8) was obtained at -20 °C to aid in identifying the exchange mechanisms and the carbonyl ligand assignment. Examination of the spectrum shows that there are four carbonyl ligands (A, B, C, G) that are in exchange. Exchange of three of the sites (A, B, C) appears to correspond to the carbonyl rotation shown in the line-shape spectrum as all three show exchange with each other. However, site B is also in exchange with site G.

This would be consistent with delocalized exchange between the two osmium atoms that are not bonded to phosphorus. The question of the actual assignment of the

carbonyl ligands still remained. Only the carbonyl ligands on the osmium bonded to the phosphorus end of the phosphidoxo ligand (D, E, F) had been identified, the other two sets (A, B, C and G, H, I) required assignment.

The set (A, B, C) has an extremely low energy barrier for the carbonyl tripodal rotation. Aime has shown that the donation of electrons from a hard base will result in a decrease in this type of barrier.[70] The oxygen portion of the phosphidoxo ligand is a hard base donor.[57] It seems highly likely then that the carbonyl ligands found on the osmium atom bound to the oxygen portion of the bridging ligand would have the lowest barrier to rotation. This, then, would place the carbonyls A, B, and C on this osmium atom, while those of G, H, and I would be found on the osmium atom sigma bonded to the acetylide.

Presumably, the delocalized exchange between sites G and B would occur *via* bridged carbonyl intermediates. This was suspected with the carbonyl scrambling observed in $Ru_3(CO)_9(\mu\text{-}H)(\mu_3\text{-}\eta^2\text{-}C{\equiv}C\text{-}t\text{-}Bu)$ but later proved incorrect by Farrugia and Rae.[24] In that particular molecule the bridging hydride is mobile and this accounts for the observed exchange. In this phosphidoxo complex, there must be delocalized carbonyl exchange. If the bridging phosphido ligand was in exchange, one would expect to see cross-peaks between all three carbonyls on each metal bridged by the phoshphido ligand, and not just on one site of each metal, as was observed. In addition, the phosphidoxo ligand is not expected to be as mobile as a hydride ligand.

The fact that the delocalized transfer was observed as a low barrier process is not

a)

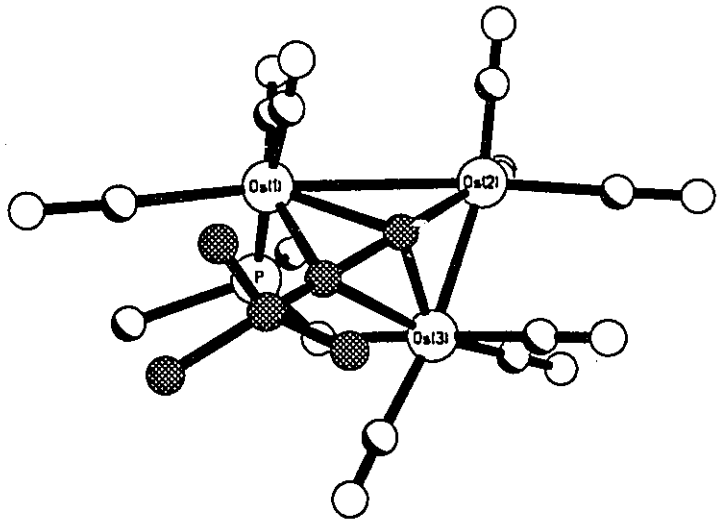

b)

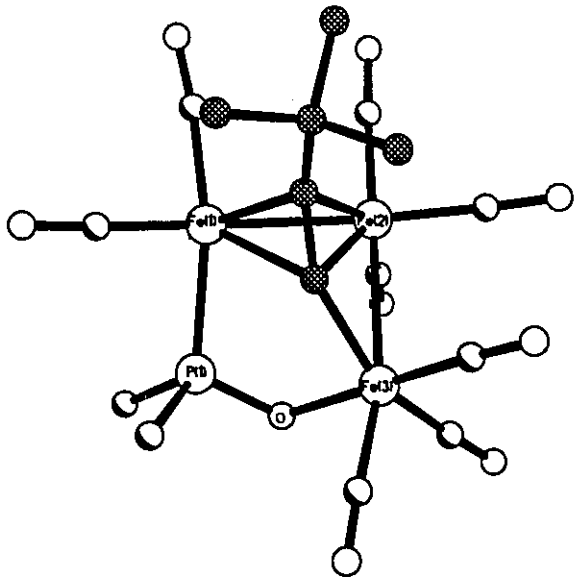

Figure 4.6 Structures of $M_3(CO)_9(\mu\text{-}Ph_2P{=}O)(\mu_3\text{-}\eta^1{:}\eta^2{:}\eta^2\text{-}CC\text{-}t\text{-}Bu)$ a) Major isomer of $Os_3(CO)_9(\mu\text{-}Ph_2P{=}O)(\mu_3\text{-}\eta^1{:}\eta^2{:}\eta^2\text{-}CC\text{-}t\text{-}Bu)$ in which the acetylide is σ bound to Os(2) b) Major isomer of $Fe_3(CO)_9(\mu\text{-}Ph_2P{=}O)(\mu_3\text{-}\eta^1{:}\eta^2{:}\eta^2\text{-}CC\text{-}t\text{-}Bu)$ in which the acetylide is σ bound to Fe(3).[57] This is believed to be a possible structure for the minor isomer of the osmium complex.

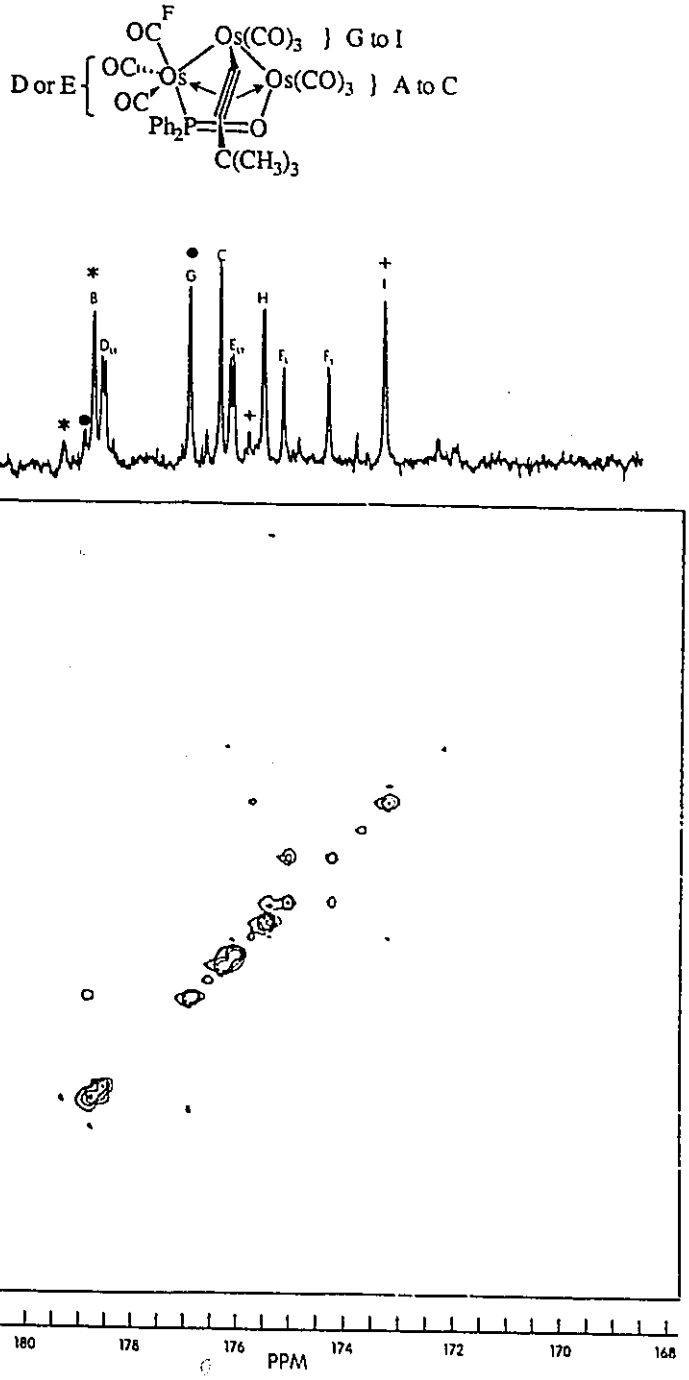

Figure 4.7 $^{13}C\{^1H\}$ 2D-EXSY carbonyl spectrum of $Os_3(CO)_9(\mu\text{-}Ph_2P{=}O)(\mu_3\text{-}\eta^1{:}\eta^2{:}\eta^2\text{-}C{\equiv}C\text{-}t\text{-}Bu)$ at 233 K. Cross-peaks between the major and minor peaks demonstrate isomer exchange. The assignment of carbonyl ligands is shown from the sketch of the molecule above the spectrum.

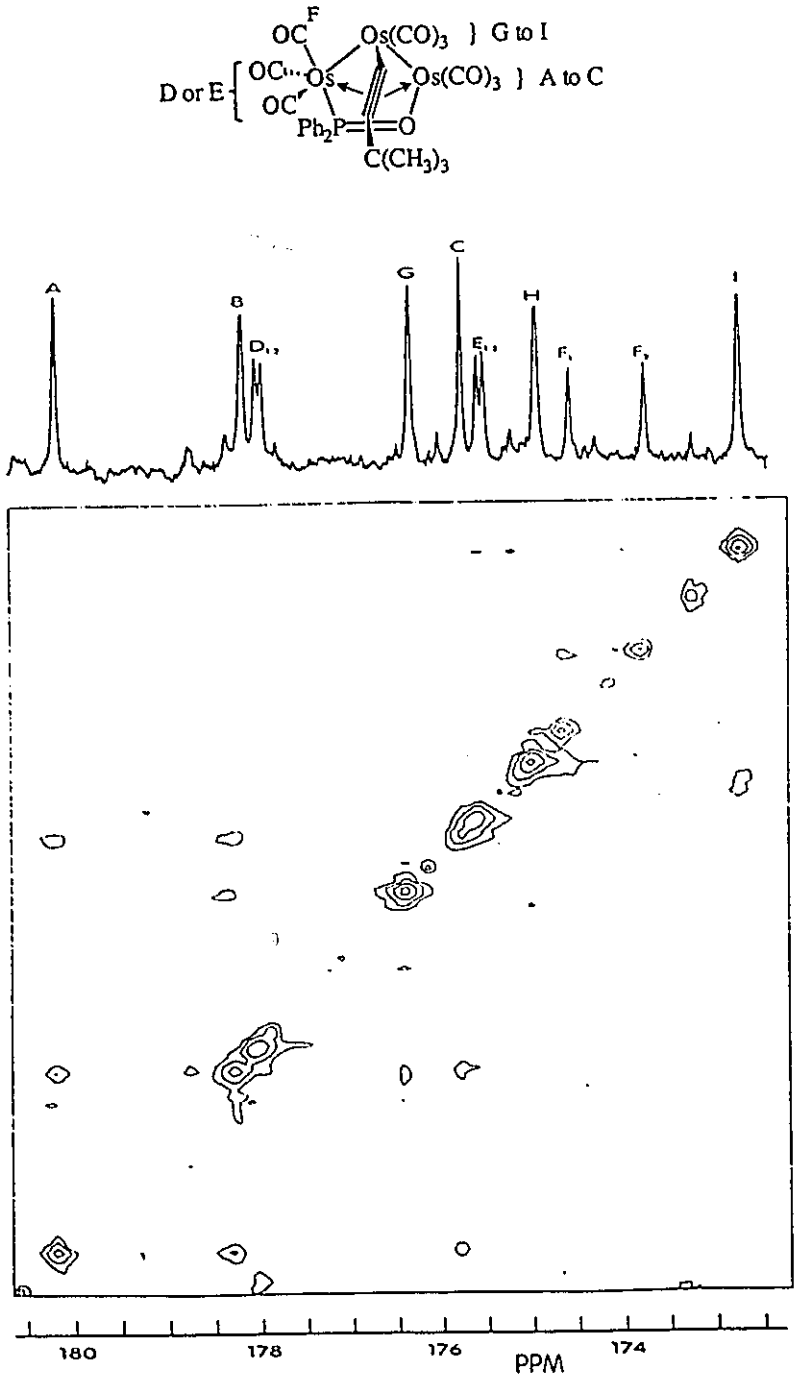

Figure 4.8 $^{13}C\{^1H\}$ 2D-EXSY carbonyl spectrum of $Os_3(CO)_9(\mu\text{-}Ph_2P{=}O)(\mu_3\text{-}\eta^1{:}\eta^2{:}\eta^2\text{-}C{\equiv}C\text{-}t\text{-}Bu)$ at 253 K. Both delocalized and localized carbonyl exchange is observed in the spectrum. The assignment of carbonyl ligands is shown from the sketch of the molecule above the spectrum.

all that difficult to rationalize chemically. Phosphine oxides are known to labilize metal carbonyl bonds and this particular ligand has been used as a reagent to facilitate ^{13}CO labelling.[144]

This is a prime example of the usefulness of the 2D experiment for mechanistic determination and assignment of signals. The delocalized CO scrambling was not expected, but the 2D spectrum offers remarkable evidence. Further studies are required to determine when the other processes begin and also to quantitate the rates.

4.5 Experimental Section

4.5.1 Preparation of the NMR Samples

The NMR sample of compound **1**, $Ru_2(CO)_6(\mu\text{-}PPh_2)(\mu_2\text{-}\eta^1\text{:}\eta^2\text{-}C{\equiv}C\text{-}i\text{-}Pr)$ was prepared as described in the experimental section of Chapter 2.

Approximately 200 mg $Fe_2(CO)_6(\mu\text{-}PPh_2)(\mu_2\text{-}\eta^1\text{:}\eta^2\text{-}HC{=}CH_2)$, **2**, was dissolved in 1 mL of deuterated chloroform-*d* (MSD Isotopes, 99.8% D) and placed in a 5 mm thin wall NMR tube. A stream of nitrogen gas was passed through the sample for a few minutes to deoxygenate it.

Approximately 100 mg of $Os_3(CO)_9(\mu\text{-}PPh_2)(\mu_2\text{-}\eta^1\text{:}\eta^2\text{-}C{\equiv}C\text{-}t\text{-}Bu)$, **3**, was dissolved in 1 mL of deuterated chloroform-d_8 (MSD Isotopes, 99.8% D) and placed in a 5 mm thin wall NMR tube. A stream of nitrogen gas was passed through the sample for a few minutes to deoxygenate it.

4.5.2 Selective Inversion Experiments

The selective inversion experiments were performed as described in Chapter 2 using the pulse program INVREC2P.AUR; only the differences in procedure are given. The values for the pulse sequence parameters that varied with experiment are found in Tables 4.4-4.6. The spin-lattice relaxation rate (T_1^{-1}) of metal carbonyl signals has a large chemical shielding anisotropy (CSA) contribution.[89-91] The CSA relaxation rate increases with the field strength.[1] The requirement that the relaxation rate be slightly less than the chemical exchange necessitated the use of an intermediate field strength. Use of a 500 MHz spectrometer for these experiments would not have been successful.

The selective inversion data were analysed with the program FLOPSI (a C version of SIFIT[19]). Normally, the ^{13}C relaxation rates were not allowed to vary, but were fixed to the measured values. A concerted mechanism was entered into the exchange map. This had the effect of constraining all three of the individual carbonyl rotations to be equal.

$Ru_2(CO)_6(\mu\text{-}PPh_2)(\mu_2\text{-}\eta^1\text{:}\eta^2\text{-}C{\equiv}C\text{-}i\text{-}Pr)$

For all of the experiments, O1 was placed at 14702.50 Hz , D1 was set to 15 seconds and the τ delay was set to 0.033 of a second. The Fourier transform size (SI) and acquisition size (TD) were set to 4K. The spectral width was set to 1326.26 Hz. This gave an acquisition time of 1.54 seconds with a digital resolution of 0.65 Hz/pt. The number of scans was 64.

Table 4.4A Parameters for the Carbonyl Rotation Process Selective Inversion Experiments for $Ru_2(CO)_6(\mu\text{-}PPh_2)(\mu_2\text{-}\eta^1\text{:}\eta^2\text{-}C{\equiv}C\text{-}i\text{-}Pr)$

Temperature (K)	Variable Delays (s)
260	0.001, 12.0, 0.3, 0.15, 0.7, 0.05, 0.35, 0.025, 0.9, 0.45, 0.40, 1.4, 2.0, 1.3, 0.25, 0.95, 1.5, 0.1, 1.1, 1.75, 1.0, 0.2, 0.5, 0.8, 0.6, 1.2, 5.0
265	0.001, 15.0, 0.3, 0.15, 0.7, 0.05, 0.35, 0.025, 0.9, 0.45, 0.40, 1.4, 2.0, 1.3, 0.25, 0.95, 1.5, 0.1, 1.1, 1.75, 1.0, 0.2, 0.5, 0.8, 0.6, 1.2, 5.0
270	0.001, 15.0, 0.3, 0.15, 0.7, 0.05, 0.35, 0.025, 0.9, 0.45, 0.40, 1.4, 2.0, 1.3, 0.25, 0.95, 1.5, 0.1, 1.1, 1.75, 1.0, 0.2, 0.5, 0.8, 0.6, 1.2, 5.0
275	0.001, 15.0, 0.3, 0.15, 0.7, 0.05, 0.35, 0.025, 0.9, 0.45, 0.40, 1.4, 2.0, 1.3, 0.25, 0.95, 1.5, 0.1, 1.1, 1.75, 1.0, 0.2, 0.5, 0.8, 0.6, 1.2, 5.0
280	0.001, 15.0, 0.15, 0.3, 0.7, 0.05, 0.35, 0.025, 0.9, 0.45, 0.075, 0.4, 0.75, 2.0, 0.85, 0.25, 0.95, 0.65, 0.1, 1.1, 0.55, 0.275, 1.0, 0.2, 0.5, 0.8, 0.6
285	0.001, 15.0, 0.15, 0.3, 0.7, 0.05, 0.35, 0.025, 0.9, 0.45, 0.075, 0.4, 2.0, 0.25, 0.65, 0.1, 0.55, 0.275, 1.0, 0.2, 0.5, 0.8, 0.6
290	0.001, 15.0, 0.1, 0.5, 0.025, 0.7, 1.0, 0.15, 2.0, 0.4, 0.05, 0.01, 0.225, 5.0, 0.035, 0.25, 0.075, 0.275, 0.175, 1.25, 0.9, 0.3, 0.03, 0.2
300	0.001, 15.0, 0.5, 0.1, 1.0, 0.25, 0.75, 0.15, 2.0, 0.4, 0.05, 0.35, 0.6, 3.0, 0.4, 0.8, 0.075, 0.175, 0.45, 0.9, 0.3, 1.5, 1.1, 0.2,

Table 4.4B Spin-Lattice Relaxation Rates for Carbonyl Rotation Process of $Ru_2(CO)_6(\mu\text{-}PPh_2)(\mu_2\text{-}\eta^1\text{:}\eta^2\text{-}C{\equiv}C\text{-}i\text{-}Pr)$

Temperature (K)	Relaxation Rates for each Site (s^{-1})
260	0.66, 0.68, 0.57, 0.55, 0.55, 0.55
265*	0.55, 0.55, 0.51, 0.51, 0.51, 0.51
270*	0.51, 0.51, 0.47, 0.47, 0.47, 0.47
275	0.47, 0.47, 0.43, 0.43, 0.43, 0.43
280	0.42, 0.43, 0.41, 0.40, 0.40, 0.41
285	0.38, 0.39, 0.38, 0.38, 0.37, 0.37
290	0.34, 0.35, 0.34, 0.34, 0.34, 0.33
300	0.32, 0.32, 0.32, 0.31, 0.31, 0.32

*extrapolated

Separate T_1 experiments were performed for most experiments, in some cases the values were extrapolated. The τ (or D2) value for the T_1 was set to 0.00001 s. The T_1 values are given in Table 4.4B. A separate ^{31}P spin-lattice relaxation rate was measured at T=300 K and was found to be 0.32 s^{-1}. The selective inversion data were analyzed with the program FLOPSI. The ^{13}C spin-lattice relaxation time was fixed to the measured values while the all of the other parameters were allowed to vary. A concerted mechanism was entered in the exchange map. This constrained all three of the individual carbonyl rotations to be equal.

$Fe_2(CO)_6(\mu\text{-}PPh_2)(\mu_2\text{-}\eta^1\text{:}\eta^2\text{-}HC{=}CH_2)$

First Carbonyl Rotation Process

The O1 was set to 16111.93 Hz for all experiments and D1 was set to 15 seconds. The Fourier transform size (SI) and acquisition size (TD) was set to 4K. The spectral width was set to 976.56 Hz. This gave an acquisition time of 2.1 s with a digital resolution of 0.48 Hz/pt. The number of scans was set to 1046.

A separate T_1 experiment for each temperature was performed. The τ (or D2) value was set to 0.00001 s. The results are given in Table 4.5B.

Table 4.5A Parameters for the First Carbonyl Rotation Process Selective Inversion Experiments of $Fe_2(CO)_6(\mu\text{-}PPh_2)(\mu_2\text{-}\eta^1\text{:}\eta^2\text{-}HC{=}CH_2)$

Temperature (K)	D2 (τ) (s)	Variable Delays
175	0.030	2.5, 0.025, 0.1, 0.05, 0.15, 0.06, 0.125, 0.085, 0.2, 0.175, 0.5, 0.25, 1.0, 0.0001
180	0.032	0.0001, 2.0, 0.075, 0.025, 0.1, 0.05, 0.15, 0.06, 0.125, 0.085, 0.2, 0.5, 0.25, 0.75

Table 4.5B The Spin-Lattice Relaxation Rates (T_1^{-1}) for the First Carbonyl Rotation Experiments for $Fe_2(CO)_6(\mu\text{-}PPh_2)(\mu_2\text{-}\eta^1\text{:}\eta^2\text{-}HC{=}CH_2)$

Temperature (K)	Relaxation Rate for each site(s)
175	4.4, 3.8, 3.1, 3.2, 3.5, 3.5
180	2.1, 2.4, 2.8, 2.3, 2.9, 2.8

The Second Carbonyl Rotation Process

The O1 was set to 15697.47 Hz for all experiments, D1 was set to 5 s and the τ delay was set to 0.025 s. The Fourier transform size (SI) and acquisition size (TD) was set to 2K. The spectral width was set to 1199 Hz. This gave an acquisition time of 0.85 s with a digital resolution of 1.17 Hz/pt. The number of scans was 778.

A separate T_1 experiment for each temperature was performed. The τ (or D2) value was set to 0.00001 s. The results are given in the Table 4.6B.

4.5.4 Line-Shape Data

The line-shape data were collected using the same samples as for the selective inversion experiments on the Bruker AC-300 MHz spectrometer. The 10 mm broad band probe was used for the first carbonyl rotation process for compound **2**, and the 5 mm quadrinuclear probe was used for all of the other processes. Both probes were tuned to carbon (75.47 MHz). The sweep width and O1 values were chosen so as to observe only the carbonyl region. These values are given in Table 4.7. The acquired data was transferred to the PC *via* NMRLINK and were processed with NMR286. This program can export the spectra in HPGL format. The calculated spectra were generated using the program EXCHANGE. The natural line-width was assumed to be 2.5 Hz. Both the calculated and experimental line-shape spectra were imported into CORELDRAW, one upon the other, to facilitate matching.

Table 4.6A Parameters for Second Carbonyl Rotation Process Selective Inversion Experiments for $Fe_2(CO)_6(\mu\text{-}PPh_2)(\mu_2\text{-}\eta^1\text{:}\eta^2\text{-}HC{=}CH_2)$

Temperature (K)	Variable Delays (s)
220	0.001, 5.0, 0.05, 0.2, 0.6, 0.1, 1.0, 0.15, 0.4, 0.8, 0.08, 0.25, 0.025, 0.3
230	0.001, 5.0, 0.05, 0.1, 0.08, 0.15, 0.025, 0.3, 0.125, 0.35, 0.25, 0.8, 0.2, 0.5, 1.0, 3.0
235	0.001, 5.0, 0.025, 0.1, 0.08, 0.15, 0.05, 0.175, 0.01, 0.3, 0.125, 0.8, 0.2, 0.5, 0.25, 1.0

Table 4.6B The Spin-Lattice Relaxation Rates (T_1^{-1}) for the Second Carbonyl Rotation Experiments for $Fe_2(CO)_6(\mu\text{-}PPh_2)(\mu_2\text{-}\eta^1\text{:}\eta^2\text{-}HC{=}CH_2)$

Temperature (K)	Relaxation Rate for each site (s^{-1})
220	0.86, 0.85, 0.87, 0.83, 0.80, 0.86
235	0.89, 0.82, 0.77, 0.76, 0.73, 0.81

Table 4.7 Line-Shape Acquisition Parameters

Compound	Size (K)	Sweep Width (Hz)	Offset Frequency (O1)
1	4	943.4	14555.64
2- First Process	4	976.56	16111.93
2- Second Process	2	1199	15697.47

4.5.5 2D Exchange Spectroscopy of $Os_3(CO)_9(\mu\text{-}PPh_2)(\mu_2\text{-}\eta^1\text{:}\eta^2\text{-}C{\equiv}C\text{-}t\text{-}Bu)$

The 2D experiments were recorded on a Bruker AM-500 MHz spectrometer using a 5 mm $^{13}C/^{1}H$ probe tuned to carbon at a frequency of 125 MHz. A phase sensitive pulse program NOESYPH.AUR was used to obtain the EXSY spectrum. The pulse sequence is as follows: D1 - 90° - t_1 - 90°- t_m - 90° -t_2 -acquire

D1 is the relaxation delay, t_1 and t_2 are a function of the size of the f_1 and f_2 dimension respectively. The mixing time, t_m, is the delay in which the chemical exchange occurs. In order to obtain a square matrix $f_2=2xf_1$ and $SW2=2xSW_1$.

Isomer Exchange

The probe temperature was allowed to equilibrate at 233 K. NE was set to 128 W (words), and SI2 was then set to 256 W to ensure a square matrix. The sweep width in f_1 was 915.751 Hz. A relaxation delay, D_1, of 1.0 s was used and the optimal mixing time (D9) was found to be 0.15 s. The number of scans was set to 256.

Carbonyl Rotation

The experimental temperature was set to 250 K. The NE was set to 256 W and SI2 was then 512W. The sweep width in f_1 was 1057.08 Hz. A relaxation delay, D1, of 1.0 s was used and the optimal mixing time (D9) was found to be 0.10 s. The number of scans was set to 256.

4.6 Conclusions

The single selective inversion technique successfully determined the temperature dependence of the rates. In all systems, the line-shape analysis was in agreement with the single selective inversion data.

Normally, the temperature range for which magnetization transfer data can be obtained is narrow and should be combined with that of the line-shape analysis to increase the confidence in the determined activation parameters. In the study of carbonyl ligand rotation in $Ru_2(CO)_6(\mu\text{-}PPh_2)(\mu_2\text{-}\eta^1\text{:}\eta^2\text{-}C{\equiv}C\text{-}i\text{-}Pr)$, the selective inversion data were obtained over a relatively wide temperature range (40 K). However, the line-shape analysis was performed to confirm the selective inversion data. The combination of data from both methods gave the following activation parameters $\Delta H^{\ddagger}$= 59 ± (3) kJ mol^{-1} and $\Delta S^{\ddagger}$ = -0.035 ± (0.003) kJ deg^{-1} mol^{-1}. These errors are quoted as ± 3 σ.

In the $Fe_2(CO)_6(\mu\text{-}PPh_2)(\mu_2\text{-}\eta^1\text{:}\eta^2\text{-}HC{=}CH_2)$ complex, two of the three chemical exchange processes are carbonyl ligand rotations. The three exchange processes are not well separated and interfere with each other in both the line-shape and selective-inversion analysis. Single selective inversion experiments were obtained over a narrow range to obtain the temperature dependence of the rate. Extrapolation of this dependence into the intermediate temperature regime gave approximate rate values for the line-shape analysis and permitted successful fitting of the complicated line-shape spectra.

The fact that the extrapolated values were accurately determined from such a narrow temperature dependence demonstrates that single selective inversion technique is

capable of providing sufficiently precise rate values.

The line-shape and selective inversion data were combined for both $Fe_2(CO)_6(\mu\text{-}PPh_2)(\mu_2\text{-}\eta^1\text{:}\eta^2\text{-}HC{=}CH_2)$ carbonyl rotation processes to determine the activation parameters. The activation parameters for both processes are as follows: 1) first process, $\Delta H^{\ddagger} = 36 \pm 2$ (3σ) kJ mol^{-1} and $\Delta S^{\ddagger} = 0.037 \pm 0.002$ (3σ) kJ mol^{-1} and 2) second process, $\Delta H^{\ddagger} = 50 \pm 2$ (3σ) kJ mol^{-1} and $\Delta S^{\ddagger} = 0.016 \pm 0.002$ (3σ) kJ mol^{-1}.

In the $Os_3(CO)_9(\mu\text{-}PPh_2)(\mu_3\text{-}\eta^1\text{:}\eta^2\text{:}\eta^2\text{-}C{\equiv}C\text{-}t\text{-}Bu)$ complex, 2D-EXSY qualitative experiments permitted the detection of a minor isomer in exchange with the major isomer at low temperature (233 K). At higher temperature (253 K), the 2D-EXSY spectrum demonstrated that both delocalized and localized carbonyl exchange processes are occurring. The delocalized exchange was not expected and demonstrates the effectiveness of the 2D experiment for exchange map determination.

CHAPTER 5

ALKENE σ TO π INTERCONVERSION

5.1 Introduction

Fluxionality of the vinyl ligand in $[(\mu\text{-H})Os_3(CO)_{10}(\mu_2\text{-}\eta^2\text{:}\eta^1\text{-HC=CH}_2)$ was first observed by Shapley *et al.* in 1975.[79] In this molecule, the vinyl ligand interconverts between the σ and π bonding modes at each respective metal atom. This motion, as shown in Figure 1.6, is described as a "windshield wiper". Later, other unsaturated organic ligands such as alkynes,[40,73-77,145-147] cyanide,[148-9] and metallocyclic ligands (such as $[RNCH_2HC=CR']$, [RNCH=CR'] or [OC(O)RC=CR] where the N or O atom also forms a bridge between the metal atoms)[150-1] were also observed to undergo this fluxional process.

Most of the dynamic NMR studies on this motion have used simple one point coalescence data to determine the barrier. In 1987, Cherkas *et al.*[40] attempted more rigorous dynamic studies using line-shape analysis. They examined a series of phosphido-bridged dimetallic carbonyls $M_2(CO)_6(\mu_2\text{-}\eta^2\text{:}\eta^1\text{-C}\equiv\text{CR})(\mu\text{-PPh}_2)$ M=Fe, Ru, Os and R=Ph, *t*-Bu, *i*-Pr in an attempt to determine the effect of the metal and of the R group. Since it

is believed that there is a correspondence between the fluxionality and the chemical reactivity, it was hoped that a more careful study of the dynamics would allow prediction of the reactivity.

The previous coalescence temperature dynamic studies had given barrier values of 43.1 kJ mol^{-1}, 46.9 kJ mol^{-1}, and 47.1 kJ mol^{-1} as one goes down the triad. The more rigorous line-shape study for the ruthenium and osmium complexes demonstrated a greater increase in the barrier down the triad with values of 49.4 and 52.3 kJ mol^{-1} respectively. In the corresponding iron complex, the carbonyl rotation occurs concurrently with the windshield wiper motion resulting in a complex line-shape that is not easily fit, and as a result the lineshape analysis for that molecule was not attempted in the study.

Alkyne systems, in general, show less variance in the barrier to the σ to π interconversion than with vinyl systems with the barrier consistently ranging from 42 to 55 kJ mol^{-1}.[40,74-78] Vinyl systems were thought to behave similarly. Casual inspection of the room temperature carbonyl spectrum of $Fe_2(CO)_6(\mu\text{-}PPh_2)(\mu_2\text{-}\eta^1\text{:}\eta^2\text{-}HC{=}CH_2)$ demonstrated that the barrier for this system was considerably higher.[82] This barrier was determined by use of both line-shape and selective inversion experiments and is presented along with a rationale for the difference in fluxional behaviour between high and low barrier systems.

5.2 Results and Discussion

The line-shape data were analyzed by following the same approach as with the

carbonyl rotation processes. In order to determine the effect of the rate of the alkene motion on the line-shape, the first and second process rates for the temperature range had to be fixed. It was also helpful to begin with reasonable estimates of the rates for the process of interest as well. Selective inversion data were first obtained for the vinyl interconversion. These were difficult to obtain as only one site (representing the carbonyl ligands in fast exchange as a result of the first exchange process) had a sharp signal, the other site representing the second set of carbonyl ligands was barely above coalescence (Figure 5.1). The broad signal was inverted as much as possible through use of the pulse sequence described in Chapter 2. The transmitter was set on the maximum of the broad peak while the pulse delay was set to one over twice the frequency difference between the maximum of both signals. The equilibrium and initial magnetizations of the partially inverted site were estimated and fit. Only the sharp signal could be fit using ONESITE (a modified version of FLOPSI) over the full range of magnetization intensities as a function of the variable delay, to extract the exchange rate.

Again, with more than one exchange process present in the system, this technique could only be applied to a narrow temperature range. As one increased the temperature, the sharp signal broadened and as one decreased the temperature, the other process of the second carbonyl rotation was slowed, and this signal became too broad to invert. The line-shape data were then obtained and combined with the selective inversion analysis to extend the range for the temperature dependence. The results are found in Table 5.1 and Figure 5.2.

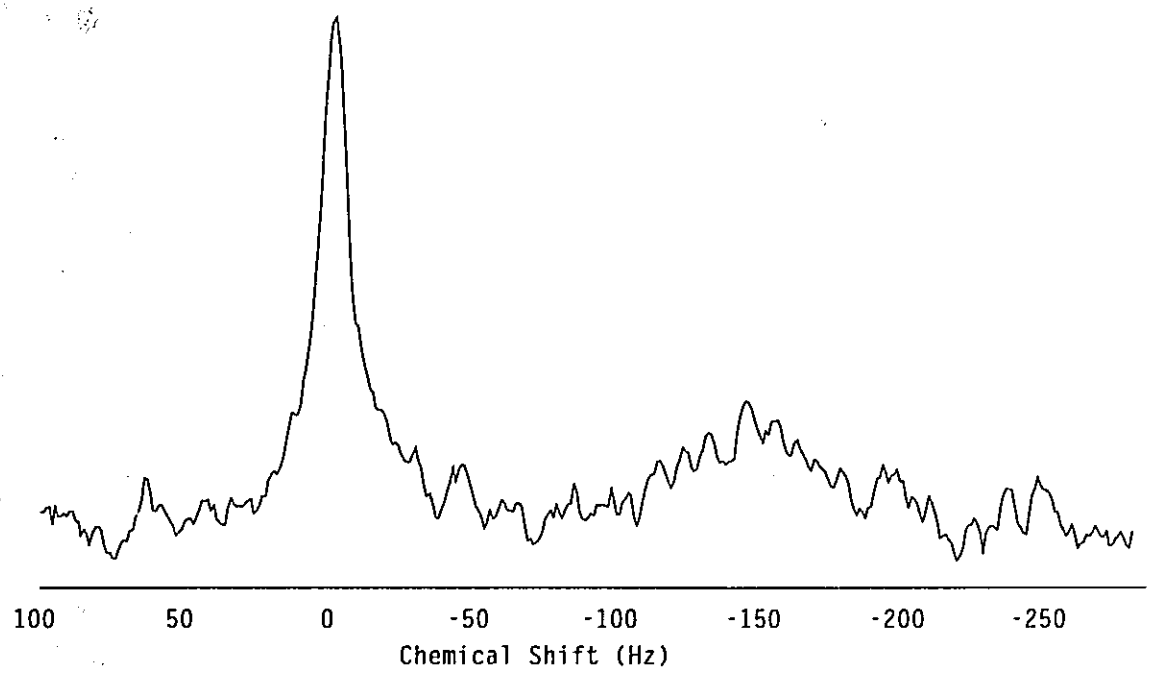

Figure 5.1 Spectrum of $Fe_2(CO)_6(\mu\text{-}PPh_2)(\mu\text{-}\eta^1{:}\eta^2\text{-}HC{=}CH_2)$ at 300K. The sharp peak represents the carbonyl ligands that are in fast exchange, slightly broadened by the vinyl windshield wiper process. The very broad peak represents the carbonyl ligands on the other iron atom. At temperatures lower than 290K, this peak is too broad to invert. Even at 300K, the rate of the vinyl exchange is slightly higher than desirable.

Table 5.1 Temperature Dependence on the Rate of the "Windshield Wiper" Exchange of the Vinyl Ligand as Determined by a Combination of Line-Shape and Selective Inversion Data

Rate (s^{-1})	Temperature (K)
9.3[a]	290
9[b]	290
16.3[a]	295
16[b]	295
33.1[a]	300
31[b]	300
80[b]	310
225[b]	325

a) selective inversion data and b) line-shape data

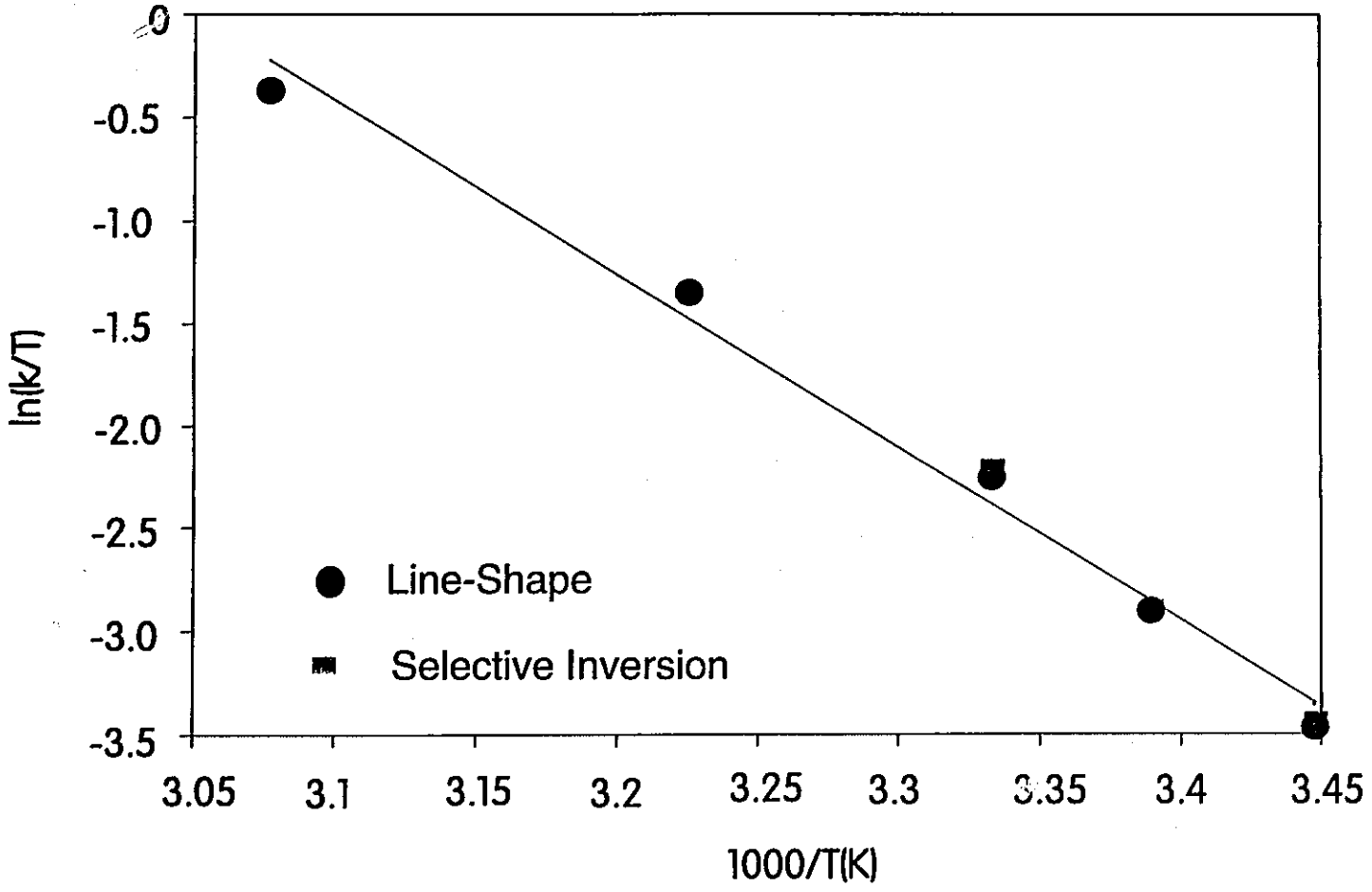

Figure 5.2 Temperature dependence of the vinyl σ to π interconversion process. Both the line-shape and selective inversion data are combined.

The combined line-shape and selective inversion data gave activation parameters of $\Delta H^{\ddagger} = 71 \pm 9$ (3σ) kJ mol^{-1} and $\Delta S^{\ddagger} = 0.017 \pm 0.003$ (3σ) kJ deg^{-1} mol^{-1}. In this case, the combination of data did not give as precise a line as with the first or second exchange process. Possible reasons for this include the need to extend the Eyring plots further from the points at which the data were collected and the unconventional use of both broad and narrow signals for the selective inversion experiment. The exchange rates for the selective inversion data are slightly outside the range that one ideally obtains. This is most noticeable for the third selective inversion data point as the exchange rate is too fast in comparison to the relaxation rate. Although, the data are not as precise, it is mostly likely a better representation of the barrier. By use of the selective inversion data alone, the barrier would have been calculated at 88 kJ mol^{-1}, which is rather extreme. However, if one ignores the third point of the selective inversion data both sets of data agree reasonably well.

The barrier for the vinyl σ to π interconversion is unusually high in comparison with other alkene and alkyne complexes that exhibit this motion. The fluxional behaviour of the alkynyl ligands is extremely consistent. There have been no examples of barriers outside the range of 42 to 55 kJ mol^{-1}. Until early 1992, it was thought that the alkenyl barriers behaved similarly. The original work by Shapley determined a barrier of 47.3 kJ mol^{-1} for a stilbenyl ligand and 43.1 kJ mol^{-1} for the vinyl ligand.[79] Subsequent work by Nubel and Brown determined barriers for rhenium binuclear complexes of 53.1 and 41.8 kJ mol^{-1} respectively with the alkenyl ligands -EtC=CH_2 and -HC=CHEt.[80] It should be

noted that these values were determined by the one point coalescence method. A more recent paper by Seyferth with a very similar compound, $Fe_2(CO)_6(\mu\text{-}SEt)(\mu\text{-}\eta^1{:}\eta^2\text{-}MeC{=}CH_2)$, also shows fast exchange at room temperature.[152] Most of the work that followed on the windshield wiper process involved alkynyl ligands that showed little deviation in the barrier.

However, the high barrier observed in compound **2**, along with several of its analogues was unexpected and led to a literature search for other windshield wiper systems that could aid in the development of a rationale for this behaviour. Other papers on alkenyl systems that show similar behaviour were found in the recent literature.

Hogarth *et al.*[84] also observed a high barrier with similar iron binuclear systems, $Fe_2(CO)_4(\mu\text{-}\eta^1{:}\eta^2\text{-}RC{=}CH_2)(\mu\text{-}PPh_2)(dppm)$ where R=Me (**4**) or Ph (**5**) and the dppm (dppm= CH_2‿PPh_2) can be in either a *cis* (**4a** and **5a**) or *trans* (**4b** and **5b**) configuration with respect to the other phosphido bridge (refer to Table 5.4). The fluxionality of these systems was monitored through the ^{31}P NMR signals of the dppm group. Two signals corresponding to the asymmetrical chemical environments of the phosphines were observed in the dppm ligand as a result of the difference in the σ and π bonding modes.

The 1-methylvinyl complexes are both in slow exchange at room temperature with considerable broadening of the two signals. The signals collapse at 80 °C, but the compounds decompose significantly shortly thereafter. The 1-phenylvinyl complexes show a marked difference in the barrier between isomers. The *trans* isomer is in fast exchange at room temperature, with an estimate of the barrier being 45 kJ mol^{-1}, while the *cis*

isomer has a barrier estimated at 63 kJ mol^{-1}.

Both the orientation of the dppm ligand and the substituent on the α carbon play a role in the barrier. It is thought that the difference is caused by steric effects. In the *cis* isomer, the phenyl substituent is directed away from all of the phenyl groups on the phosphido ligands, whereas in the *trans* isomer this interaction is expected to be considerable. In other words, the system relieves stress by being fluxional. This could also be an explanation for the slow *trans* methyl complex and the fast *trans* phenyl complex since the methyl substituent is smaller than the phenyl substituent.

Another example of an alkenyl complex with a high barrier was reported by Tiripicchio *et al.*[78] and involved the binuclear species $Mn_2(\mu\text{-}H)(\mu,\eta^1{:}\eta^2\text{-}CR{=}CH_2)(CO)_6(dppm)$ where R = Ph or H. Again, ^{31}P NMR signals of the dppm ligand was used to monitor the fluxionality of the systems. The 1-phenyl analogue is rigid at room temperature, showing two distinct environments, while the vinyl analogue shows only one signal demonstrating fluxionality at that temperature. At -50 °C, the process is frozen out and two signals are observed. The corresponding alkynyl analogues show no differentiation in the barrier upon substitution on the ligand and are fluxional at room temperature.

Steric constraints are evoked to explain the difference in behaviour between the vinyl and the 1-phenylvinyl complexes, this time however, in the opposite sense. Tirippichio *et al.*[78] propose that it is likely that the bulk of the phenyl group in the α position is responsible for its stereochemical rigidity. In other words, the bulkier the

substituent the more that it is prefers to stay in one favourable position. This is in direct contradiction to the explanation given by Hogarth *et al.*.[84] It is of interest that of the two systems, it is the vinyl system that is fluxional since this is not the case with the vinyl ligand in $Fe(CO)_6(\mu\text{-}PPh_2)(\mu_2\text{-}\eta^1\text{:}\eta^2\text{-}HC{=}CH_2)$.

Other work in the recent literature involving asymmetric complexes of the type $Ru_2\{\mu\text{-}O{=}C(NMe_2,\mu_2\text{-}\eta^1\text{:}\eta^2\text{-}C(Ph){=}CR\}(CO)_5(PPh_3)$ where R=Ph or H noticed barrier differentiation upon β substitution.[153] In particular, it is noted that the windshield wiper was stopped by substitution of an H for a Ph group. These complexes are asymmetric so care must be taken in comparing them to the other systems. Not only does the σ to π interconversion involve a change between degenerate and nondegenerate isomerization, but now each metal is distinguished by more than one type of asymmetrically bound ligand. However, since they are comparing two systems that differ only by a substituent on the vinyl group, this work has relevance to this discussion. The explanation that was given for the difference in the barrier was that during the transition state the β carbon atom would become electron deficient. This is based on work by Hoffmann, in which he determined that during the transition state, the ring formed by the two metal atoms and the bridging carbon would take on a negative charge while the C_β would take on a positive charge (Figure 1.6). An attached phenyl group on C_β would be able to delocalize the charge.[153]

Along the very same lines, Deeming *et al.*[81], in 1990, proposed that there is a

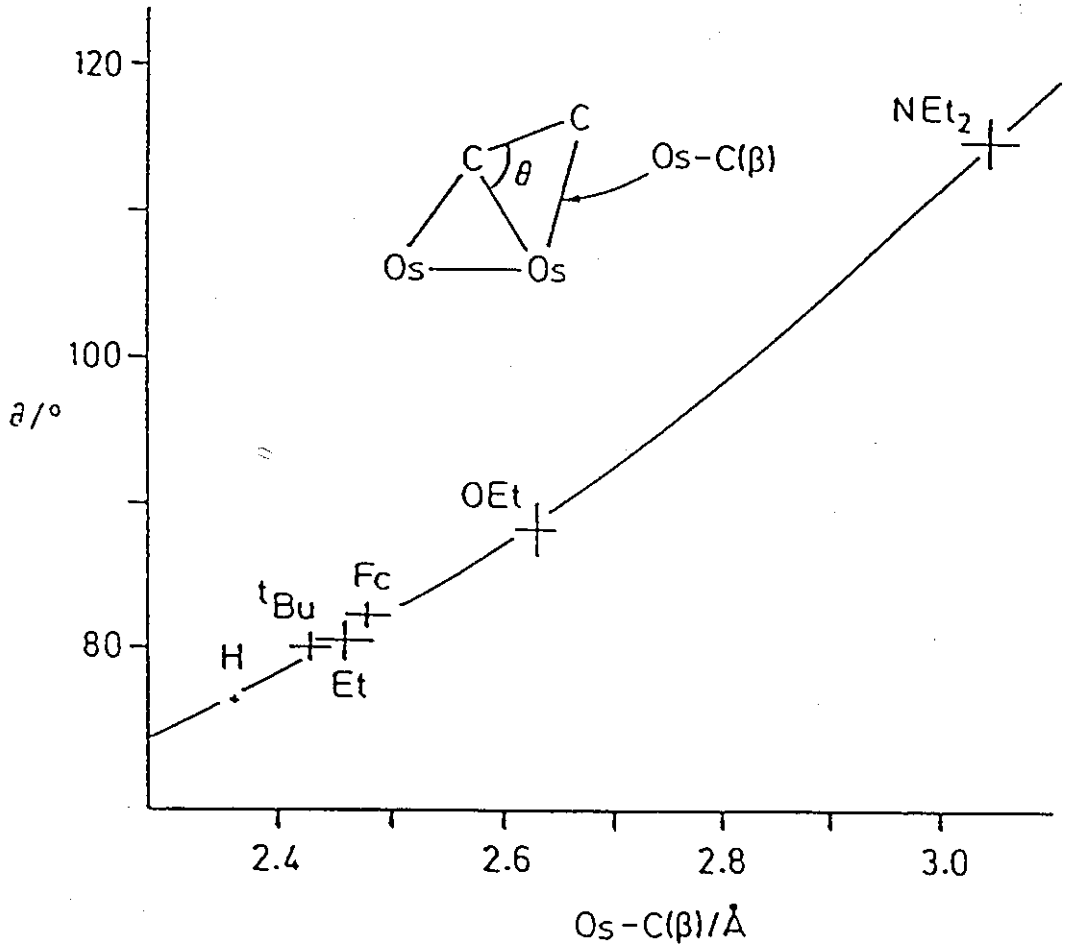

Figure 5.3 Plot of the angle θ against the Os-C_β bond distance. The series of compounds $[Os_3(CO)_{10}(\mu\text{-}H)(\mu\text{-}\eta^1\text{:}\eta^2\text{-}HC{=}CHR)]$ where R=H, ^{t}Bu, Et, Fc=$C_5H_4FeC_5H_5$, OEt, and NEt_2 are examined. *Figure 5.3 is reproduced from reference 81.*

correlation between the kinetic energy barrier to the vinyl oscillation and the M-C_β distance. They were studying the effect of substituents on the C_β position and found that the M-C_β distance is increased as the π-donor ability increases. As the π-donor ability increases, one is able to stabilize the transition state. Although they show a smoothly varying curve (Figure 5.3) correlating the Os-C_β distance with substituent, they are unable to differentiate the barriers to much extent even when they use such subtitutients as OEt and $C_5H_4FeC_5H_5$. They also thought that there should be no differentiation between barriers upon substitution in the α position. Of course, the work by Tiripicchio[78] in which the 1-phenylvinyl system is slower than the vinyl (and others involving pure vinyl ligands which were observed to be in fast exchange) negate this explanation.

Another interesting set of alkene derivatives that show differentiation of the barrier was found in a study by Bruce *et. al.*.[83] In this set, the bridging hydride in $Os_3(CO)_{10}(\mu\text{-}H)(\mu\text{-}\eta^1\text{:}\eta^2\text{-}HC{=}CHR)$ is replaced by isolobal group $MPPh_3$ where M= Au, Ag, and Cu, and R=C_6F_5 or C_6H_5 (refer to Table 5.5 for diagram of structure). Only the complex $Os_3(CO)_{10}(\mu\text{-}AuPPh_3)(\mu_2\text{-}\eta^1\text{:}\eta^2\text{-}HC{=}CHC_6F_5)$ in which M=Au and R=C_6F_5, is not fluxional at room temperature. Although the barrier is not quantitated, the carbonyl region of the ^{13}C NMR spectra shows 10 distinct signals, even though it was acquired with a low field NMR instrument (80 MHz). This demonstrates that the interconversion barrier is quite high. All of the other analogues show one broad signal at room temperature, demonstrating a much lower barrier. Substituting a C_6F_5 for a C_6H_5 group in the C_β position is expected to decrease the distance from the C_β to the metal atom, and hence

increase the barrier. However, it is not clear why substitution of the gold for silver or copper in the bridging ligand would decrease the barrier in the C_6F_5 systems.

The work described in these papers demonstrates that with vinyl compounds, a rationalization that will allow prediction of the height of the σ to π interconversion barrier has not yet been proposed that will hold for all systems.

5.2.1 Relationship Between Structural Features and Dynamics

So far all of the arguments that have been proposed have focussed on the nature of the substituents on the oscillating alkenyl or alkynyl ligand. These arguments cannot predict the ease of fluxionality. The change in barrier with the the substitution of the silver and copper bridging ligands in the study by Bruce *et al.*[83] leads ones to suspect that an examination of the structure and bonding in the entire system, if undertaken, might reveal the presence of structural features that could influence the chemical exchange barrier.

In order to draw some conclusions on the effect of the structural features on the observed dynamics in high barrier systems, one must find analogous systems that will differ only in bridged ligands with the metal framework remaining constant, yet still show a marked difference in the barrier to interconversion. Such a system has been studied by Cherkas *et al.*[40] where -HC=CH_2 in compound **2** is replaced by -C≡C-*t*-Bu. In the acetylide case, the σ to π interconversion is facile and rapid. Exchange occurs significantly below room temperature. One can see from Table 5.2 that the only

Table 5.2 Comparison of $Fe_2(CO)_6(\mu\text{-}PPh_2)(\mu_2\text{-}\eta^1\text{:}\eta^2\text{-}HC{=}CH_2)$ and $Fe_2(CO)_6(\mu\text{-}PPh_2)(\mu_2\text{-}\eta^1\text{:}\eta^2\text{-}C{\equiv}C\text{-}t\text{-}Bu)$ Through Selected Bond Distances

Bond Definition	Selected Bond Lengths in Å		
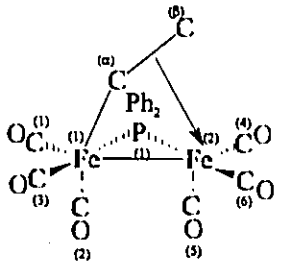	-$HC{=}CH_2$	-$C{\equiv}C$-*t*-Bu	Difference
Fe(1)-P(1)	2.215 (1)	2.2095 (8)	+0.0060 (13)
Fe(2)-P(1)	2.258 (1)	2.2231 (7)	+0.0350 (12)
asymmetry:	**0.0430 (14)**	**0.0140 (11)**	**0.029 (2)**
π: Fe(2)-C_α	2.084 (3)	2.123 (3)	-0.039 (4)
Fe(2)-C_β	2.169 (3)	2.326 (3)	-0.157 (4)
Δ:	**0.085 (4)**	**0.203 (4)**	**-0.118 (6)**
σ: Fe(1)-C_α	1.964 (3)	1.905 (3)	+0.059 (6)
C_α-C_β	1.379 (5)	1.223 (4)	N.A.
Fe(1)-Fe(2)	2.597 (1)	2.5959 (6)	+0.0010 (12)
Fe-CO: Fe(1)-C(1)	1.764 (3)	1.776 (3)	-0.012 (4)
Fe(1)-C(2)	1.810 (3)	1.797 (3)	+0.013 (4)
Fe(1)-C(3)	1.813 (3)	1.813 (3)	+0.000 (4)
Fe(2)-C(4)	1.786 (3)	1.785 (3)	+0.001 (4)
Fe(2)-C(5)	1.789 (3)	1.777 (3)	+0.012 (4)
Fe(2)-C(6)	1.798 (3)	1.829 (3)	-0.031 (4)

significant differences in bond distances occur in the bridging ligands, with the metal-metal and metal-carbonyl distances being virtually the indistinguishable from one another. A small difference is observed in the Fe(2)-C(6) distances, but if one averages the bond distances over the tripod, this difference is not significant.

The first pronounced difference occurs in both the σ and π ligand to metal bonding distances and the subsequent geometry arising from these bonding distances. The π bonds to the α and β carbon are weaker in the acetylide system than in the vinyl system with the more significant difference of the two occurring with the β carbon interaction. The β carbon is weakly bonded in the acetylide case: the distance between C_α and C_β is 1.223 Å. In comparison, the C≡C bond distance in free acetylene is only slightly shorter at 1.203 Å.[157] On the other hand, in the vinyl system the distance between C_α and C_β is 1.379 Å, which is significantly longer than the C=C bond distance in free ethylene (1.330 Å).[157] This demonstrates that the vinyl ligand is π bound more strongly.

The stonger π interaction is reflected by the difference between the M-C_α and M-C_β bonding distances. If these two distances are very similar then the π interaction is quite strong. In the vinyl system, the difference is 0.085 Å, compared with 0.203 Å for the alkynyl system. The difference becomes smaller as both of the M-C_α and M-C_β bonds become stronger. In contrast, the σ interaction is much stronger in the acetylide case than that of the vinyl case with a bond length difference of +0.059 Å. This is not unexpected as a change from an sp^2 to sp^3 carbon leads to a difference of +0.043 Å.[154]

This difference in bonding also leads to a difference in geometry. When

the α and β carbons are bonded almost equally by the π interaction, C_β moves out of the plane defined by Fe(1)-Fe(2)-C_α. In comparison, when the β carbon is bonded much more weakly by the π interaction, the ligand is more coplanar with the M-M axis (Figure 5.4).

Taking these structural features into consideration, it is not difficult to rationalize why the vinyl complex has a higher barrier than the analogous acetylide system. The vinyl ligand that is bound more strongly by the π interaction will require more energy to break those bonds and this results in a higher barrier. In addition, the geometry of the acetylide system more closely resembles that of the most probable transition state and as such will have a lower barrier.

The second significant difference observed is the asymmetry in the bonding of the phosphido bridge. There is a statistically significant asymmetry in the bond distances in both cases, but it is much more pronounced in the vinyl case (0.043 Å compared with 0.014 Å).

The vinyl group is π-bound to Fe(2) [Fe(2)-C_α = 2.084(3) Å and Fe(2)-C_β = 2.169(3)Å] and is σ-bound to Fe(1) [Fe(1)-C_α = 1.964(3) Å], so the stronger phosphorus to metal interaction occurs with the electron-poor metal atom. Both the vinyl group and the phosphido ligand are each formally 3 electron donors. When the vinyl group bonds in the bridging σ and π fashion, it must bond asymmetrically, one electron to the σ interaction and two electrons to the π interaction. This imbalance can be counteracted by placing the phosphido electrons asymmetrically, two electrons for the metal with the σ-vinyl interaction and one for the metal with the π-vinyl interaction. This is clearly

a)

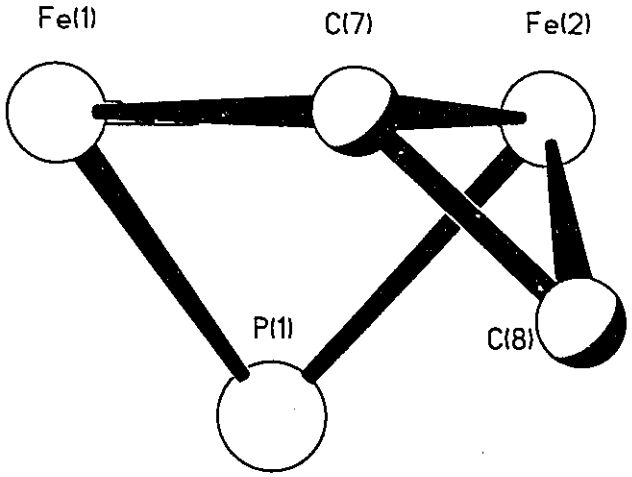

b)

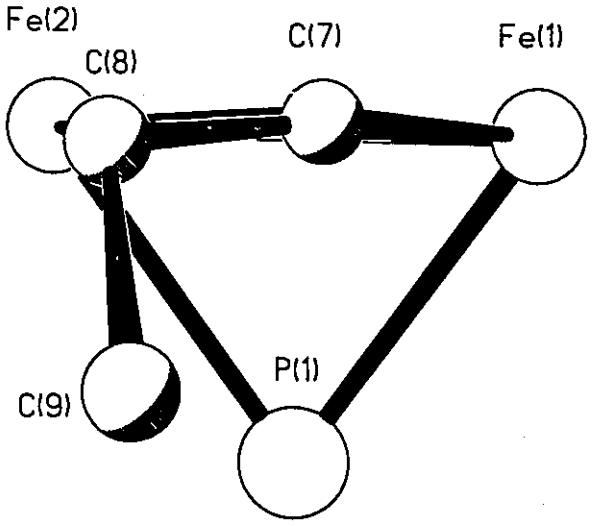

Figure 5.4 Comparison of low barrier acetylide and high barrier vinyl bonding orientation. a) Vinyl- $Fe_2(CO)_6(\mu\text{-}PPh_2)(\mu\text{-}\eta^1\text{:}\eta^2\text{-}HC{=}CH_2)$[82] b) Acetylide-$Fe_2(CO)_6(\mu\text{-}PPh_2)(\mu\text{-}\eta^1\text{:}\eta^2\text{-}CC\text{-}t\text{-}Bu)$[40]

justified given the observed asymmetry in the two metal to phosphorus bond distances.

This structural feature would also produce a higher barrier in the vinyl complex. The fact that the π interaction is significantly stronger in the vinyl case imposes a large electronic imbalance between the two metals. This would be a driving force for the σ-π interconversion. If the system can compensate an electronic imbalance then the barrier to interconversion will be higher. The ground state would be more energetically favourable and hence would be lowered relative to the ground state in a system in which there is a significant electronic difference between the two metals. Evidence for this compensation of the electronic difference is seen by the asymmetric bonding of the phosphido ligand.

In summary, there appear to be two structural features that are used to propose separate criteria that can be used to predict the interconversion barrier: 1) the strength of the π-interaction as determined by the difference in M-C_α and M-C_β bond lengths, and 2) the asymmetry in electron donation to each metal as determined through the metal to ligand distances.

One can separate to some extent the role of these two criteria in the case of the alkynyl system, by examination of the acetylide bridged complexes down the metal triad (M=Fe, Ru, Os)[40]. In the ruthenium and osmium cases, there is no asymmetry in the phosphido bridging bonds, so the only factor differentiating the two metal atoms in each complex is the alkynyl bridge itself, with the phosphido bridge playing only a small role in the iron case.

Table 5.3 Comparison of Selected Bond Distances for $M_2(CO)_6(\mu\text{-}PPh_2)(\mu_2\text{-}\eta^1\text{:}\eta^2\text{-}C{\equiv}C\text{-}t\text{-}Bu)$ Where M= Fe, Ru and Os

Bond Distances in Å

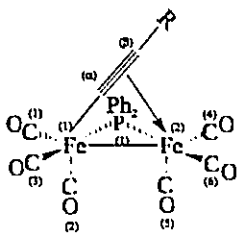

	M=Fe	M=Ru	M=Os
M(1)-P(1)	2.2095 (8)	2.3399 (8)	2.359 (3)
M(2)-P(1)	2.2231 (7)	2.3406 (8)	2.362 (3)
asymmetry:	**0.0140 (11)**	**0.0010 (11)**	**0.003 (4)**
π: M(2)-C_α	2.123 (3)	2.285 (3)	2.310 (12)
M(2)-C_β	2.326 (3)	2.417 (3)	2.377 (12)
Δ:	**0.203 (4)**	**0.132 (4)**	**0.063 (17)**
σ: M(1)-C_α	1.905 (3)	2.044 (3)	2.036 (12)
C_α-C_β	1.223 (4)	1.218 (4)	1.228 (18)
M(1)-M(2)	2.5959 (6)	2.7523 (3)	2.7950 (6)
M-CO: M(1)-C(1)	1.776 (3)	1.918 (4)	1.904 (14)
M(1)-C(2)	1.797 (3)	1.933 (4)	1.908 (13)
M(1)-C(3)	1.813 (3)	1.943 (4)	1.933 (16)
M(2)-C(4)	1.785 (3)	1.931 (4)	1.887 (15)
M(2)-C(5)	1.777 (3)	1.886 (4)	1.873 (13)
M(2)-C(6)	1.829 (3)	1.955 (4)	1.916 (13)

Note: Representative single M-M bond distances can be inferred from the average of the unbridged M-M bond lengths of 2.673, 2.8542, and 2.877 Å from $M_3(CO)_{12}$, respectively.[40]

As discussed previously, the barrier to the interconversion increases as one goes down the trial. One can cleary see the effect of the strength of the π interaction through the acetylide to metal distances. The σ interaction appears to be similar through the triad, with perhaps a small increase in the osmium case. However, the errors in the bond lengths for the osmium system make it difficult to determine this with any degree of certainty. The only obvious difference between metals as one moves down the triad is that the metal to π interaction becomes more significant. The difference in bond lengths between M(2)-C_α and M(2)-C_β (defined as Δ in Table 5.3) decreases by almost a factor of two from one metal to the next in the series. Along with this difference in bond distance, there is a change in geometry. As the π interaction decreases the C_α-C_β axis becomes more coplanar with the M-M bond axis. This is also consistent with the $Fe_2(CO)_6(\mu\text{-}PPh_2)(\mu_2\text{-}\eta^1\text{:}\eta^2\text{-}HC{=}CH_2)$ complex.

Although Deeming's theory on π-donor substituent effect does not hold, there appears to be some merit in the correlation between the barrier and the M(2)-C_β distance. However, it cannot simply be as a result of the M-C_β bond strength because as one goes down the triad, one observes an increase in the barrier (43.1, 46.9, 47.3 kJ mol^{-1}, by one-point coalescence method) with the most significant difference between the iron and ruthenium complexes. Yet, if one only compares the M(2)-C_β distance between these two metals, the difference (once the radii of the metals are taken into consideration) is not significant enough to explain the barrier difference. In order to see the correct trend, one must compare the strength of both π bonds.

The above evidence in support of these factors has only involved systems with diphenylphosphide as the other bridging ligand. Perhaps a more extensive examination of systems with other bridging ligands will determine its overall applicability and shed more light on the importance of each criterion. Unfortunately, the subset of systems that one can examine is small. The bond distances for all of the bridging ligands and an approximation of the interconversion barrier must have been reported. Many of the molecules studied involve a bridging hydride that was not detected using X-ray crystallography techniques. In other cases, either the X-ray or the dynamic data are not reported.

There are some systems reported in the literature from which one can gain insight. Only one relevant crystal structure was reported in the Hogarth study,[84] that of the *cis* 1-methylvinyl isomer $Fe_2(CO)_4(\mu^2\text{-}\eta^1\text{:}\eta^2\text{-MeC=CH}_2)(\mu\text{-PPh}_2)$(dppm) **4a** (refer to Table 5.4). This compound replaces one carbonyl ligand on each metal atom with a bridging dppm ligand and a methyl group is substituted at the C_α position. The barrier was not calculated, but is similar to that of $Fe_2(CO)_6(\mu\text{-PPh}_2)(\mu_2\text{-}\eta^1\text{:}\eta^2\text{-HC=CH}_2)$ in that observable broadening of the ^{31}P NMR signals is observed at room temperature and coalescence does not occur until 80 °C. There is an analogous iron acetylide (-C≡C-*t*-Bu) system that is present only as the *trans* isomer. The barrier for this system is exceptionally low ($\Delta G^{\ddagger}$=34.7 kJ mol^{-1}).

With regards to the asymmetry, a comparison of the alkene system with that of metals are now significantly different. The comparison of bond distances to determine

Table 5.4 Comparison of Selected Bond Distances for *cis* $Fe_2(CO)_4(\mu^2\text{-}\eta^1\text{:}\eta^2\text{-}MeC{=}CH_2)(\mu\text{-}PPh_2)(dppm)$ and *trans* $Fe_2(CO)_4(\mu^2\text{-}\eta^1\text{:}\eta^2\text{-}C{\equiv}C\text{-}t\text{-}Bu)(\mu\text{-}PPh_2)(dppm)$

Selected Bond Lengths in Å			
Bond Definition	alkenyl (cis) $MeC{=}CH_2$ 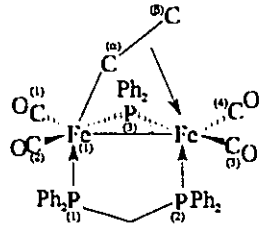	alkynyl (trans) $-C{\equiv}C\text{-}t\text{-}Bu$ 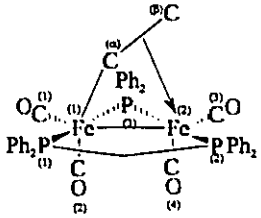	Difference
Fe(1)-P(3)	2.252(3)	2.197(2)	0.055(5)
Fe(2)-P(3)	2.279(3)	2.222(2)	0.057(5)
asymmetry:	**-0.027(4)**	**-0.025(3)**	**-0.002(6)**
Fe(1)-P(1)	2.258(3)	2.211(2)	0.047(5)
Fe(2)-P(2)	2.241(3)	2.257(2)	-0.016(5)
asymmetry:	**+0.017(4)**	**-0.046(3)**	**+0.063(7)**
π:Fe(2)-C_α	2.124(8)	2.126(7)	-0.002(11)
Fe(2)-C_β	2.126(8)	2.314(8)	-0.188(11)
Δ:	**0.002(11)**	**0.188(11)**	**-0.186(16)**
σ:Fe(1)-C_α	2.002(7)	1.883(8)	+0.119(11)
Fe(1)-Fe(2)	2.658(3)	2.622(1)	+0.036(3)
Fe-CO: Fe(1)-C(1)	1.764(10)	1.755(8)	0.009(13)
Fe(1)-C(2)	1.802(9)	1.742(9)	0.060(13)
Fe(2)-C(3)	1.793(9)	1.769(8)	0.024(12)
Fe(2)-C(4)	1.778(10)	1.754(9)	0.024(13)
C_α-C_β	1.403(12)	1.261(11)	N.A.

an electronic imbalance is a simplistic approach. It is difficult to obtain meaningful conclusions with the separate asymmetries from the two phosphido ligands. Clearly, with the addition of a third asymmetry in the metal-carbonyl bonding, this approach is not useful. High level theoretical calculations would be required to determine the electronic difference between the two metal atoms. However, the differences in bonding as one goes from the *trans* alkyne to the *cis* alkene are quite dramatic and, as such, are worth discussion. The relevant bond distances for the two systems are listed in the Table 5.4.

The first obvious difference between the acetylide system and the vinyl system is in the asymmetry in the bonding of the dppm ligand. In the acetylide system, the Fe(1)-P(1) bond is considerably shorter than Fe(2)-P(2) bond, whereas in the vinyl system this asymmetry is reversed with the Fe(1)-P(1) bond being slightly longer than the Fe(2)-P(2) bond. In contrast, the bonds to the diphenylphosphido ligand show no difference between systems. As a result, in the vinyl system, the two bridging phosphido ligands appear to counteract one another while in the acetylide they are asymmetric in the same sense.

The second major difference occurs with the σ and π interactions of the vinyl and acetylide group. The σ interaction of the acetylide (Fe(1)-C_α) is much stronger while its π interaction to C_β (Fe(2)-C_β) is much weaker than the corresponding interactions of the vinyl group. The π interaction to C_α are equal between systems. This demonstrates that the acetylide ligand induces a more significant electronic imbalance than the vinyl ligand.

By use of the π interaction criterion, one would predict that the acetylide system is highly fluxional, while the vinyl system is not. The differences between the two π

bonds are 0.188 Å (acetylide) and 0.002 Å (vinyl). There is a slight compensating asymmetry with the vinyl system but the two phosphido ligands seem to counteract one another. Clearly, the dominant factor in this system is that of the π interaction.

In next case to be examined, the Os-$AuPPh_3$ systems of Bruce *et al.*[83], this factor does not dominate and the asymmetry in the bonding of the other bridging ligands appears to determine the interconversion barrier. The important bond distances for $Os_3(CO)_{10}(\mu\text{-}AuPPh_3)(\mu\text{-}\eta^1\text{:}\eta^2\text{-}HC{=}CHC_6F_5)$ and $Os_3(CO)_{10}(\mu\text{-}AuPPh_3)(\mu\text{-}\eta^1\text{:}\eta^2\text{-}HC{=}CHC_6H_5)$ are given in Table 5.5. Unfortunately, the structures of the silver and copper analogues were not reported and cannot be compared.

In both of these systems, there are three groups bridging the Os(1)-Os(2) bond that must be considered: the $\mu\text{-}\eta^1\text{:}\eta^2$-vinyl, the μ-$Au(PPh_3)$ and the μ-$Os(3)(CO)_4$. There is an asymmetry between the Os(1)-CO and Os(2)-CO bond lengths, but it appears that the asymmetry is the same for both systems, within experimental error. These distances were not listed in the paper but were extracted from the published coordinates. The first striking difference observed between the two analogues is the asymmetry in the Os-Au bond distances. In the C_6F_5 analogue, the Au to Os_1 and Os_2 distances are nearly equal. The asymmetry in the two bonds is only 0.011(1) Å, while in the Ph analogue the asymmetry in these bonds is -0.057(1) Å. The asymmetry in the bridging $Os(CO)_4$ group

Table 5.5 Comparison of Selected Bond Distances for $Os_3(CO)_{10}(\mu\text{-}AuPPh_3)(\mu\text{-}\eta^1\text{:}\eta^2\text{-}HC{=}CHC_6F_5)$ and $Os_3(CO)_{10}(\mu\text{-}AuPPh_3)(\mu\text{-}\eta^1\text{:}\eta^2\text{-}HC{=}CHC_6H_5)$

Selected Bond Distances in Å

Bond Definition

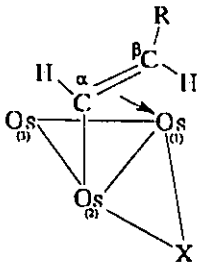

	X=Au(PPh_3) R=C_6F_5	X=Au(PPh_3) R=C_6H_5	Difference
Os(1)-Os(2)	2.894(1)	2.882(1)	+0.012(1)
Os(1)-Os(3)	2.922(1)	2.924(1)	-0.002(1)
Os(2)-Os(3)	2.854(1)	2.864(1)	-0.010(1)
Asymmetry:	**+0.068(1)**	**+0.060(1)**	**+0.008(2)**
Os(1)-Au(1)	2.766(1)	2.738(1)	0.028(1)
Os(2)-Au(1)	2.777(1)	2.795(1)	-0.018(1)
Asymmetry:	**-0.011(1)**	**-0.057(1)**	**0.046(2)**
π-interactions			
Os(1)-C_α	2.276(6)	2.251(14)	+0.025(15)
Os(1)-C_β	2.403(7)	2.448(16)	-0.045(18)
Δ:	**-0.127(9)**	**-0.197(21)**	**0.070(23)**
σ interaction			
Os(2)-C_α	2.133(8)	2.107(15)	+0.026(17)
C_α-C_β	1.396(10)	1.393(24)	+0.003(28)

is similar between systems (0.068(1) Å for the C_6F_5 system and 0.060(1) Å for C_6H_5).

Thus, the only significant difference between the two systems is that the asymmetry in the bridging $Os(CO)_4$ group is negated by the asymmetry in the bridging $AuPPh_3$ ligand in the Ph system, while it is not in the C_6F_5 system. The high barrier C_6F_5 analogue shows a compensation for the asymmetry in the bridging alkene, *via* the two other bridging ligands. Whereas in the low barrier Ph analogue, the asymmetry in the two other briding ligands negate each other so there is no compensation of the asymmetry induced by the vinyl ligand.

Secondly, the difference between the Os(2)-C_α and Os(2)-C_β bond distances is significant for both systems with the Ph analogue showing a greater difference (-0.197(21) Å compared with -0.127(9) Å in the C_6F_5 system). The errors for these bond distances are large for the C_6F_5 system, so one cannot predict with any degree of certainty which barrier would be higher. However, by use of the π-interaction criterion, one would conclude that both systems should have a low barrier, as the difference between the two distances is still significant.

It is expected that the C_β distance to the osmium atom would be shorter in the C_6F_5 analogue compared to the C_6H_5 analogue and this is observed. The Os-C_β distance is statistically lower (2.403(7) Å compared with 2.448(16) Å). However, this is not a very drastic shortening.

In the comparison of the $Os_3(CO)_{10}(\mu\text{-}AuPPh_3)(\mu\text{-}\eta^1\text{:}\eta^2\text{-}HC{=}CHR)$, R=$C_6F_5$ and C_6H_5 systems quite clearly the strength of the π interaction is not the dominant factor and

the asymmetry in bonding of the other ligands allows prediction of the barrier. The other supporting evidence for this conclusion is that substitution of a copper or silver metal atom for the gold in the C_6F_5 analogues appears to decrease the barrier. Although there are no crystal structure data for the remaining compounds in this study, the NMR data show a low barrier for the silver and copper analogues. This leads one to conclude that the metal in the bridging group is an important consideration.

The μ-η^1-η^2 bound vinyl ligand induces a large polarization in the metal-metal bond. The ability of the bridging ligands to counteract this polarization must be a factor. Gold is a large third row transition metal and as such is the most polarizable in the series. The substitution of the C_6F_6 for C_6H_6 in the vinyl ligand must induce a larger polarization in the Os-Os bond and this is turn affects the bridging gold ligand which can compensate more readily than the copper or silver ligand.

There is another possible explanation for the observed fluxionality in the copper and silver analogues. The copper and silver metal is expected to bond PPh_3 more weakly than to gold, and competing equilibria between the bound and unbound species might occur.[154]

5.3 Experimental Section

The NMR sample of $Fe_2(CO)_6(\mu\text{-}PPh_2)(\mu_2\text{-}\eta^1\text{:}\eta^2\text{-}HC{=}CH_2)$ was prepared as described in experimental section of Chapter 4 and was used for both the selective inversion and line-shape spectra.

Table 5.6 Parameters for the Vinyl Windshield Wiper Selective Inversion Experiments

Temperature (°C)	Variable Delays
27.4	0.001, 20.0, 0.1, 0.025, 0.25, 0.15, 0.075, 0.5, 0.2, 0.4, 0.3, 1.0, 5.0
21.9	0.001, 20.0, 0.1, 0.025, 0.125, 0.5, 0.15, 0.05, 0.075, 0.25, 1.0, 5.0
16.9	0.001, 20.0, 0.1, 0.025, 0.125, 0.5, 0.15, 0.05, 0.075, 0.25, 1.0, 5.0

5.3.1 Selective Inversion Experiment

The selective inversion experiments were performed as described in Chapter 2 using the pulse program INVREC2P.AUR, only the differences in procedure are given. The values for the pulse sequence parameters that varied with experiment are found in Table 5.6.

In a normal two-site selective inversion experiments, ideally one inverts one peak and then follows the recovery of both sites. In this experiment there was only one sharp peak in the accessible temperature range. The strategy employed in determining the exchange rate was to invert the broad signal as much as possible and follow the magnetization intensity of the sharp peak. For all experiments, O1 was placed on the maximum of the broad signal (15844.74 Hz) and the τ delay was set to the inverse of twice the frequency difference between the two signals (0.003432 s). The Fourier transform size (SI) and acquisition size (TD) were set to 2K. The spectral width was set to 1028.81 Hz. This gave an acquisition time of 1.0 s with a digital resolution of 1.0047 Hz/pt. The number of scans was set to 256.

A separate T_1 experiment was performed at 27.4 °C for the sharp site. The τ (or D2) value was set to 0.00001 s. At this temperature, the T_1 value is 4.8 s. The relaxation rate is much shorter that the chemical exchange rate and as a result its value does not have much affect on the chemical exchange rate determination. For this reason, separate T_1 experiments for each temperature were not required.

The selective inversion data were analyzed by use of a modified version of

FLOPSI for a two site system in which only one site is followed (ONESITE). The ^{13}C spin-lattice relaxation time was fixed to 0.2 s, while the M_0-M_∞ and the M_∞ values were allowed to vary.

5.3.2 Line-Shape Data

The line-shape data were obtained, processed and analyzed as described in the experimental section of Chapter 4. The Fourier transform size (SI) and acquisition time (TD) were set to 4K. The sweep width was set to 2793 Hz with an O1 value of 15844.74 Hz, resulting in a spectrum with only the carbonyl signals.

5.4 Conclusions

The selective inversion and line-shape data were combined to obtain the activation parameters for the σ to π interconversion of the vinyl ligand in $Fe_2(CO)_6(\mu\text{-}PPh_2)(\mu_2\text{-}\eta^1\text{:}\eta^2\text{-}HC{=}CH_2)$. The activation parameters are as follows, $\Delta H^{\ddagger} = 71 \pm 9$ (3σ) kJ mol^{-1} and $\Delta S^{\ddagger} = 0.017 \pm 0.003$ (3σ) kJ deg^{-1} mol^{-1}. The activation barrier was higher than expected and this led to a proposed rationalization for the observed high barrier.

It is possible to predict the presence of fluxionality at room temperature given the X-ray crystal structure. The two criteria- strength of the π interaction and the asymmetry in the bonding of the other bridging ligands have so far allowed prediction of the degree of fluxionality in all cases found in the literature to date. It would help tremendously to have more data. For instance, no crystal structure data were available for the iron vinyl

system in which the phosphido bridge was replaced by a sulphido bridge and since that system exhibited a low barrier, it might provide an interesting comparison. There were a myriad of other compounds which unfortunately were missing either the kinetic information, or the bond distances.

The evidence that has been presented to rationalize the barrier height is strongly corroborating. Notwithstanding this, there are some problems in the use of the proposed approach to rationalize the barrier. The first is that it involves a comparison of structure data observed in the solid state with the dynamic behaviour observed in solution. It is not known how closely the bonding in solution corresponds with that of the solid state. Comparing bond lengths alone to determine electronic contributions conclusively is not sufficient. This is especially so if one attempts to compare asymmetric molecules. Accurate theoretical calculations to determine the electron density at each metal atom are required.

It is not clear to what extent that the two criteria used for predicting the fluxionality are independent. In the last example, it was demonstrated that the asymmetry criterion is more prominant, whereas in another example, the π interaction criterion was the more important factor. In all likelihood, the manner in which the alkene or alkyne ligand bonds strongly affects the degree to which the other ligands are capable of compensating the polarized metal-metal bond.

It would appear that the ability of a system to induce and compensate for the polarization induced by the alkene or alkyne is key to understanding the ability of the

system to undergo σ to π interconversion. If there is an electronic imbalance induced between the two metals by the alkene or alkyne ligand then the barrier is low. The ground state for such a system is not as stable as that of a system that is capable of compensating this asymmetry with other ligands. In addition, the large difference in the strength of the M-C_α and M-C_β bounds would give a ground state that more closely approximates the transition state and this too would decrease the barrier. It is clear that the barrier to the fluxionality is more strongly dominated by electronic factors than by steric factors.

CHAPTER 6

CONCLUSIONS AND FUTURE WORK

6.1 Conclusions

It is possible to design a single selective inversion experiment for complex multi-site and multi-exchange systems. The set of initial conditions that are chosen affect the ability to measure the exchange rates. The partial derivative criterion is valid and can be used to aid in determining an acceptable set of initial conditions.

There is more than one acceptable set of optimal conditions and as long as there is sufficient excitation from one site with respect to another in any given rate process, there appears to be no bias in the data between the different initial sets.

The strengths and weaknesses of each of the dynamic NMR methods in the slow regime are complementary and the optimal experiment for complex multi-site and multi-exchanging systems is a combination of the methods. The methods are co-dependent in complex systems. One cannot determine the initial conditions for 1D and 2D magnetization transfer methods without an approximation of the rate and knowledge of the correct temperature regime and one cannot analyze the line-shape data without the

exchange map. The approximate rate and correct temperature regime is best determined from preliminary line-shape analysis, and the exchange map is best determined from a qualitative 2D experiment.

Quantitative 2D-EXSY analyses are prone to large errors unless highly digitized spectra are obtained and the data are fit with multiple mixing times. Multiple mixing times are not always feasible because of time constraints. On the other hand, the quantitative results from the single selective inversion experiment are generally more expedient and prone to less error.

It was concluded that the concerted mechanism for the trigonal carbonyl rotation process is more likely than a successive pairwise mechanism for the compounds under study.

It appears that the barrier to the σ to π interconversion is dominated more by electronic effects than by steric effects. There appear to be two structural features in the complexes that can be used to predict the interconversion barrier: 1) strength of the π-interaction as determined by the difference in M-C_α and M-C_β distances, and 2) asymmetry in electron donation to each metal as determined through the metal to ligand distances.

Use of these two criteria has so far allowed prediction of the barrier in all cases found in the literature to date. If the π interaction is strong, as determined by near equality in the M-C_α and the M-C_β distances, more energy is required to break the bonds in the interconversion process. In addition, a difference in the geometry of the bound

ligand is observed when the M-C_β distance is considerably longer than the M-C_α distance. When the M-C_β distance is long, the geometry more closely resembles the transition state and this too reduces the barrier to interconversion. A ligand that bonds in a μ_2-η^1:η^2 fashion necessarily imposes an electronic imbalance between the two metals. If a system can compensate for that asymmetry in the alkene or alkyne bonding, then the ground state should be more stable and hence the barrier to interconversion will be higher.

It is not clear to what extent the two criteria used for predicting the fluxionality are independent. In all likelihood, the manner in which the alkene or alkyne bonds strongly affects the degree to which the other ligands are capable of compensating. However, it would appear that the ability of a system to induce and compensate for the polarizabilty in the alkene or alkyne is key to understanding the ability of the system to undergo σ to π interconversion.

6.2 Future work

6.2.1 Future Possibilities for NMR Improvements

In all dynamic NMR methods especially one-dimensional methods, the covariance in the errors is significant. In multi-site and multi-exchange systems, the number of parameters upon which the covariance depends is large. For example, in a six site and four rate process, one would need to solve the variance-covariance matrix over 22 dimensions and this is difficult computationally. Currently none of the programs used for the selective inversion analysis address this problem. Consequently, any reported errors

for the actual rate values should be regarded with suspicion.

In this work, the lack of confidence in the error is alleviated somewhat by the fact that it was the activation parameters that were sought and not the rate value at any one individual temperature. A reasonable error can be approximated by quoting the variance determined from the linear least-squares fit of the temperature dependence to the 99% confidence level.

Although the number of parameters for the covariance-variance matrix is large, one need only solve for the largest covariance to determine the confidence level. The program SIFIT by McClung determines the covariance-variance elements but does not solve the matrix. It may be possible to reduce the dimensionality of the problem by searching for and then solving for the largest error. Failing this, powerful computers and programs are becoming more accessible, and an efficient program may already exist that can solve the matrix despite the large number of dimensions.

New methods of spectral data processing have been developed by NMR spectroscopy workers in response to the prevalence of powerful computers. Fourier transform has traditionally been used to process the frequency information into the time domain. Other mathematical procedures exist that may produce more accurate results. Linear Prediction (LP) and the maximum entropy method (MEM) are examples of procedures that can be found in the recent literature.[155] Incorporation of these techniques should be explored to attempt to reduce the error of these dynamic NMR techniques.

Reference deconvolution is an example of a spectral data processing technique that

has been incorporated into line-shape analysis.[114] The true line-shape can be corrupted by instrumental contributions, the largest arising from imperfect shimming. This can cause significant broadening that will be interpreted as exchange. In this technique, the spectrum is deconvoluted with the line shape of an imperfect reference signal and reconvoluted with the ideal line-shape for the reference signal that does not undergo exchange. At the same time, an identical instrumental contribution is removed from all of the other signals in the spectrum. This allowed greater precision in the line-shape fitting routine.[114]

6.2.2 Possibilities for Further Research in Metal Carbonyl Cluster Chemisty

The proposed rationalization for the height of the activation barrier in the σ to π interconversion leads to possible future research in both theoretical and synthetic areas. High level calculations should be attempted to determine if the two criteria influence the barrier as expected. *Ab initio* calculations are becoming more prevalent for inorganic transition metal complexes, but they are still not common place. In particular, these calculations should be able to determine if an electronic imbalance between the two metal atoms lowers the barrier. If *ab initio* calculations are not possible, Extended Hückel Molecular Orbital (EHMO) calculations might be successful in the comparison of two very similar compounds that demonstrate a large difference in the barrier such as $Os_3(CO)_{10}(\mu\text{-}AuPPh_3)(\mu\text{-}\eta^1\text{:}\eta^2\text{-}HC{=}CHC_6F_5)$ and $Os_3(CO)_{10}(\mu\text{-}AuPPh_3)(\mu\text{-}\eta^1\text{:}\eta^2\text{-}HC{=}CHC_6H_5)$.

It appears that the bridging ligands play a significant role in the barrier. Most of

the dynamic NMR studies involved simple coalescence rate data. It would be interesting to conduct a rigorous dynamic NMR study of this barrier with a variety of bridging ligands such as $AsPh_3$, $Ph_2P{=}O$, and $AuPPh_3$. There have been no reported cases of high barrier alkyne systems Synthetically, the challenge is to "stop" the alkyne σ to π interconversion. The results from the kinetic study as a function of bridging ligand might provide sufficient direction for this goal.

REFERENCES

1) Harris, R.K., *Nuclear Magnetic Resonance Spectroscopy*; Pitman Books Limited: London, 1983.

2) Sandstrom, J., *Dynamic NMR spectroscopy*; Academic Press: London, 1982.

3) Jackman, L.M.; Cotton, F.A., *Dynamic Nuclear Magnetic Resonance Spectroscopy*; Academic Press: New York, 1975.

4) Perrin, C.L.; Dwyer, T. *Chem. Rev.*, **1990**, *90*, 935-967.

5) Sanders, J.K.M.; Mersh, J.D. *Prog. Nucl. Magn. Reson. Spectrosc.*, **1982**, *15*, 353-400.

6) Sanders, J.K.M.; Hunter, B.K., *Modern NMR Spectroscopy. A Guide For Chemists*; Oxford University Press: Oxford, 1988.

7) Orrell, K.G.; Sik, V.; Stephenson, D. *Prog. Nucl. Magn. Reson. Spectrosc.*, **1990**, *22*, 141-208.

8) Stephenson, D.S.; Binsch, G. *J. Magn. Reson.*, **1978**, *32*, 145-152.

9) Noggle, J.H.; Schirmer, R.E., *The Nuclear Overhauser Effect: Chemical Applications*; Academic Press: 1971.

10) Bahadur, G.A.; Baldwin, J.E.; Field, L.D.; Lehtonen, E.M.M.; Usher, J.J.; Abraham, E.P.; White, R.L.; Valleho, C.A. *J. Chem. Soc. ,Chem. Commun.*, **1981**, 917.

11) Bain, A.D.; Cramer, J.A. *J. Magn. Reson.*, **1993**, *A 103*, 217-222.

12) Forsen, S.; Hoffman, R.A. *J. Chem. Phys.*, **1964**, *40*, 1189-1196.

13) Forsen, S.; Hoffman, R.A. *J. Chem. Phys.*, **1963**, *39*, 2892-2901.

14) Orrell, K.G.; Sik, V. *Ann. Rep. NMR Spectrosc.*, **1987**, *19*, 79-173.

15) McConnell, H.M.; Thompson, D.D. *J. Chem. Phys.*, **1957**, *26*, 958-959.

16) McConnell, H.M. *J. Chem. Phys.*, **1958**, *28*, 430-431.

17) Gutowsky, H.S.; Holm, C.H. *J. Chem. Phys.*, **1956**, *25*, 1228-1234.

18) Led, J.J.; Gesmar, H. *J. Magn. Reson.*, **1982**, *49*, 444-463.

19) Muhandiram, D.R.; McClung, R.E.D. *J. Magn. Reson.*, **1987**, *71*, 187-192.

20) Willem, R. *Prog. Nucl. Magn. Reson. Spectrosc.*, **1987**, *20*, 1-94.

21) Abel, E.W.; Coston, T.P.J.; Orrell, K.G.; Sik, V.; Stephenson, D. *J. Magn. Reson.*, **1986**, *70*, 34-53.

22) Perrin, C.L.; Gipe, R.K. *J. Am. Chem. Soc.*, **1984**, *106*, 4036.

23) Ramachandran, R.; Knight, C.T.G.; Kirkpatrick, R.J.; Oldfield, E. *J. Magn. Reson.*, **1985**, *65*, 136-141.

24) Farrugia, L.J.; Rae, S.E. *Organometallics*, **1992**, *11*, 196-206.

25) Grassi, M.; Mann, B.E.; Pickup, B.T.; Spencer, C.M. *J. Magn. Reson.*, **1986**, *69*, 92-99.

26) Alger, J.R.; Shulman, R.G. *Q. Rev. Biophys.*, **1984**, *17*, 83.

27) Knight, C.T.G.; Merbach, A.E. *Inorg. Chem.*, **1985**, *24*, 576.

28) Pardy, R.B.A.; Taylor, M.J.; Constable, E.C.; Mersh, J.D.; Sanders, J.K.M. *J. Organomet. Chem.*, **1982**, *231*, C25.

29) Beringhelli, T.; D'Alfonso, G.; Molinari, H.; Hawkes, G.E.; Sales, K.D. *J. Magn. Reson.*, **1988**, *80*, 45-59.

30) Brown, M.; Chaloner, P.A.; Morris, G.A. *J. Chem. Soc., Perkin Trans. II*, **1987**, 1583.

31) Brown, M.; Evans, P.L.; Lucy, A.R. *J. Chem. Soc., Perkin Trans. II*, **1987**, 1597.

32) Brown, M.; Kent, A.G. *J. Chem. Soc., Perkin Trans. II*, **1987**, 1597.

33) Howarth, O.W.; Kelly, P. *J. Chem. Soc., Chem. Commun.*, **1988**, 1236.

34) Led, J.J; Gesmar, H.; Abildgaard, F. *Methods Enzymol.*, **1989**, *176*, 311-329.

35) Boyd, J.; Brindle, K.M.; Campbell, I.D.; Radda, G.K. *J. Magn. Reson.*, **1984**, *60*, 149-155.

36) Shungu, D.C.; Buster, D.C.; Briggs, R.W. *J. Magn. Reson.*, **1990**, *89*, 102-122.

37) Hsu, V.L.; Handsmacher, R.E.; Armitage, I.M. *J. Am. Chem. Soc.*, **1990**, *112*, 6745-6747.

38) Led, J.J; Neesgaard, E. *Biochemistry*, **1987**, *26*, 183.

39) Carty, A.J. *Pure and Appl. Chem.*, **1982**, *1*, 113-130.

40) Cherkas, A.A.; Randall, L.H.; MacLaughlin, S.A.; Mott, G.N.; Taylor, N.J.; Carty, A.J. *Organometallics*, **1988**, *7*, 969-977.

41) Lukehart, C.M., *Fundamental Transition Metal Organometallic Chemistry*; Brooks/Cole Publishing Company: Monterey, CA, 1984.

42) Muetterties, E.L. *Pure and Appl. Chem.*, **1978**, *50*, 941.

43) Aime, S.; Castiglioni, M.; Gobetto, R.; Osella, D. *Polyhedron*, **1984**, *3*, 175-181.

44) Meutterties, E.L. *Bull. Soc. Chim. Belg.*, **1975**, *84*, 959.

45) Chini, P.; Longoni, G.; Albano, V.G. *Adv. Organomet. Chem.*, **1976**, *14*, 285.

46) Masters, C., *Homogeneous Transition-Metal Catalysis*; Chapman and Hall: New York, 1981.

47) Parshall, G.W., *Homogeneous Catalysis*; John-Wiley & Sons: New York, 1980.

48) Hartley, F.R.; Vezey, P.N. *Adv. Organomet. Chem.*, **1977**, *15*, 189.

49) Jardine, F.H. *Prog. Inorg. Chem.*, **1981**, *28*, 63.

50) Orchin, M. *Acc. Chem. Res.*, **1981**, *14*, 259.

51) Nucciarone, D.; MacLaughlin, S.A.; Taylor, N.J.; Carty, A.J. *Organometallics*, **1988**, *7*, 106-117.

52) Aime, S.; Milone, L. *Prog. Nucl. Magn. Reson. Spectrosc.*, **1977**, *11*, 183-210.

53) Rosenberg, E.; Thorsen, C.B.; Milone, L.; Aime, S. *Inorg. Chem.*, **1985**, *24*, 231-233.

54) Aime, S.; Gobetto, R.; Osella, D.; Milone, L.; Rosenberg, E. *Organometallics*, **1982**, *1*, 640-644.

55) Cotton, F.A.; Hunter, D.L.; Lahuerta, P. *Inorg. Chem.*, **1975**, *14*, 511-514.

56) Cotton, F.A.; Hunter, D.L.; Lahuerta, P. *J. Am. Chem. Soc.*, **1975**, *97*, 1046-1050.

57) Fogg, D.E.; Carty, A.J.; Meyer, A.; Taylor, N.J. *Organometallics*, **1987**, *6*, 2252-2254.

58) Adams, R.D.; Cotton, F.A. *J. Am. Chem. Soc.*, **1973**, *95*, 6589-6594.

59) Evans, J.; Johnson, B.F.G.; Lewis J.; Norton, J.R.; Cotton, F.A. *J. Chem. Soc., Chem. Commun.*, **1988**, 1236.

60) Adams, R.D.; Brice, M.D.; Cotton, F.A. *J. Am. Chem. Soc.*, **1973**, *95*, 6594-6602.

61) Cotton, F.A.; Troup, J.M. *J. Am. Chem. Soc.*, **1974**, *96*, 4155-4159.

62) Cotton, F.A.; Hunter, D.L. *Inorg. Chim. Acta*, **1974**, *11*, L9-L10.

63) Agapiou, A; Pederson, S.E.; Zyzyck, L.A.; Norton, J.R. *J. Chem. Soc., Chem. Commun.*, **1977**, 393-394.

64) Cotton, F.A.; Kruczynski, L.; Shapiro, B.L.; Johnson, L.F. *J. Am. Chem. Soc.*, **1972**, *94*, 6191-6193.

65) Cotton, F.A.; Hanson, B.E.; Jamerson, J.D. *J. Am. Chem. Soc.*, **1977**, *99*, 6588-6593.

66) Cotton, F.A. *Bull. Soc. Chim. Fr.*, **1973**, *9*, 2587-2592.

67) Forster, A.; Johnson, B.F.G.; Lewis, J.; Matheson, T.W.; Robinson, B.H.; Jackson, W.G. *J. Chem. Soc., Chem. Commun.*, **1974**, 1042-1044.

68) Cotton, F.A.; Lahuerta, P.; Stults, B.R. *Inorg. Chem.*, **1976**, *15*, 1866-1871.

69) Hawkes, G.E.; Lian, L.Y.; Randall, E.W.; Sales, K.D.; Aime, S. *J. Magn. Reson.*, **1985**, *65*, 173-177.

70) Aime, S.; Gambino, O.; Milone, L.; Sappa, E.; Rosenberg, E. *Inorg. Chim. Acta*, **1975**, *15*, 53-56.

71) Aime, S.; Milone, L.; Sappa, E. *J. Chem. Soc., Dalton Trans.*, **1976**, 838-840.

72) Wilson, S.T.; Coville, N.J.; Shapley, J.R.; Osburn, J.A. *J. Am. Chem. Soc.*, **1974**, *96*, 4038-4040.

73) Nubel, P.O.; Brown, T.L. *Organometallics*, **1984**, *3*, 29-32.

74) Lee, K.W.; Brown, T.L.; Cordes, A.W.; Pennington, W.T. *J. Am. Chem. Soc.*, **1985**, *107*, 631-641.

75) Mul, W.P.; Elsevier, C.J.; Polm, L.H.; Vrieze, K.; Zoutberg, M.C.; Heijdenrijk, D.; Stam, C.H. *Organometallics*, **1991**, *10*, 2247-2259.

76) Alcock, N.W.; Kemp, T.J.; Pringle, P.J.; Beragamini, P.; Traverso, O. *J. Chem. Soc., Dalton Trans.*, **1987**, 1659-1663.

77) Deranlyagala, S.P.; Grundy, K.R. *Organometallics*, **1985**, *4*, 424-426.

78) Alonso, F.J.G.; Riera, V.; Ruiz, M.A.; Tiripicchio, A.; Camellini, M.T. *Organometallics*, **1992**, *11*, 370-386.

79) Shapley, J.R.; Richter, S.I.; Tachikawa, M.; Keister, J.B. *J. Organomet. Chem.*, **1975**, *94*, C43-C46.

80) Dyke, A.F.; Knox, S.A.R.; Morris, M.J.; Naish, P.J. *J. Chem. Soc., Dalton Trans.*, **1983**, 1417-1426.

81) Deeming, A.J.; Felix, M.S.B.; Nuel, D.; Powell, N.I.; Tocher, D.A.; Hardcastle, K.I. *J. Organomet. Chem.*, **1990**, *384*, 181-191.

82) MacLaughlin, S.A.; Doherty, S.; Taylor, N.J.; Carty, A.J. *Organometallics*, **1992**, *11*, 4315-4325.

83) Bruce, M.I.; Snow, M.R.; Matisons, J.G.; Horn, E. *J. Organomet. Chem.*, **1985**, *286*, 271-287.

84) Hogarth, G.; Lavender, M.H. *J. Chem. Soc., Dalton Trans.*, **1992**, 2759-2764.

85) Dahlquist, F.W.; Longmuir, K.J.; DuVernet, R.B. *J. Magn. Reson.*, **1975**, *17*, 406-410.

86) Alger, J.R.; Prestegard, J.H. *J. Magn. Reson.*, **1977**, *27*, 137.

87) Aime, S.; Osella, D.; Milone, L.; Rosenberg, E. *J. Organomet. Chem.*, **1981**, *213*, 207-213.

88) Gesmar, H.; Led, J.J. *J. Magn. Reson.*, **1986**, *68*, 95-101.

89) Spiess, Von H.W.; Mahnke, H. *Berichte der Bunsen-Gesellschaft*, **1972**, *76*, 990-995.

90) Mahnke, H.; Sheline, R.K.; Spiess, H.W. *J. Chem. Phys.*, **1974**, *61*, 55-60.

91) Gleeson, J.W.; Vaughan, R.W. *J. Chem. Phys.*, **1983**, *78*, 5384-5392.

92) Fukushima, E.; Roeder, S.B.W., *Experimental Pulse NMR*; Addison-Wesley: Don Mills, Ontario, 1981.

93) Hoffman, R.A.; Forsen, S. *J. Chem. Phys.*, **1966**, *45*, 2049-2060.

94) Draper, N.; Smith, H., *Applied Regression Analysis*; 2nd Ed., John Wiley and Sons Inc.: Toronto, 1981.

95) Morris, G.A.; Freeman, R. *J. Magn. Reson.*, **1978**, *29*, 433-462.

96) Derome, A.E., *Modern NMR Techniques for Chemistry Research*; Pergamon Press: Oxford, 1988.

97) Weiss, G.H.; Ferretti, J.A. *J. Magn. Reson.*, **1983**, *55*, 397-407.

98) Weiss, G.H.; Byrd, R.A.; Ferretti, J.A. *J. Magn. Reson.*, **1987**, *71*, 97-105.

99) Weiss, G.H.; Kiefer, J.E.; Ferretti, J.A. *J. Magn. Reson.*, **1992**, *97*, 227-234.

100) Bain, A.D. *J. Magn. Reson.*, **1990**, *89*, 153-160.

101) Bain, A.D.; Lao, L. *Isotopes in the physical and biomedical sciences, vol. 2. Isotopic applications in NMR studies*; Buncel, E.; Jones, J.R., Eds. Elsevier: Amsterdam, 1991; p. 411-429.

102) Bain, A.D.; Cramer, J.A. *J. Phys. Chem.*, **1993**, *97*, 2884-2887.

103) Neuhaus, D.; Williamson, M.P., *The nuclear Overhauser effect in structural and conformational analysis*; Verlag Chemie: New York, 1988.

104) Pelczer, I.; Szalma, S. *Chem. Rev.*, **1991**, *91*, 1507-1524.

105) Perrin, C.L. *J. Magn. Reson.*, **1989**, *82*, 619-621.

106) Pardue, H.L. *Anal. Chimica Acta*, **1989**, *216*, 69-107.

107) Nadjari, R.; Grivet, J.-Ph. *J. Magn. Reson.*, **1992**, *98*, 259-270.

108) Bodenhausen, G.; Ernst, R.R. *J. Magn. Reson.*, **1981**, *45*, 367.

109) Bodenhausen, G.; Ernst, R.R. *J. Am. Chem. Soc.*, **1982**, *104*, 1304.

110) Yarnykh, V.L.; Ustynyuk, Y.A. *J. Magn. Reson.*, **1993**, *A 102*, 131-136.

111) Campbell, I.D.; Dobson, C.M.; Ratcliffe, R.G.; Williams, R.J.P. *J. Magn. Reson.*, **1978**, *29*, 397-417.

112) Inglefield, P.T.; Krakower, E.; Reeves, L.W.; Stewart, R. *Mol. Phys.*, **1968**, *15*, 65-86.

113) Mann, B.E. *J. Magn. Reson.*, **1976**, *21*, 17-23.

114) Green, D.V.S.; Hillier, I.H.; Morris, G.A.; Whalley, L. *Magn. Reson. Chem.*, **1990**, *28*, 820-823.

115) Warren, J.D.; Clark, R.J. *Inorg. Chem.*, **1970**, *9*, 373-379.

116) Mann, B.E. *J. Chem. Soc., Chem. Commun.*, **1971**, 1173-1174.

117) Kruczynski, L.; Takats, J. *J. Am. Chem. Soc.*, **1974**, *96*, 932-934.

118) Kreiter, C.G.; Stuber, S.; Wackerle, L. *J. Organomet. Chem.*, **1974**, *66*, C49-C52.

119) Akhtar, M.; Ellis, P.D.; MacDiarmid, A.G.; Odom, J.D. *Inorg. Chem.*, **1972**, *11*, 2917-2921.

120) Kotzian, M.; Kreiter, C.G.; Michael, G.; Ozkar, S. *Chem. Ber.*, **1983**, *116*, 3637-3658.

121) Ozkar, S.; Kreiter, C.G. *J. Organomet. Chem.*, **1983**, *256*, 57-69.

122) Rigatti, G.; Boccalon, G.; Ceccon, A; Giacometti, G. *J. Chem. Soc., Chem. Commun.*, **1972**, 1165-1166.

123) Kirschner, R.M.; Marks, T.J.; Kristoff, J.S.; Ibers, J.A. *J. Am. Chem. Soc.*, **1973**, *95*, 6602.

124) Harris, D.C.; Rosenberg, E.; Roberts, J.D. *J. Chem. Soc., Dalton Trans.*, **1974**, 2398-2403.

125) Adams, R.D.; Brice, M.D.; Cotton, F.A. *Inorg. Chem.*, **1974**, *13*, 1080-1085.

126) Evans, J.; Johnson, B.F.G.; Lewis, J.; Norton, J.R. *J. Chem. Soc., Chem. Commun.*, **1973**, 79-80.

127) Bullitt, J.G.; Cotton, F.A.; Marks, T.J. *J. Am. Chem. Soc.*, **1970**, *92*, 2155-2156.

128) Gansow, O.A.; Burke, A.R.; Vernon, W.D. *J. Am. Chem. Soc.*, **1972**, *94*, 2550-2552.

129) Cotton, F.A.; Kruczynski, L.; White, A.J. *Inorg. Chem.*, **1974**, *96*, 1402-1407.

130) Adams, R.D.; Cotton, F.A. *Inorg. Chim. Acta*, **1973**, *7*, 153-156.

131) Cotton, F.A.; Hanson, B.E.; Jamerson, J.D. *J. Am. Chem. Soc.*, **1977**, *99*, 6588-6593.

132) Cotton, F.A.; Hanson, B.E. *Inorg. Chem.*, **1977**, *16*, 3369-3371.

133) Tachikawa, M.; Richter, S.I.; Shapley, J.R. *J. Organomet. Chem.*, **1977**, *128*, C9-C14.

134) Lawson, R.J.; Shapley, J.R. *Inorg. Chem.*, **1978**, *17*, 772-774.

135) Matheson, T.W.; Robinson, B.H. *J. Organomet. Chem.*, **1975**, *88*, 367-373.

136) Johnson, B.F.G.; Lewis, J.; Matheson, T.W. *J. Chem. Soc., Chem. Commun.*, **1974**, 441-442.

137) Martinengo, S.; Chini, P.; Albano, V.G.; Cariati, F.; Salvatori, T. *J. Organomet. Chem.*, **1973**, *59*, 379-394.

138) Milone, L.; Aime, S.; Randall, E.W.; Rosenberg, E. *J. Chem. Soc., Chem. Commun.*, **1975**, 452-454.

139) Cattermole, P.E.; Orrell, K.G.; Osborne, A.G. *J. Chem. Soc., Dalton Trans.*, **1974**, 328-332.

140) Aime, S. *Inorg. Chim. Acta*, **1982**, *62*, 51-56.

141) Hawkes, G.E.; Lian, L.Y.; Randall, E.W.; Sales, K.D.; Aime, S. *J. Chem. Soc., Dalton Trans.*, **1985**, 225-227.

142) Aime, S.; Milone, L.; Osella, D.; Valle, M.; Randall, E.W. *Inorg. Chim. Acta*, **1976**, *20*, 217-220.

143) Kruczynski, L.; Lishing Man, L.K.K.; Takats, J. *J. Am. Chem. Soc.*, **1974**, *96*, 4006-4008.

144) Darensbourg, Donald J.; Darensbourg, Marcetta Y.; Walker, Nyal *Inorg. Chem.*, **1981**, *20*, 1981-1921.

145) Seyferth, Dietmar; Hoke, Jeffrey B.; Wheeler, D.R. *J. Organomet. Chem.*, **1988**, *341*, 421-437.

146) Koridize, A.A.; Kizas, O.A.; Petrovskii, P.V.; Kolobova, N.E.; Struchkov, Y.T.; Yanovsky, A.I. *J. Organomet. Chem.*, **1988**, *338*, 81-87.

147) Lee, K-W; Brown, T.L. *Organometallics*, **1985**, *4*, 1025-1030.

148) Curtis, M.D; Han, K.R.; Butler, W.M. *Inorg. Chem.*, **1980**, *19*, 2096-2101.

149) Aspinall, H.C.; Deeming, A.J.; Donovan-Muntzi, S. *J. Chem. Soc., Dalton Trans.*, **1983**, 2669-2671.

150) Hickey, J.P.; Huffman, J.C.; Todd, L.J. *Inorg. Chim. Acta*, **1978**, *28*, 77-82.

151) Aime, S.; Milone, L.; Sappa, E.; Tiripicchio, A.; Camellini, M. *J. Chem. Soc., Dalton Trans.*, **1979**, 1155-1159.

152) Seyferth, D.; Archer, C.M.; Ruschke, D.P.; Cowie, M.; Hilts, R.W. *Organometallics*, **1991**, *10*, 3363-3380.

153) Xue, Z.L.; Sieber, W.J.; Knobler, C.B.; Kaesz, H.D. *J. Am. Chem. Soc.*, **1990**, *112*, 1825-1833.

154) Carty, A., Private Communication, 1993.

155) Gesmar, H.; Led, J.J.; Abildgaard, F. *Prog. Nucl. Magn. Reson. Spectrosc.*, **1990**, 22, 255-288.

156) Szymanski, S.; Witanowski, M.; Gryff-Keller, A.M. *Annual reports on NMR spectroscopy*; Webb, G.A., Ed. Academic Press: London, 1978; p. 227-289.

157) Streitwieser, A.; Heathcock, C.H. *Introduction to Organic Chemistry*; 2nd Ed., MacMillan Publishing Co., Inc.: New York, 1981.

APPENDIX

Theory of NMR Exchange[1.156]

In the quantum-mechanical model, every observable (i.e the frequency of transition) is determined from the action of an operator, Â on a wavefunction (or state). If the wavefunction is an eigenfunction of the operator, the result will be a constant:

$$\hat{A}|r\rangle = a|r\rangle \qquad \text{A.1}$$

The observable cannot be not determined directly, but rather one determines the expectation value or the average over a state. Mathematically, this is defined as follows:

$$\langle\hat{A}\rangle = \langle r|\hat{A}|r\rangle \qquad \text{A.2}$$

The wavefunction may be represented as a linear combination of eigenfunctions of the operator Â (A.3), and $|a\rangle, and\ |b\rangle$ are always chosen to be orthonormal, that

is $\langle a|b\rangle = \langle b|a\rangle = 0$, *and* $\langle a|a\rangle = \langle b|b\rangle = 1$.

$$|r\rangle = c_1|a\rangle + c_2|b\rangle \qquad \text{A.3}$$

With any spectroscopic technique, the eigenvalues and eigenfunctions are defined by the Schrödinger equation (A.4)

$$\hat{\mathcal{H}}\Psi = E\Psi \qquad \text{A.4}$$

In NMR spectroscopy, the basis states or eigenfunctions for protons with s=½ are $|\alpha\rangle$ *and* $|\beta\rangle$ and the combination is given in equation A.5.

$$\Psi = C_\alpha|\alpha\rangle + C_\beta|\beta\rangle \qquad \text{A.5}$$

The expectation value for the operator, $\hat{O}$ is given by A.6.

$$\begin{aligned}\langle\Psi|\hat{O}|\Psi\rangle &= \langle C_\alpha|\alpha\rangle + C_B|\beta\rangle\ |\hat{O}|\ C_\alpha|\alpha\rangle + C_\beta|\beta\rangle\rangle \qquad \text{A.6}\\ &= C_\alpha C_\alpha^*\langle\alpha|\hat{O}|\alpha\rangle + C_\alpha C_\beta^*\langle\alpha|\hat{O}|\beta\rangle\\ &+ C_\beta^* C_\alpha\langle\beta|\hat{O}|\alpha\rangle + C_\beta C_\beta^*\langle\beta|\hat{O}|\beta\rangle\end{aligned}$$

and this can also be written as equation A.7

$$< \hat{O} > = trace\ (\rho^{\dagger} O) \qquad \text{A.7}$$

where ρ is the density matrix (A.9) defined as equation A.8 and **O** is the matrix of eigenfunctions (A.9)

$$\rho = \begin{pmatrix} C_\alpha C_\alpha^* & C_\alpha C_\beta^* \\ C_\alpha^* C_\beta & C_\beta^* C_\beta \end{pmatrix} \qquad \text{A.8}$$

$$O = \begin{pmatrix} \langle\alpha|\hat{O}|\alpha\rangle & \langle\alpha|\hat{O}|\beta\rangle \\ \langle\beta|\hat{O}|\alpha\rangle & \langle\beta|\hat{O}|\beta\rangle \end{pmatrix} \qquad \text{A.9}$$

In Liouville space, the space for all linear operators, the density matrix (ρ) is written as a linear combination of the following orthoganol vectors (A.10) and ρ is written as a vector (A.11).

$$\boldsymbol{\rho} = C_\alpha C_\alpha^* \begin{pmatrix} 1 & 0 \\ 0 & 0 \end{pmatrix} + C_\alpha C_\beta^* \begin{pmatrix} 0 & 1 \\ 0 & 0 \end{pmatrix} + C_\beta^* C_\alpha \begin{pmatrix} 0 & 0 \\ 1 & 0 \end{pmatrix} + C_\beta^* C_\beta \begin{pmatrix} 0 & 0 \\ 0 & 1 \end{pmatrix} \qquad \text{A.10}$$

$$\rho = \begin{pmatrix} C_\alpha C_\alpha^* \\ C_\alpha^* C_\beta \\ C_\beta C_\alpha^* \\ C_\beta^* C_\beta \end{pmatrix} \qquad \text{A.11}$$

The energy corresponding to a transition between the α and β states is given by applying the Hamiltonian operator (A.12) to the α or β state. The expectation value

$$\hat{\mathcal{H}} = -\gamma \hbar B \cdot \hat{I}_j \qquad \text{A.12}$$

resulting from the application of the spin angular momentum in the z direction ($\hat{I}_z$) defines the difference between the spin population in the energy levels.

$$\langle \hat{I}_z \rangle = \begin{pmatrix} C_\alpha C_\alpha^* \\ C_\alpha C_\beta^* \\ C_\beta C_\alpha^* \\ C_\beta^* C_\beta \end{pmatrix} \cdot \begin{pmatrix} \frac{1}{2} \\ 0 \\ 0 \\ -\frac{1}{2} \end{pmatrix} = \frac{1}{2}(C_\alpha C_\alpha^* - C_\beta^* C_\beta) \qquad \text{A.13}$$

The diagonal elements $C_\alpha C^*_\alpha$ and $C_\beta C^*_\beta$ define the level populations and their difference defines the equilibrium magnetization intensity.

On the other hand, the $\hat{I}_x$ and $\hat{I}_y$ angular momentum operators are responsible for creating the transition from one level to the other. They are more conveniently reformulated as the raising and lowering operators, $\hat{I}_+$ and $\hat{I}_-$ (A.14 and A.15).

$$\hat{I}_+ = \hat{I}_x + i\hat{I}_y \qquad \text{A.14}$$

$$\hat{I}_- = \hat{I}_x - i\hat{I}_y \qquad \text{A.15}$$

The raising operator, $\hat{I}_+$, takes $\beta \rightarrow \alpha$ and is written in the form of a ket-bra (A.16), so when $\hat{I}_+$ is applied to β , α results (A.17).

$$\hat{I}_+ = |\alpha\rangle\langle\beta| \qquad \text{A.16}$$

$$\hat{I}_+ |\beta\rangle = |\alpha\rangle\langle\beta|\beta\rangle = |\alpha\rangle \qquad \text{A.17}$$

The spin angular momementum operators can also be represented as the basis sets in equation A.10.

$$\hat{I}_+ = \begin{pmatrix} 0 & 1 \\ 0 & 0 \end{pmatrix}, \hat{I}_- = \begin{pmatrix} 0 & 0 \\ 1 & 0 \end{pmatrix}, \hat{I}_z = \begin{pmatrix} 1 & 0 \\ 0 & -1 \end{pmatrix}, and\ \boldsymbol{E} = \begin{pmatrix} 1 & 0 \\ 0 & 1 \end{pmatrix} \qquad \text{A.18}$$

where **E** is the unit matrix

It then follows from equation A.11 and A.18 that ρ can be written in the form of equation A.19, representing the components along the vectors.

$$\hat{\rho} = \begin{pmatrix} E \\ \hat{I}_{+} \\ \hat{I}_{z} \\ \hat{I}_{-} \end{pmatrix} \qquad \text{A.19}$$

The time-dependence of the Schrödinger equation is given by A.20 and integration of that equation results in the eigenfunction defined in A.21.

$$-i\hbar\frac{\partial}{\partial t}\Psi = \hat{\mathcal{H}}\Psi \qquad \text{A.20}$$

$$\Psi = e^{(i\mathcal{H}t)}\Psi_{O} \qquad \text{A.21}$$

The time dependence of ρ is defined by equation A.22. If ρ is chosen to be the raising operator, that is $\rho = |\Psi_1\rangle\langle\Psi_2|$, then A.23 results.

$$i\hbar\frac{\partial}{\partial t}\rho = [\hat{\mathcal{H}}, \rho] = \hat{\mathcal{H}}\rho - \rho\hat{\mathcal{H}} \qquad \text{A.22}$$

$$i\hbar\frac{\partial}{\partial t}\rho = \hat{\mathcal{H}}|\Psi_1\rangle\langle\Psi_2| - |\Psi_1\rangle\langle\Psi_2|\hat{\mathcal{H}} \qquad \text{A.23}$$

$$= \mathscr{E}_1|\Psi_1\rangle\langle\Psi_2| - |\Psi_1\rangle\langle\Psi_2|\mathscr{E}_2$$

$$= (\mathscr{E}_1 - \mathscr{E}_2)|\Psi_1\rangle\langle\Psi_2|$$

This corresponds to the transition from one energy level to the other, with an eigenvalue of $(\mathscr{E}_1 - \mathscr{E}_2)$. From classical mechanics, we know that this value is given by the Larmor frequency $\omega = \gamma B_0$.

To summarize, the components of ρ along the eigenvectors are defined by equation A.19 and the elements that give its time dependence are the raising and lowering operators $\hat{I}_+$ and $\hat{I}_-$. The elements that determine its equilbrium value are **E** and $\hat{I}_z$. The time-dependence components, $\rho(t)$, are then given by A.24.

$$\rho(t) = \begin{pmatrix} 0 \\ e^{+\gamma B_0}\rho(0) \\ 0 \\ e^{-\gamma B_0}\rho(0) \end{pmatrix} \qquad \text{A.24}$$

and the components at equilibrium are given by ρ_0 (A.25)

$$\rho_0 = \begin{pmatrix} C_\alpha C_\alpha^* + C_B C_\beta^* \\ 0 \\ C_\alpha C_\alpha^* - C_\beta C_\beta^* \\ 0 \end{pmatrix} = \begin{pmatrix} N \\ 0 \\ M_z \\ 0 \end{pmatrix} \qquad \text{A.25}$$

where N is the total number of spin population in the system and M_z is the magnetization intensity that is observed in the spectrum. These are given by the sum and the difference of the spin populations in the upper and lower levels.

Now relaxation can be incorporated into the time dependence equation and this known as the Wangness-Bloch-Redfield (WBR) master equation (A.26) and integration gives A.27.

$$i\hbar\frac{\partial}{\partial t}\rho = [\hat{\mathcal{H}}, \hat{\rho}] - \hat{R}(\rho - \rho_0) = \hat{\mathcal{L}} - \hat{R}(\rho - \rho_0) \qquad \text{A.26}$$

$$\rho(t) = e^{(i\hat{\mathcal{L}}t - \hat{R}t)}\,\rho_0 \qquad \text{A.27}$$

where $\hat{\mathcal{L}}$ is the Liouville superoperator that may be represented as in equation A.28. from A.19 and A.24.

$$\hat{\mathcal{L}} = \begin{bmatrix} \omega_0 & 0 & 0 \\ 0 & 0 & 0 \\ 0 & 0 & -\omega_0 \end{bmatrix} \cdot \begin{bmatrix} \hat{I}_+ \\ \hat{I}_z \\ \hat{I}_- \end{bmatrix} \qquad \text{A.28}$$

and in the presence of no exchange, **R** is simply composed of the spin-lattice and spin-spin relaxation rates (A.29).

$$\boldsymbol{R} = \begin{bmatrix} \frac{1}{T_2} & 0 & 0 \\ 0 & \frac{1}{T_1} & 0 \\ 0 & 0 & \frac{1}{T_2} \end{bmatrix} \qquad \text{A.29}$$

Using equation A.28 and A.29, the density matrix representing a single site is given below.

$$\rho_j(t) = \begin{bmatrix} i\omega_j - \left(\frac{1}{T_2}\right)_j & 0 & 0 \\ 0 & -\left(\frac{1}{T_1}\right)_j & 0 \\ 0 & 0 & -i\,\omega_j - \left(\frac{1}{T_2}\right)_j \end{bmatrix} \qquad \text{A.30}$$

The signal line-shape is described using only the $\hat{I}_+$ and $\hat{I}_-$ elements and hence is described by a simple damped exponential equation (A.31).

$$\rho(t) = e^{(i\omega_0 t - t/T_2)}\,\rho_0 \qquad \text{A.31}$$

Exchange

In order to incorporate exchange, there must be at least two sites described by $\rho_1(t)$ and $\rho_2(t)$ (A.32) that are linked by exchange (A.33)

$$\rho_1(t) = \begin{pmatrix} \hat{I}_{1+} \\ \hat{I}_{1z} \\ \hat{I}_{1-} \end{pmatrix} \textit{ and } \rho_2(t) = \begin{pmatrix} \hat{I}_{2+} \\ \hat{I}_{2z} \\ \hat{I}_{2-} \end{pmatrix} \qquad \text{A.32}$$

$$\rho_{exch} = \begin{pmatrix} [\rho_1(t) - k] & k \\ k & [\rho_2(t) - k] \end{pmatrix} \qquad \text{A.33}$$

The exchange matrix (A.34) is then determined by combining equations A.32 and A33.

$$\rho_{exch}(t) = \begin{pmatrix} \hat{I}_{1+} \\ \hat{I}_{2+} \\ \hat{I}_{1z} \\ \hat{I}_{2z} \\ \hat{I}_{1-} \\ \hat{I}_{2-} \end{pmatrix} = \begin{pmatrix} \rho_+ & 0 & 0 \\ 0 & \rho_z & 0 \\ 0 & 0 & \rho_- \end{pmatrix} \qquad \text{A.34}$$

where ρ_+, ρ_z, and ρ_- are defined as follows

$$\rho_+(t) = \begin{pmatrix} \hat{I}_{1+} \\ \hat{I}_{2+} \end{pmatrix} = \begin{pmatrix} +i\omega_1 - \left(\frac{1}{T_2}\right)_1 - k & k \\ k & +i\omega_2 - \left(\frac{1}{T_2}\right)_2 - k \end{pmatrix} \quad \text{A.35}$$

$$\rho_z(t) = \begin{pmatrix} \hat{I}_{1z} \\ \hat{I}_{2z} \end{pmatrix} = \begin{pmatrix} -\left(\frac{1}{T_1}\right)_1 - k & k \\ k & -\left(\frac{1}{T_1}\right)_2 - k \end{pmatrix} \quad \text{A.36}$$

$$\rho_-(t) = \begin{pmatrix} \hat{I}_{1-} \\ \hat{I}_{2-} \end{pmatrix} = \begin{pmatrix} -i\omega_1 - \left(\frac{1}{T_2}\right)_1 - k & k \\ k & -i\omega_2 - \left(\frac{1}{T_2}\right)_2 - k \end{pmatrix} \quad \text{A.37}$$

Diagonalization of these matricies will give the density matrix elements for each site under the condition of exchange.

Line-Shape Analysis

In line-shape analysis, it is the chemical shift that is modulated and thus one only deals with the raising and lowering elements (ρ_+ and ρ_-) The relaxation quantity, r, given by equation A.38 is extracted from the raising and lowering density matricies (A.35 and A.37) and defines the Larmor Frequency and natural line-width for each site. When k becomes large compared to the difference in frequency between both sites, the lines broaden and move together until they reach an average value.

$$r = i\omega - \frac{1}{T_2} \qquad \text{A.38}$$

Magnetization Transfer Exchange

In magnetization transfer, the exchange occurs only when z magnetization is formed, and then one need only diagonalize the z density matrix, ρ_z (A.36). Now r is simply the spin-lattice relaxation rate, $(T_1)^{-1}$. One can now see that equation A. 36 resembles the familiar exchange-relaxation matrix **A** (A.39) and the time-dependence of the magnetization found in Chapter 2 is given by equation A.40.

$$A_{ij} = \begin{cases} k_{ji} & i \neq j, \\ -\sum_{l=i}^{n} k_{il} - \frac{1}{T_{1i}} & i = j, \end{cases} \qquad \text{A.39}$$

$$\frac{d}{\partial t}\begin{bmatrix} M_1(\infty) - M_1(t) \\ M_2(\infty) - M_2(t) \end{bmatrix} = \boldsymbol{A}\begin{bmatrix} M_1(\infty) - M_1(t) \\ M_2(\infty) - M_2(t) \end{bmatrix} \qquad \text{A.40}$$